CANADIAN THESES ON MICROFICHE

THÈSES CANADIENNES SUR MICROFICHE

NOTICE

The quality of this microfiche is heavily dependent upon the quality of the original thesis submitted for microfilming. Every effort has been made to ensure the highest quality of reproduction possible.

If pages are missing, contact the university which granted the degree.

Some pages may have indistinct print especially if the original pages were typed with a poor typewriter ribbon or if the university sent us an inferior photocopy.

Previously copyrighted materials (journal articles, published tests, etc.) are not filmed.

Reproduction in full or in part of this film is governed by the Canadian Copyright Act, R.S.C. 1970, c. C-30. Please read the authorization forms which accompany this thesis.

AVIS

La qualité de cette microfiche dépend grandement de la qualité de la thèse soumise au microfilmage. Nous avons tout fait pour assurer une qualité supérieure de reproduction.

S'il manque des pages, veuillez communiquer avec l'université qui a conféré le grade.

La qualité d'impression de certaines pages peut laisser à désirer, surtout si les pages originales ont été dactylographiées à l'aide d'un ruban usé ou si l'université nous a fait parvenir une photocopie de qualité inférieure.

Les documents qui font déjà l'objet d'un droit d'auteur (articles de revue, examens publiés, etc.) ne sont pas microfilmés.

La reproduction, même partielle, de ce microfilm est soumise à la Loi canadienne sur le droit d'auteur, SRC 1970, c. C-30. Veuillez prendre connaissance des formules d'autorisation qui accompagnent cette thèse.

THIS DISSERTATION HAS BEEN MICROFILMED EXACTLY AS RECEIVED

LA THÈSE A ÉTÉ MICROFILMÉE TELLE QUE NOUS L'AVONS REÇUE

Canada

THE UNIVERSITY OF ALBERTA

APPLICATION OF DIRAC PHENOMENOLOGY TO PROTON

INELASTIC SCATTERING

by

(C)   JON INGVAR JOHANSSON

A THESIS

SUBMITTED TO THE FACULTY OF GRADUATE STUDIES AND RESEARCH

IN PARTIAL FULFILMENT OF THE REQUIREMENTS FOR THE DEGREE

OF MASTER OF SCIENCE

IN

NUCLEAR PHYSICS

DEPARTMENT OF PHYSICS

EDMONTON, ALBERTA
FALL 1986

THE UNIVERSITY OF ALBERTA

RELEASE FORM

NAME OF AUTHOR: JON INGVAR JOHANSSON

TITLE OF THESIS: APPLICATION OF DIRAC PHENOMENOLOGY TO

PROTON INELASTIC SCATTERING

DEGREE: MASTER OF SCIENCE

YEAR THIS DEGREE GRANTED: FALL 1986

Permission is hereby granted to THE UNIVERSITY OF ALBERTA LIBRARY to reproduce single copies of this thesis and to lend or sell such copies for private, scholarly or scientific research purposes only.

The author reserves other publication rights, and neither the thesis nor extensive extracts from it may be printed or otherwise reproduced without the author's written permission.

....

(Signature)

DRPT. OF PHYSICS

(Permanent address)

UNIVERSITY OF ALBERTA

EDMONTON AB

T6C 2J1

Date: JULY 29/86

THE UNIVERSITY OF ALBERTA

FACULTY OF GRADUATE STUDIES AND RESEARCH

The undersigned certify that they have read and recommend to the Faculty of Graduate Studies and Research for acceptance a thesis entitled APPLICATION OF DIRAC PHENOMENOLOGY TO PROTON INELASTIC SCATTERING submitted by Jon Ingvar Johansson in partial fulfillment of the requirements for the degree of MASTER OF SCIENCE in Physics.

....
Supervisor

....

....

....

Date: ...July 4, 1986...

ABSTRACT

We consider the inelastic scattering of intermediate energy protons leading to the excitation of collective states in even-even nuclei. This work is done in the framework of Dirac phenomenology. We calculate the inelastic scattering amplitude in the distorted wave Born approximation in which we describe the relative motion of the nucleon and target by Dirac spinors. These spinors are solutions of the Dirac equation with complex scalar and vector optical potentials. The transition operator is obtained by deforming these potentials and keeping terms which are first order in the nuclear deformation. The states of the target nucleus are treated nonrelativistically.

A computer program based on these considerations has been written and tested. Calculations of cross section, analyzing power and polarization transfer coefficients will be compared with experimental data. We also compare our calculations with those of other authors. The calculations are found to agree well with data when the deformation parameter of the state is small but agreement gets worse with increasing size of the deformation, indicating the importace of coupled channels effects. We also find that the full relativistic calculation does a better job of describing the data than some nonrelativistic calculations, even if there is some correction for relativity.

ACKNOWLEDGEMENTS

TABLE OF CONTENTS

LIST OF TABLES

LIST OF FIGURES

I - INTRODUCTION

A scattering experiment is done to gain data which will aid in the understanding of nuclear structure and nuclear reactions. When the incident particle has a low kinetic energy (a few tens of Mev) the observed results can generally be well explained by decribing the involved particles with the Schrödinger theory of scattering, but with the advent of machines which routinely accelerate protons to a kinetic energy of five hundred Mev or more the Schrödinger descriptions of these projectiles has been found to be inadequate [Cl82]. At a kinetic energy of five hundred Mev a proton has a velocity of over eighty per cent of the speed of light so a proper relativistic description is in order.

Such a relativistic description of proton elastic scattering has been developed in the past few years [Cl82], and does a very good job of describing the elastic scattering observables. This model is based on the Dirac equation with an optical potential consisting of a term which is a scalar under Lorentz transformation and a term which transforms as the zeroth component of a four-vector. The description of the cross section resulting from the Dirac based calculations is at least as good as that of the Schrödinger calculations and the description of the spin observables (analyzing power and spin rotation parameter) is much better.

The Dirac optical potential has gained respectability since relativistic impulse approximation (RIA) calculations have shown that these vector and scalar potentials arise naturally from a relativistically invariant free nucleon-nucleon scattering amplitude [Mc83]. These microscopic calculations give reasonable agreement with the deep,

phenomenologically determined optical potentials. These RIA potentials result in a good

description of the elastic scattering of 500 Mev. protons from ^{40}Ca [Sh83].

Another interesting point is the observation that a central potential that has a

"wine-bottle-bottom" shape can give a better description of elastic scattering data than a

potential which has the standard Woods-Saxon shape [Me81]. Such a potential shape is

an artifact of the reduction of the Dirac equation to a two-component Schrödinger-like

equation. This effective potential has been used in the calculation of inelastic scattering

observables [Sa84] and is found to give slightly better predictions than the standard

(Woods-Saxon) potential.

Recently it has been pointed out that there is a relation between elastic scattering

and the inelastic scattering to collective states [Am80]. The assumption of a local, surface

peaked transition density leads to an expression for the inelastic cross section in terms of

the elastic cross section at a shifted angle. This relation gives a good description of the

inelastic cross section for 800 Mev. protons scattering from ^{208}Pb. This relation is also

found to hold when the calculation is done in the framework of the relativistic distorted

wave impulse approximation. [Pi83].

A good description of elastic scattering may result in a good description of the

inelastic scattering. The present work has been carried out with this hope in mind. We

extend the phenomenological Dirac optical model to the calculation of proton inelastic

scattering leading to collective excited states. The inelastic scattering amplitude is

calculated in the distorted wave Born approximation (DWBA). The relative motion of the

proton and nucleus is described by a four-component Dirac spinor and the target nucleus

is descibed nonrelativistically. We obtain the transition operator by deforming the scalar

and vector potentials and keeping terms which are first order in the nuclear deformation.

In chapter II we outline some of nonrelativistic scattering theory. In chapter III we discuss the phenomenolgical Dirac optical model and we show the fits obtained to elastic scattering data. In chapter IV we show the calculation of the T-matrix element for inelastic scattering to collective states. The relation of this T-matrix to the scattering observables is shown in appendix B. Chapter V contains the predictions for the inelastic observables and comparisons to data. A conclusion is given in chapter VI.

II - SCATTERING THEORY

Here we consider the formal nonrelativistic theory of the scattering of spin-0 projectiles from a spin-0 target. This is the simplest scattering system, and a knowledge of the structure of the theory for this system makes the extension to more complicated systems and relativistic calculations fairly easy. For the sake of simplicity we consider only interaction potentials for which $r^2V(r)$ goes to zero as $r \rightarrow \infty$, so we ignore the Coulomb potential. Also for simplicity we take $\hbar = c = 1$.

It should be pointed out here that the observables which are calculated in later chapters are related to the T-matrix (Appendix B), and the inclusion of the scattering operator and its properties may seem extraneous. However, the scattering operator is the most fundamental operator of scattering theory in the sense that it relates the asymptotic outgoing state of the system to the asymptotic incoming state. These are the experimentally observable states, and so the scattering operator contains all the information about the scattering process. Rather than pulling the T-matrix out of the proverbial hat I will try to present an overview of the relationships between the commonly used objects of scattering theory, which we will in fact calculate in later chapters, and the S-matrix, but due to lack of space there will still be some things pulled out of that hat.

II-1 The S-matrix and the On-shell T-matrix

In a scattering experiment the initial state of the system $\Psi_{in}(t)$ is prepared at $t=-\infty$. The system then evolves in time according to the Hamiltonian into a state $\Psi^{(+)}(t)$ which has the same quantum numbers (momentum, spin, etc.) as $\Psi_{in}(t)$. $\Psi^{(+)}(t)$ continues to evolve, and in the limit $t \to \infty$ becomes a free wave $\Psi_{out}(t)$ which contains some scattered (spherical) wave in addition to the incident plane wave, $\Psi_{in}(t)$.

Alternatively we can specify a state in the future ($t=\infty$), $\Psi_{out}(t)$, which arises from a state $\Psi^{(-)}(t)$ (and has the same quantum numbers as $\Psi_{out}(t)$), which in turn evolves from a state $\Psi_{in}(t)$ in the remote past. $\Psi^{(-)}(t)$ is a solution of the same Schrödinger equation as $\Psi^{(+)}(t)$ but asymptotically it is an incoming spherical wave. The assumption of time reversal invariance gives a relation between $\Psi^{(+)}$ and $\Psi^{(-)}$ [Ja70]

$$[\Psi^{(+)}(t)]^* = \Psi^{(-)}(-t) \qquad \text{II-1}$$

The functions $\Psi^{(\pm)}(t)$ are solutions of the Lippmann-Schwinger equation

$$\Psi^{(\pm)}(t) = \Psi^{(0)}(t) + \int G_0^{(\pm)}(t-t') V \Psi^{(\pm)}(t')dt' \qquad \text{II-2}$$

where V is the interaction potential of the problem and the free Green functions $G_0^{(\pm)}$ are solutions of

$$(i\partial/\partial t - H_0) G_0^{(\pm)}(t) = \delta(t) \qquad \text{II-3}$$

Note that (II-2) contains the boundary conditions

$$LIM_{t \to -\infty} \Psi^{(\pm)}(t) = \Psi_{in/out}(t) \qquad \text{II-4}$$

Also note that if the full wave is $\Psi^{(+)}(t)$ then $\Psi^{(0)}(t)$ is $\Psi_{in}(t)$ and if the full wave is $\Psi^{(-)}(t)$ then $\Psi^{(0)}(t)$ is $\Psi_{out}(t)$.

Equation II-3 can be written (see II-10 and below) as

$$(E - H_0) G_0^{(\pm)}(E) = 1 \qquad\qquad \text{II-5}$$

and we can write a formal solution as

$$G_0^{(\pm)}(E) = [E - H_0 \pm i\epsilon]^{-1} \qquad\qquad \text{II-6}$$

where the $\pm i\epsilon$ tells us which way to close the integration contour around the poles in the Green function. These shifts of the pole into the complex plane reflect the boundary conditions that are imposed on the time dependent Green functions.

The asymptotic (free) wave functions are related to the full wave functions by the Möller operators, $\Omega_\pm$, such that

$$\Psi(t) = \Omega_+ \Psi_{in}(t)$$

$$= \Omega_- \Psi_{out}(t) \qquad\qquad \text{II-7}$$

so Ω_+ propagates $\Psi_{in}(t)$ from $t=-\infty$ to a time t, and Ω_- propagates $\Psi_{out}(t)$ from $t=+\infty$ to a time t. The Möller operators are defined as the limits

$$\Omega_\pm = \text{LIM}_{t\to-\infty} \exp(iHt) \exp(-iH_0t) \qquad\qquad \text{II-8}$$

It is possible to form an operator which relates the asymptotic states at $t=-\infty$ to those at $t=\infty$. This is the scattering operator, S, which is defined as

$$S = \Omega_-^\dagger \Omega_+$$

This operator relates the asymptotic states by

$$\Psi_{out}(t) = S \Psi_{in}(t) \qquad\qquad \text{II-9a}$$

and

$$\Psi_{in}(t) = S^\dagger \Psi_{out}(t) \qquad\qquad \text{II-9b}$$

The sets of states { $\Psi_{in}(t)$} and { $\Psi_{out}(t)$} are assumed to be complete so from II-9 we

get that $SS^\dagger = S^\dagger S = 1$, i.e. S is a unitary operator. When evaluated on the basis of asymptotically free states this operator is called the S-matrix.

It is more convenient to work with wave functions which are functions of energy instead of time so we Fourier transform the wave functions by

$$\Psi(E) = \int e^{iEt}\Psi(t)dt \qquad\qquad\qquad II\text{-}10$$

and similarly for the Green functions $G_0^{(\pm)}(t)$. The Lippmann-Schwinger equation then becomes

$$\Psi^{(\pm)}(E) = \Psi^{(0)}(E) + [E - H_0 \pm i\epsilon]^{-1} V \Psi^{(\pm)}(E) \qquad\qquad II\text{-}11$$

S is a time independent operator so equations II-9 become

$$\Psi_{out}(E) = S\cdot\Psi_{in}(E) \qquad\qquad\qquad II\text{-}12a$$

$$\Psi_{in}(E) = S^\dagger \Psi_{out}(E) \qquad\qquad\qquad II\text{-}12b$$

Note that in II-12a, if the full state is $\Psi^{(+)}(E,\alpha)$, i.e. the state has quantum numbers α, then Ψ_{in} is $\Psi^{(0)}(E,\alpha)$, ie $\Psi^{(0)}$ has the same quantum numbers, but Ψ_{out} is a linear combination of all possible final states and can not be assigned definite quantum numbers. Similarly if the full state is $\Psi^{(-)}(E,\alpha)$ then Ψ_{out} is $\Psi^{(0)}(E,\alpha)$, but Ψ_{in} is then a linear combination of all possible initial states.

The total Hamiltonian for the system is $H = H_0 + V$ so we can write a formal solution of the Lippmann-Schwinger equation as

$$[E - H]\Psi^{(\pm)} = [E - H_0]\Psi^{(0)} = [E - H]\Psi^{(0)} + V\Psi^{(0)} \qquad II\text{-}13$$

or

$$\Psi^{(\pm)} = \Psi^{(0)} + [E - H \pm i\epsilon]^{-1} V\Psi^{(0)} \qquad\qquad II\text{-}14$$

Note that this is purely a formal solution since we must still evaluate $[E - H \pm i\epsilon]^{-1}$

which would require that we know the eigenfunctions of H.

The S-matrix elements are specified by

$$S_{fi} = < \Psi^{(-)} (E_f) \mid \Psi^{(+)} (E_i) >$$ II-15

$$= < \Psi^{(+)} (E_f) \mid \Psi^{(+)} (E_i) > + \{ < \Psi^{(-)} (E_f) \mid - < \Psi^{(+)} (E_f) \mid \} \mid \Psi^{(+)} (E_i) >$$

and using our formal solutions II-13 we can write

$$\mid \Psi^{(-)} (E_f) > - \mid \Psi^{(+)} (E_f) > = \{ [E_f - H - i\epsilon]^{-1} V -$$

$$- [E_f - H + i\epsilon]^{-1} V \} \mid \Psi^{(0)} (E_f) >$$

also the functions $\Psi^{(\pm)}(E_f)$ are orthonormal so

$$< \Psi^{(\pm)} (E_f) \mid \Psi^{(\pm)} (E_i) > = \delta_{fi}$$ II-16

where $\delta_{fi} = \delta(E_f - E_i) \, \delta_{\alpha\beta}$. Here α and β are all the quantum numbers besides energy

which are required to specify $\Psi^{(+)} (E)$. Finally it is useful to recall the relation

$$[E - H \pm i\epsilon]^{-1} = P [E - H]^{-1} - i\pi\delta(E - H)$$ II-17

where the P denotes the principal value of the integral. The elements of the scattering

matrix then become

$$S_{fi} = \delta_{fi} + < \Psi^{(0)} (E_f) \mid V [E_f - H + i\epsilon]^{-1} - V [E_f - H - i\epsilon]^{-1} \mid \Psi^{(+)} (E_i) >$$

$$= \delta_{fi} + \{ P[E_f - E_i]^{-1} - i\pi \, \delta(E_f - E_i) -$$

$$P[E_f - E_i]^{-1} - i\pi \, \delta(E_f - E_i) \} < \Psi^{(0)} (E_f) \mid V \mid \Psi^{(+)} (E_i) >$$

$$= \delta_{fi} - 2\pi i\delta(E_f - E_i) < \Psi^{(0)} (E_f) \mid V \mid \Psi^{(+)} (E_i) >$$

$$= \delta_{fi} - 2\pi i\delta(E_f - E_i) \, T_{fi}$$ II-18

where we have defined the T-matrix on the energy shell (final energy = initial energy)

as

$$T_{fi} = < \Psi^{(0)} (E_f) \mid V \mid \Psi^{(+)} (E_i) > \qquad E_f = E_i \qquad \text{II-19}$$

II-2 The Off-shell T-matrix

First consider the Green functions, G_0 for the free Hamiltonian, and G, for the total Hamiltonian

$$G_0 = [E - H_0]^{-1} \qquad \text{II-20}$$

$$G = [E - H]^{-1} = [E - H_0 - V]^{-1} \qquad \text{II-21}$$

Note that for simplicity we have dropped the $\pm$ie, but this is implied with the proper sign when the boundary conditions are specified. Using the identity

$$1/A - 1/B = 1/B (B - A) 1/A \qquad \text{II-22}$$

we can find integral equations relating G_0 and G; i.e. setting $A = E - H_0$ and $B = E - H_0 - V$ gives

$$G = G_0 + G_0 V G \qquad \text{II-23}$$

Similarly interchanging A and B gives

$$G_0 = G - G V G_0 \qquad \text{II-24}$$

We can iterate II-23 to get

$$G = G_0 + G_0 V G_0 + G_0 V G_0 V G_0 + ...$$

$$= G_0 + G_0 [V + V G_0 V + V G_0 V G_0 V + ...] G_0$$

$$= G_0 + G_0 T G_0 \qquad \text{II-25}$$

where the off-shell T-matrix is defined by

$$T = V + V\,G_0\,V + V\,G_0\,V\,G_0\,V + ... \qquad\qquad \text{II-26a}$$

$$= V + V\,G_0\,T \qquad\qquad \text{II-26b}$$

Comparing equations II-14 and II-7 we see that the Möller operator can be written as

$$\Omega_{\pm} = 1 + G_{\pm}\,V \qquad\qquad \text{II-27}$$

and using this in the expression II-19 for the T-matrix gives

$$T_{fi} = \,< \Psi^{(0)}\,(E_f)\,|\,V\,|\,\Psi^{(+)}\,(E_i)\,>$$

$$= \,< \Psi^{(0)}\,(E_f)\,|\,V\,\Omega_{+}\,|\,\Psi^{(0)}\,(E_i)\,>$$

$$= \,< \Psi^{(0)}\,(E_f)\,|\,V + V\,G_{+}\,V\,|\,\Psi^{(0)}\,(E_i)\,>$$

then using II-23 to iterate the operator between the plane wave states this is (recalling II-26a)

$$T_{fi} = \,< \Psi^{(0)}\,(E_f)\,|\,V + V\,G_0\,V + V\,G_0\,V\,G_0\,V + ...\,|\,\Psi^{(0)}\,(E_i)\,>$$

$$= \,< \Psi^{(0)}\,(E_f)\,|\,T\,|\,\Psi^{(0)}\,(E_i)\,> \qquad\qquad \text{II-28}$$

II-3 Invariance Properties of the S-Matrix

We say that a system is invariant with respect to some unitary operation if the Hamiltonian is invariant, that is

$$H = U^{-1}HU$$

First consider the effect of translations on a system. The operator which generates a rigid translation of the system through a vector a is

$$D(a) = \exp(-ia \cdot P) \qquad \qquad \text{II-29}$$

where P is the total momentum operator of the system, $-i\nabla$. Consider the effect of this operator in one dimension.

$$D(a)f(x) = \exp(-iaP)f(x)$$

$$= \Sigma_n (-a)^n / n! \ (d/dx)^n f(x)$$

$$= f(x-a)$$

so if the system is in a state Ψ then a translation of the state through a vector a is produced by

$$\Psi(x-a) = D(a) \Psi(x) \qquad \qquad \text{II-30}$$

Recall that the Hamiltonian of the system is $H=H_0+V$, where H_0 is the kinetic energy operator of the system. The translation operator commutes with H_0 and if the system is translationally invariant then H also commutes with $D(a)$ i.e. $H = D^{-1}(a)H$ $D(a)$. So if the system is translationally invariant the translation operator must commute with the Möller operators since

$$D(a) \ \Omega_{\pm} = D(a) \ \text{LIM}_{t\to-\infty} \exp(iHt) \exp(-iH_0t)$$

$$= \text{LIM}_{t\to-\infty} \exp(iHt) \exp(-iH_0t) \ D(a)$$

$$= \Omega_{\pm} D(a)$$

and since the scattering matrix is $S = \Omega_-^{\dagger} \Omega_+$ we have that S is invariant under translations

$$S = D^{-1}(a) \ S \ D(a) \qquad \qquad \text{II-31}$$

Also since S commutes with $D(a)$ for all a, S must commute with the momentum operator of the system, $[S , P] = 0$, and taking matrix elements of this commutator gives

$$\langle p'' \mid SP \mid p'\rangle - \langle p'' \mid PS \mid p'\rangle = 0$$

or

$$\langle p'' \mid S \mid p'\rangle \, (p'' - p') = 0 \qquad\qquad \text{II-32}$$

so the S-matrix is nonzero only if $p'' = p'$, i.e. if the total momentum is conserved. So we see that imposing translational invariance on our system leads to conservation of linear momentum. Taking matrix elements of II-31 gives

$$\langle p' \mid S \mid p\rangle = \langle p' \mid D^{-1}(a) \, S \, D(a) \mid p\rangle$$

$$= \langle p_t' \mid S \mid p_t\rangle \qquad\qquad \text{II-33}$$

where $\mid p_t\rangle$ is the translated wave function. And we see that S is invariant under translations.

Now consider the effect of rotations on our system. If the system is rotated through an angle Θ, about a direction n, we define a vector $\Theta = \Theta n$, and the rotation operator is

$$R(\Theta) = \exp(i\Theta \cdot J) \qquad\qquad \text{II-34}$$

where J is the total angular momentum operator of the system.

If the system is rotationally invariant then $R(\Theta)$ must commute with the Hamiltonian, so by the same arguments as were used for translational invariance $R(\Theta)$ commutes with $\Omega_\pm$ and so, with S. This is true for any Θ so S must commute with J, and through steps similar to those which give II-32 we get that rotational invariance of the system implies conservation of angular momentum. Finally, as in the translational case, we must have

$$\langle p' \mid S \mid p \rangle = \langle p' \mid R^{-1}(\Theta) \, S \, R(\Theta) \mid p \rangle$$

$$= \langle p_R' \mid S \mid p_R \rangle \qquad\qquad \text{II-35}$$

so the S-matrix is invariant under rotations of the system as well.

The operator S commutes with the kinetic energy operator, H_0, and with the total angular momentum of the system, J (which is just L for spinless particles) The operators, H_0, L^2, and L_z form a complete set of observables (i.e. they have simultaneous eigenfunctions $\mid E, \ell, m \rangle$ with the eigenvalues E, $\ell(\ell+1)$, m). The representation of this wave function in coordinate space is

$$\langle x \mid E, \ell, m \rangle = 4\pi \, i^{\ell} \, (Mk)^{1/2} \, j_{\ell}(kr) \, Y_{\ell m}(\Omega) \qquad\qquad \text{II-36}$$

where the factor $(Mk)^{1/2}$ comes from the normalization

$$\langle E', \ell', m' \mid E, \ell, m \rangle = (2\pi)^3 \, \delta(E'-E) \, \delta_{\ell',\ell} \, \delta_{m',m} \qquad\qquad \text{II-37}$$

S commutes with H_0, and L so the S-matrix is diagonal in the angular momentum representation, and it has the form

$$\langle E', \ell', m' \mid S \mid E, \ell, m \rangle = (2\pi)^3 \, \delta(E'-E) \, \delta_{\ell',\ell} \, \delta_{m',m} \, s_{\ell}(E) \qquad\qquad \text{II-38}$$

where $s_{\ell}(E)$ is the eigenvalue of S corresponding to the eigenfunction $\mid E, \ell, m \rangle$. Note that $s_{\ell}(E)$ is independent of m. This can be easily shown since S commutes with L, so it commutes with $L_{\pm}$ and we can write

$$L_+ \, S \, L_- = S \, L_+ \, L_-$$

and taking matrix elements of this we get

$$\langle \dots, m\text{-}1 \mid S \mid \dots, m\text{-}1 \rangle = \langle \dots, m \mid S \mid \dots, m \rangle$$

which must be true for all m so the matrix element can not depend on m.

II-4 The Scattering Amplitude

The potential due to the scattering center is $V(r)$, and in the center of momentum system the wave function is a solution of the Schrödinger equation

$$(p^2/2M + V(r)) \Psi = E \Psi \qquad\qquad \text{II-39}$$

or defining $k^2=2mE$ and $U(r)=2mV(r)$ we can write this as

$$(\nabla^2 + k^2) \Psi = -U(r) \Psi \qquad\qquad \text{II-40}$$

At $t=-\infty$ the incident particle is at $z=-\infty$ and is incident along the z-axis. The nuclear potential goes to zero faster than $r^2U(r)$ as $r\to\infty$ so the asymptotic incident wave function feels no potential and is just the plane wave

$$\Psi_I(r) = \exp(ikz) \qquad\qquad \text{II-41}$$

After scattering the total wave function contains the part of the plane wave which was not scattered, travelling along the z-axis, as well as a scattered, outward travelling, spherical wave

$$\Psi_O(r) = f(\theta,\phi) \exp(ikr)/r \qquad\qquad \text{II-42}$$

The total wave function is then

$$\Psi_{TOT}(r) = \Psi_I(r) + \Psi_O(r) = \exp(ikz) + f(\theta,\phi) \exp(ikr)/r \qquad\qquad \text{II-43}$$

where $f(\theta,\phi)$ is the scattering amplitude (i.e. the amplitude of the scattered wave).

The plane wave can be expanded as

$$\exp(ikz) = \sum_{\ell} i^{\ell} (2\ell+1) j_{\ell}(kr) P_{\ell}(\cos\theta) \qquad\qquad \text{II-44}$$

At large r the spherical Bessel function has the form

$$j_{\ell}(kr) \to_{r \to \infty} 1/kr \, \sin(kr - \ell\pi/2) \qquad\qquad \text{II-45}$$

and far from the scattering center the plane wave can be written as

$$\exp(ikz) \to_{r \to \infty} 1/kr \sum_{\ell} i^{\ell} \, (2\ell+1) \, \sin(kr - \ell\pi/2) \, P_{\ell}(\cos\theta) \qquad \text{II-46}$$

The Schrödinger equations for $\Psi_{1}(r)$ and $\Psi_{TOT}(r)$ differ only by the presence of the potential $U(r)$, and if $U(r)$ goes to zero fast enough $\Psi_{1}(r)$ and $\Psi_{TOT}(r)$ can differ at most by a constant phase for each partial wave, so we write for the total wave function

$$\Psi_{TOT}(r) \to_{r \to \infty} 1/kr \sum_{\ell} B_{\ell} \, \sin(kr - \ell\pi/2 + \delta_{\ell}) \, P_{\ell}(\cos\theta) \qquad \text{II-47}$$

With a little manipulation we can write:

$$\sin(kr - \ell\pi/2 + \delta_{\ell}) = \exp(-i\delta_{\ell}) \{ \sin(kr - \ell\pi/2) +$$

$$+ 1/2i \, \exp(ikr - i\ell\pi/2)[\exp(2i\delta_{\ell}) - 1]\}$$

and the total wave function can then be written as

$$\Psi_{TOT}(r) \to_{r \to \infty} 1/kr \sum_{\ell} B_{\ell} \exp(-i\delta_{\ell}) \, \sin(kr - \ell\pi/2) \, P_{\ell}(\cos\theta)$$

$$+ \exp(ikr)/kr \sum_{\ell} B_{\ell} \, (-i)^{\ell} \sin(\delta_{\ell}) \, P_{\ell}(\cos\theta) \qquad \text{II-48}$$

Comparing this with II-46 we see that

$$B_{\ell} \exp(-i\delta_{\ell}) = i^{\ell} \, (2\ell + 1)$$

and the partial wave expansion for the scattering amplitude for spin-0 spin-0 scattering is

$$f(\theta) = 1/2ik \sum_{\ell} (2\ell+1) \, [\exp(2i\delta_{\ell}) - 1] \, P_{\ell}(\cos\theta) \qquad \text{II-49}$$

II-5 Relation Between The Scattering Amplitude And The T-matrix

The free Green function can be written in terms of the eigenfunctions and eigenenergies of the free Hamiltonian as [Ja70]

$$G_0(r,r') = (2\pi)^{-3} \int \exp(ik'\cdot r) \exp(-ik'\cdot r') / (E - E') \, d^3k' \qquad \text{II-50}$$

where $E=k^2/2M$ and $E'=k'^2/2M$ so

$$G_0^{\pm}(r,r') = (2\pi)^{-3} \, LIM_{\varepsilon\to 0} \, 2M \int \exp[ik'\cdot (r - r')] / (k^2 - k'^2 \pm i\varepsilon) \, d^3k' \qquad \text{II-51}$$

Finding the residues at the poles $k'=\pm\sqrt{(k^2 \pm i\varepsilon)}$ and taking the limit $\varepsilon\to 0$ gives the free Green function as

$$G_0^{\pm}(r,r') = -M/(2\pi) \exp[\pm ik | r - r' |)] / | r - r' | \qquad \text{II-52}$$

We can write equation II-10 as

$$\Psi^{(\pm)}(k,r) = \exp(ik\cdot r) + \int G_0^{\pm}(r,r') \, V(r') \, \Psi^{(\pm)}(k,r') \, d^3r' \qquad \text{II-53}$$

Here we consider only the nuclear force, so $V(r')$ falls off rapidly and in the asymptotic region $r \gg r'$ there is no significant contribution to the integral. In this case we can make the approximations

$$| r - r' | \to r - \hat{r}\cdot r'$$

$$| r - r' |^{-1} \to 1/r$$

and the Green function in the asymptotic region is

$$G_0^{\pm}(r,r') = -M/(2\pi) \exp[\pm i(kr - k'\cdot r')] / r \qquad \text{II-54}$$

where $k'=k\hat{r}$. The Lippmann-Schwinger equation is then

$$\Psi^{(\pm)}(k,r) = \exp(ik\cdot r) - \exp(ikr)/r \, M/(2\pi) \int \exp[- i(k'\cdot r')] V(r') \, \Psi^{(\pm)}(k,r') \, d^3r'$$

Comparing this expression with II-43 we see that the scattering amplitude is

$$f(\theta) = -M/(2\pi) \int \exp[-i(k'\cdot r')] \, V(r') \, \Psi^{(+)}(k,r') \, d^3r'$$

$$= -M/(2\pi) \int \Psi^{(0)}(k',r') \, V(r') \, \Psi^{(+)}(k,r') \, d^3r' \qquad \text{II-55}$$

and finally comparing this last with II-18 we get the relationship between the scattering

amplitude and the T-matrix as

$$f(\theta) = -M/(2\pi) \, T^{(+)} \qquad \text{II-56}$$

II-6 The S-matrix Elements

Using equations II-18 and II-56 we can relate the S-matrix and the scattering

amplitude through

$$< k' \mid S - 1 \mid k > = i \, (2\pi)^2/M \, \delta(E_{k'} - E_k) \, f(\theta) \qquad \text{II-57}$$

We can use the transformation matrix

$$< k \mid E, \ell, m > = (Mk)^{-1/2} \, (2\pi)^{3/2} \, \delta(E_k - E) \, Y_{\ell m}(\hat{k}) \qquad \text{II-58}$$

to evaluate the left hand side of II-57, by using the completness of $\{ \mid E, \ell, m > \}$, i.e.

$$< k' \mid S - 1 \mid k > = \int dE \sum_{\ell m} < k' \mid S - 1 \mid E, \ell, \hat{m} > \cdot < E, \ell, m \mid k > . \qquad \text{II-59}$$

Recall that we have shown that $\mid E, \ell, m >$ is an eigenfunction of S with the eigenvalue

s_ℓ so we can write

$$< k' \mid S - 1 \mid k > = \int dE \sum_{\ell m} (s_\ell - 1) < k' \mid E, \ell, m > < E, \ell, m \mid k > \qquad \text{II-60}$$

and with II-58 this becomes

$$< k' \mid S - 1 \mid k > = \sum_{\ell m} (s_\ell - 1) (2\pi)^3/Mk \; \delta(E_{k'} - E_k) \; Y_{\ell m}(\hat{k}') \; Y_{\ell m}^*(\hat{k})$$

$$= \sum_{\ell} (s_\ell - 1) (2\pi)^3/Mk \; \delta(E_{k'} - E_k) \; (2\ell+1)/4\pi \; P_\ell(\cos\theta) \qquad \text{II-61}$$

Comparing II-61 with II-57 we see that the scattering amplitude is

$$f(\theta) = 1/2ik \sum_{\ell} (2\ell+1) (s_\ell - 1) P_\ell(\cos\theta) \qquad \text{II-62.}$$

This last result, when compared with II-49, gives the relation between the partial-wave

S-matrix elements and the phase shift as

$$s_\ell = \exp(2i\, \delta_\ell) \qquad \text{II-63}$$

We will be calculating these S-matrix elements in later chapters when we do the fits to

the elastic scattering of a spin-1/2 projectile scattering from a spin-0 target.

II-7 Scattering From Two Potentials

Let us consider what happens if we can write the potential in the scattering

problem as two separate pieces

$$V = U + W \qquad \text{II-64}$$

The wave function of the system is a solution of the Schrödinger equation with the

Hamiltonian

$$H = H_0 + U + W \qquad \text{II-65}$$

and the T-matrix is from II-19

$$T_{fi} = < \Psi^{(0)} (E_f) \mid U + W \mid \Psi^{(+)} (E_i) > \qquad \text{II-66}$$

Suppose that we can find a solution for the Hamiltonian involving only U

$$\cdot H_1 = H_0 + U \qquad\qquad \text{II-67}$$

so $\dashv$

$$H_1 \chi^{(+)} = E \chi^{(+)} \qquad\qquad \text{II-68}$$

where the energy eigenvalue is the same as the eigenvalue corresponding to the Hamiltonian II-65.

There are three Green functions for this problem:

$$G_0 = [\, E - H_0 \,]^{-1} \qquad\qquad \text{II-69a}$$

$$G_1 = [\, E - H_0 - U \,]^{-1} \qquad\qquad \text{II-69b}$$

$$G = [\, E - H_0 - U - W \,]^{-1} \qquad\qquad \text{II-69c}$$

and using equation II-22 we can write a relation between G and G_1 as

$$G^{(+)} = G_1^{(+)} + G_1^{(+)} W G^{(+)} \qquad\qquad \text{II-70}$$

Also we can write Lippmann-Schwinger equations for the wave functions

$$\chi^{(+)} = \Psi^{(0)} + G_1^{(+)} U \, \Psi^{(0)} \qquad\qquad \text{II-71a}$$

$$\Psi^{(+)} = \Psi^{(0)} + G_1^{(+)} (\, U + W \,) \, \Psi^{(0)} \qquad\qquad \text{II-71b}$$

Using II-70 in II-71b we write,

$$\Psi^{(+)} = \Psi^{(0)} + (\, G_1^{(+)} + G_1^{(+)} W G^{(+)} \,)(\, U + W \,) \, \Psi^{(0)}$$

$$= (\, 1 + G_1^{(+)} U \,) \, \Psi^{(0)} + G_1^{(+)} W [\, 1 + G^{(+)} (\, U + W \,) \,] \, \Psi^{(0)}$$

with II-71 this last equation can be written as

$$\Psi^{(+)} = \chi^{(+)} + G_1^{(+)} W \, \Psi^{(+)} \qquad\qquad \text{II-72}$$

Now consider the scattering amplitude II-66

$$T_{fi} = <\Psi_f^{(0)} | U + W | \Psi_i^{(+)}>$$

Using II-72 the matrix element can be written as

$$T_{fi} = <\Psi_f^{(0)} | U | \chi_i^{(+)}> + <\Psi_f^{(0)} | W + U G_1^{(+)} W | \Psi_i^{(+)}>$$

The first term on the right hand side can be rewritten using II-71a

$$<\Psi_f^{(0)} | U | (1 + G_1^{(+)} U) \Psi_i^{(0)}> = <(1 + G_1^{(+)} U)^\dagger \Psi_f^{(0)} | U | \Psi_i^{(0)}>$$

$$= <(1 + U^\dagger G_1^{(-)})^\dagger \Psi_f^{(0)} | U | \Psi_i^{(0)}>$$

$$= <\chi_f^{(-)} | U | \Psi_i^{(0)}>$$

Similarly for the second term

$$<\Psi_f^{(0)} | (1 + U G_1^{(+)}) W | \Psi_i^{(+)}> = <\chi_f^{(-)} | W | \Psi_i^{(+)}>$$

where we have used the condition for time reversal invariance

$$\chi^{(-)}(k, r) = [\chi^{(+)}(-k, r)]^* \qquad \qquad \text{II-73}$$

The transition amplitude for scattering from two potentials is then

$$T_{fi} = <\chi_f^{(-)} | U | \Psi_i^{(0)}> + <\chi_f^{(-)} | W | \Psi_i^{(+)}> \qquad \qquad \text{II-74}$$

The presence of the total wave function in the second term generally precludes solving the problem exactly but there are various ways to approximate the solution.

II-8   Optical Potentials and Distorted Waves

We introduce a potential U into the T-matrix II-19 by

$$T_{fi} = <\Psi_f^{(0)} | V - U + U | \Psi_i^{(+)}>$$

$$= <\Psi_f^{(0)} | \omega + U | \Psi_i^{(+)}> \qquad \qquad \text{II-75}$$

where the residual interaction is defined by

$$\omega = V - U$$
<div align="right">II-76</div>

We take the potential U to be the optical potential for the problem so the distorted wave is a solution of

$$(H_0 + U) \chi = E \chi$$
<div align="right">II-77</div>

The Green function associated with this distorted wave is

$$G^{(+)} = [E - H_0 - U + i\varepsilon]^{-1}$$
<div align="right">II-78</div>

so the distorted wave can be written as

$$\chi^{(+)} = (1 + G^{(+)} U) \Psi^{(0)}$$
<div align="right">II-79</div>

and using II-73 the T-matrix is then

$$T_{fi} = < \chi_f^{(-)} | U | \Psi_i^{(0)} > + < \chi_f^{(-)} | \omega | \Psi_i^{(+)} >$$
<div align="right">II-80</div>

ω is the difference between the total potential, V, for the scattering and the optical potential, which is spherically symmetric and describes only the elastic scattering. This residual part of the interaction potential is the portion that may support changes of state during the process. For example if we are considering inelastic scattering the first term of II-80 will be zero and the T-matrix will be given by the second term of II-80. The form of the residual interaction for excitation to collective states will be discussed in chapter IV. We expand the total wave function in the second term using II-72 and keep only the first term in the expansion so

$$T_{fi} = < \chi_f^{(-)} | \omega | \chi_i^{(+)} >$$
<div align="right">II-81</div>

This is the T-matrix for inelastic scattering in the Distorted Wave Born Approximation (DWBA). This is the approximation that we use later to calculate excitations to collective

states.

Another commonly used distorted wave approximation is the distorted wave impulse approximation (DWIA). To derive the DWIA matrix element we start with the inelastic part of II-80

$$T_{fi} = <\chi_f^{(-)} | \omega | \Psi_i^{(+)} >$$

We restrict ourselves to the case of a single nucleon in both the incoming and outgoing channels, then the residual interaction is the sum of the two body residual interactions

$$\omega = \sum_j \omega_j = \sum_j (v_{0j} - U/A)$$
II-82

where v_{0j} is the interaction between the projectile and the jth nucleon in the nucleus and U is the average potential, for example an optical potential. Expanding the total wave function as in II-72 we can write the T-matrix element as

$$T_{fi} = <\chi_f^{(-)} | \omega | \chi_i^{(+)} + G_1^{(+)} \omega \Psi_i^{(+)} >$$

$$= <\chi_f^{(-)} | \omega + \omega G_1^{(+)} \omega + ... | \chi_i^{(+)} >$$

$$= <\chi_f^{(-)} | t | \chi_i^{(+)} >$$

where we have defined the t-matrix by

$$t = \omega + \omega G_1^{(+)} t$$
II-83

$$= \sum_j \omega_j + \sum_j \omega_j G_1^{(+)} t$$

Now we introduce an effective two body t-matrix

$$t_j = \omega_j + \omega_j G_1^{(+)} t_j$$
II-84

then we can do a little algebra to get

$$t = \sum_j t_j + \sum_j t_j \, G_1^{(+)} \sum_{k \neq j} t_k + \dots$$

The free two body t-matrix obeys

$$t_j^{(0)} = v_{0j} + v_{0j} \, G^{(0)} \, t_j^{(0)} \qquad \qquad \text{II-85}$$

The DWIA is formed in two steps. First we approximate the total t-matrix by the sum of

the two body t-matrices in nuclear matter, then we approxinate these by the free two

body t-matrices so the transition matrix element in DWIA is

$$T_{fi} = <\chi_f^{(-)} \mid \sum_j t_j^{(0)} \mid \chi_i^{(+)}> \qquad \qquad \text{II-86}$$

II-9 The Optical Potential From Plane Wave Impulse Approximation

It is possible, in the plane wave impulse approximation (PWIA), to find an

expression for the optical potential in terms of the scattering amplitude at zero momentum

transfer. The T-matrix element can be obtained by starting from expresion II-28 and

approximating the transition operator by the sum of free two-body transition operators (

impulse approximation). The result is

$$T_{fi} = <\Psi_f^{(0)} \, \Phi_0 \mid \sum_j t_j^{(0)} \mid \Phi_0 \, \Psi_i^{(0)} > \qquad \qquad \text{II-87}$$

where the Φ_0 is the nuclear ground state wave function. The free t-matrices are

proportional to the scattering amplitude for the spin-1/2 on spin-1/2 system. With the

assumptions of rotational invariance, parity conservation and time reversal invariance the

scattering amplitude can be written in terms of five complex amplitudes which are

functions of energy, angle and isospin

$$M(q) = A + B \, \sigma_1 \cdot N \, \sigma_2 \cdot N + C \, (\, \sigma_1 + \sigma_2 \,) \cdot N +$$

$$+ D \, \sigma_1 \cdot K \, \sigma_2 \cdot K + E \, \sigma_1 \cdot P \, \sigma_2 \cdot P \qquad \text{II-88}$$

where the coordinate system is chosen as

$$K = (\, k_f - k_i \,) / | \, k_f - k_i \, |, \quad N = (\, k_i \times k_f \,) / | \, k_i \times k_f \, |,$$

$$P = (\, k_i + k_f \,) / | \, k_i + k_f \, | \qquad \text{II-89}$$

and k_i and k_f are the initial and final wave vectors.

From II-56 the free t-matrix is

$$t_j^{(0)} = -2\pi/m \, M_j$$

so the matrix element of the free t-matrices between nuclear ground states is

$$< \Phi_0 \, | \, \sum_j t_j^{(0)} \, | \, \Phi_0 > = -2\pi/m < \Phi_0 \, | \, \sum_j M_j \, | \, \Phi_0 >$$

If the target has even numbers of neutrons and protons the spin averages over the target will give zero, so the only terms that survive in M are

$$M(q) = A(q) + C(q) \, \sigma_1 \cdot N \qquad \text{II-90}$$

The T-matrix can then be written as

$$T_{fi} = -2\pi/m \, [\, A(q) + C(q) \, \sigma_1 \cdot N \,] \, F(q) \qquad \text{II-91}$$

where $A(q)$ is the Fourier transform of $A(E,\theta)$ and the form factor is the Fourier transform of the density

$$F(q) = \int \exp(iq \cdot r) \, \rho(r) \, d^3r \qquad \text{II-92}$$

Recall from II-74 that the elastic scattering term of the T-matrix for an optical potential U is

$$T_{fi} = < \chi_f^{(-)} \mid U \mid \Psi_i^{(0)} >$$ II-93

In the plane wave approximation this is

$$T_{fi} = < \Psi_f^{(0)} \mid U \mid \Psi_i^{(0)} >$$

$$= \int \exp(-i k_f \cdot r) \, U \, \exp(i k_i \cdot r) \, d^3 r$$

$$= \int \exp(i q \cdot r) \, U \, d^3 r$$ II-94

where the momentum transfer is $q = k_i - k_f$. We can Fourier transform II-94 to write

the optical potential in terms of the T-matrix element

$$U = \int \exp(-i q \cdot r) \, T_{fi} \, d^3 q$$ II-95

Using II-90 in II-94 the optical potential is

$$U = -2\pi/m \int \exp(-i q \cdot r) \, [\, A(q) + C(q) \, \sigma_1 \cdot N \,] \, F(q) \, d^3 q$$

$$= U_{cent} + U_{s.o.}$$

For heavy nucleii [Ja70] A(q) varies slowly compared with F(q) so we can write

$$U_{cent} \cong -2\pi/m \, A(0) \, \rho(r)$$ II-96

The spin-orbit term is a little more complicated but if we realize that for elastic scattering

the magnitude of the wave vector does not change we can write

$$N = (\, k_i \times k_f \,) \, / \mid k_i \times k_f \mid = (\, k_i \times k_f \,) \, / \, (k^2 \sin\theta)$$

and also $k_f = k_i - q$ so $k_i \times k_f = q \times k_i$, then the spin-orbit potential is

$$U_{s.o.} = -2\pi/m \, i \, \sigma_1 \cdot \nabla \{ \int \exp(-i q \cdot r) \, [\, C(q) / \, (k^2 \sin\theta) \,] \, F(q) \, d^3 q \, \} \times k_i$$

$$= -2\pi/m \, i \, \sigma_1 \cdot (1/r \, \partial H/\partial r) \, r \times k_i$$

$$= -2\pi/m \, i/r \, \partial H/\partial r \, \sigma_1 \cdot L$$ II-97

Again for heavy nuclei the function H simplifies to

$$H \approx [\text{LIM}_{q \to 0} \, C(q) / (k^2 \sin\theta)] \, \rho(r)$$
II-98

In this approximation the potential involves the product of the T-matrix and the density. This is the $t\rho$ approximation for the optical potential, and results in a potential with the same general form as the nonrelativistic phenomenological optical potential.

III - ELASTIC SCATTERING

There are several relativistic approaches to nuclear physics which suggest that the optical potential for nucleon-nucleus scattering involves large Lorentz scalar and vector contributions. First, the phenomenological Dirac optical model [Cl82] uses strong vector and scalar potentials to give good fits to elastic spin observables. The relativistic impulse approximation (RIA) [Mc83,Wa85] calculations find deep scalar and vector potentials from a Lorentz-invariant representation of nucleon-nucleon scattering amplitudes. Finally, relativistic mean field calculations [Ho81b] relate these potentials to large scalar (sigma) and vector (omega) meson fields and give a good description of ground state charge densities. In this chapter we explore the first two of these types of calculations.

III-1 Phenomenology

The phenomenological optical model is formed by varying the parameters of the potential until the elastic scattering observables calculated using this potential agree well with the experimental elastic scattering data.

The nonrelativistic phenomenological optical potential is constructed from a complex central term, which is usually parameterized as a Woods-Saxon function, and a

spin-orbit term which is parameterized as the derivative of a Woods-Saxon function [Sh68]. This spin-orbit term is required to explain the elastic polarization of the scattered particles and improves the calculated cross sections at backward angles.

Feshbach [Fe58] has developed a formal theory of elastic scattering which has been described by Jackson [Ja70] and we briefly outline here.

Write the total Hamiltonian of the system as

$$H = H_0 + V(r,\xi) + H(\xi) \qquad \qquad \text{III-1}$$

where H_0 is the kinetic energy operator of the projectile, $\xi = r_1,...,r_A$ denotes all nuclear coordinates, $V(r,\xi)$ is the potential for interaction between the projectile and the target and $H(\xi)$ is the internal Hamiltonian of the target. $H(\xi)$ has a complete set of eigenfunctions $\{\Phi_j(\xi)\}$ which we can use to expand the total wave function

$$\Psi(r,\xi) = \sum_j \Psi_j(r)\, \Phi_j(\xi) \qquad \qquad \text{III-2}$$

where $\Psi_j(r)$ describes the motion of the projectile relative to the target. The elastic channel in this expansion is $\Psi_0(r)\, \Phi_0(\xi)$ so we define an elastic channel projection operator, P, such that

$$P\,\Psi(r,\xi) = \Psi_0(r)\,\Phi_0(\xi) \qquad \qquad \text{III-3}$$

and another projection operator, Q, which projects all states except the elastic channel

$$Q\,\Psi(r,\xi) = \sum_{j\neq 0} \Psi_j(r)\,\Phi_j(\xi) \qquad \qquad \text{III-4}$$

After some manipulation of the Schrödinger equation associated with III-1 the generalized optical potential is defined by

$$U = \langle \Phi_0 | V(r,\xi) | \Phi_0 \rangle + \langle \Phi_0 | VQ\,[\,E - QHQ\,]^{-1}\, QV | \Phi_0 \rangle \qquad \qquad \text{III-5}$$

If $V(r,\xi)$ is a local interaction and exchange effects are ignored $< \Phi_0 \mid V(r,\xi) \mid \Phi_0 >$ is a

local single particle potential $V(r)$ which is real and represents the leading term in the

interaction between the incident nucleon and the target ground state. The second term

represents scattering which involves an intermediate excited state of the nucleus [Ja70]

and it is this term which contributes the imaginary part of the optical potential. If

scattering through intermediate states is an unimportant process then the optical potential

can be approximated by the first term of III-5.

The shape of the real part the central potential can be guessed from the

following argument. The intrinsic nuclear wave functions are functions of the nuclear

coordinates only, and we assume that the total potential is the sum over all the nucleons

in the nucleus of the two body interaction between the projectile and a target nucleon, so

the matrix element of the potential between nuclear ground states is

$$< \Phi_0(\xi) \mid V (r, \xi) \mid \Phi_0(\xi) > = < \Phi_0(\xi) \mid \Sigma_{i=1,A} \, v_i (r - r_i) \mid \Phi_0(\xi) >$$

$$= \int d^3r' \, v (r - r') < \Phi_0(\xi) \mid \Sigma_{i=1,A} \, \delta (r_i - r') \mid \Phi_0(\xi) >$$

The matter density of the nucleus is

$$\rho(r') = < \Phi_0(\xi) \mid \Sigma_{i=1,A} \, \delta (r_i - r') \mid \Phi_0(\xi) > \qquad \text{III-6}$$

so the matrix element we are considering can be written as

$$< \Phi_0 \mid V \mid \Phi_0 > = \int d^3r' \, v (r - r') \, \rho(r')$$

and if the nucleon-nucleon interaction is short range, we can use a point (δ-function)

interaction so our matrix element is just proportional to the matter density of the nucleus

$$< \Phi_0 \mid V \mid \Phi_0 > = \text{const.} \, \rho(r) \qquad \text{III-7}$$

We therefore choose functions for the optical potential that are roughly the shape of the nuclear density, for example the Woods-Saxon function, which we use

$$f (r, r_x, a) = [1 + \exp ((r - R_x) / a)]^{-1}$$ III-8

where $R_x = r_x A^{1/3}$, r_x is the radius parameter and a is the diffuseness.

The relativistic phenomenological optical model is based on the Dirac equation. The optical potential is formed from a Lorentz scalar term, $U_S(r)$, and a term, $U_V(r)$, which transforms as the time-like component of a Lorentz four-vector. The equation we solve is then (with $\hbar=c=1$)

$$[\alpha \cdot p + \beta (m + U_S)] \Psi = (E - U_V - V_C) \Psi$$ III-9

where α and β are the standard 4x4 Dirac matrices, m is the rest mass of the projectile, E is the total projectile energy in the center of momentum frame and V_C is the coulomb potential due to a charge distribution of the form

$$\rho(r) = N \{ 1 - ERF [(r - R) / (2a)] \}$$ III-10

where ERF(x) is the error function. The normalization constant, N, is determined by integrating the charge density over all space to get the total charge. This form for the coulomb potential is very close to the Woods-Saxon form if we make

$$R_{W-S} = R_{ERF}$$

$$a_{W-S} = a_{ERF} (\pi)^{1/2} / 2 \quad ,$$

this also matches the gradients at r=R [Co85a]. The scalar and vector potentials are parameterized as

$$U_S = V_S f (r, r_{S1}, a_{S1}) + i W_S f (r, r_{S2}, a_{S2})$$ III-11a

$$U_V = V_V f (r, r_{V1}, a_{V1}) + i W_V f (r, r_{V2}, a_{V2})$$ III-11b

where the f's are the Woods-Saxon functions III-8.

Equation III-9 can be reduced [Cl82] to a Schrödinger-like equation which contains effective central and spin-orbit terms that can be compared with the nonrelativistic optical potential. The effect of the nonrelativistic spin-orbit potential is implicit in the use of the Dirac equation since this equation describes a spin-1/2 particle. The Dirac phenomenology has twelve free parameters as does the Schrödinger based phenomenology but the reduction of the Dirac equation to a Schrödinger-like equation gives effective central and spin-orbit potentials which are fairly complicated functions of the Dirac potentials and allows more freedom in the form of the effective potentials. These effective potentials also explicitly contain the energy of the incoming particle.

If we write the four component Dirac wave function in terms of two-component wave functions, u and d as

$$\Psi = (\,u^\dagger_i\,,\,d^\dagger_i\,)^\dagger \qquad \text{III-12}$$

we can write III-9 as two coupled equations for u and d

$$(\,m + U_S\,)\,u + \sigma\cdot p\,d = (\,E - U_V - V_C\,)\,u \qquad \text{III-13a}$$

$$\sigma\cdot p\,u - (\,m + U_S\,)\,d = (\,E - U_V - V_C\,)\,d \qquad \text{III-13b}$$

where p is the projectile momentum operator and σ is the usual Pauli spin vector. From the second of these equations we can write the lower component in terms of the upper one

$$d = (\,E - U_V - V_C + m + U_S\,)^{-1}\,\sigma\cdot p\,u \qquad \text{III-14}$$

Substituting III-14 into III-13a results in a second order equation for u which contains the first derivative of u (the Darwin term). To get rid of the Darwin term so that we have an equation which looks like the Schrödinger equation we make the substitution

$$\Psi_S = s^{-1/2}\, u \qquad\qquad\qquad \text{III-15}$$

where we choose a form for s which will make the two wave functions asymptotically the same in the absence of the Coulomb interaction

$$s = (E - U_V - V_C + m + U_S) / (E + m) \qquad\qquad \text{III-16}$$

we get, after a little algebra, the Schrödinger-like equation

$$[-\nabla^2 / (2m) + U_{cent}(r) + U_{s.o.}(r)\, \sigma \cdot L]\, \Psi_S = T\, \Psi_S \qquad\qquad \text{III-17}$$

where T is the kinetic energy of the incoming proton. The effective central potential is

$$U_{cent}(r) = - [(E - U_V - V_C)^2 - (m + U_S)^2 - (E^2 - m^2)] / (2m)$$

$$- [1/r\, s'/s - 3/4\, (s'/s)^2 + 1/2\, s''/s] / (2m) \qquad\qquad \text{III-18a}$$

and the spin-orbit potential is

$$U_{s.o.}(r) = - s' / (2mrs) \qquad\qquad\qquad \text{III-18b}$$

Note that a prime on s denotes differentiation with respect to r. Equation III-17 is "Schrödinger-like" because the energy of the projectile is explicitly contained in the potentials.

This reduction of the Dirac equation actually results in a central potential which is quite different from the regular Woods-Saxon form [Cl82]. With the Woods-Saxon central potential the shape must remain basically the same as the projectile energy increases but the strength is free to change from attractive to repulsive. The effective central potential has a much more dramatic energy dependence. At low energies the potential is close to the conventional Woods-Saxon shape and attractive, and as the projectile energy increases the strength of the potential decreases in magnitude and eventually becomes repulsive at about 200 Mev. The center of the potential becomes

more repulsive as incident energy is increased but there remains an attractive pocket at

the nuclear surface. Figure III-1 shows the real part of the effective central potential for

protons scattering from ^{40}Ca at an incident proton energy of 500 Mev. The relativistic

optical model parameters from which this was calculated are given in table III-1. The

attractive pocket is believed to be necessary for calculating the spin observables correctly

[Cl83]. Figure III-2 shows the imaginary effective central potential which is very similar

to the usual Woods-Saxon form, and figures III-3 and III-4 show the real and imaginary

parts of the effective spin-orbit potential which are very similar in shape to the derivative

of a Woods-Saxon function and are surface peaked.

Calculation of the observables for elastic scattering is simplest if we write the

wave function in the partial wave series IV-18 and then integrate the differential equation

numerically. The integration is carried out to a range where the nuclear part of the

potential has died away, say ten to fifteen Fermi's usually, then the partial wave can be

normalized to a Coulomb function [Co81], and the phase shift for that partial wave can

be calculated at the same time. The elastic observables can then be calculated in terms of

these phase shifts (Appendix B). The elastic scattering fits for various nuclei and

energies will be shown in a later section.

The optical potential parameters are determined by varying the parameters and

seeing how well the calculated observables (cross section, analyzing power, and Q if

available) agree with the experimental ones. A convenient measure of the fit is the

chi-squared defined by

$$\chi^2 = \Sigma_{Data} [(O_{Ex} - O_{Th}) / \Delta O_{Ex}]^2$$

III-19

where O_{Ex} is the experimental value, ΔO_{Ex} is the error and O_{Th} is the theoretical value. The elastic data are searched on till a minimum χ^2 is found.

The scattering amplitude for the scattering of spin-1/2 particles from spin-0 particles is given in equation II-90. There are two complex amplitudes which means that we need three observables to determine these amplitudes up to an arbitrary phase. The observables usually measured are cross section and analyzing power, but these are not enough to uniquely determine the potential parameters. In part this is due to the freedom of fitting inside the band made by the error bars and in part due to the lack of the third observable. Kobos et al. [Ko85] have shown that the addition of Q parameter data can if not uniquely determine, then at least reduce the number of parameter sets.

III-2   Impulse Approximation

We have seen that in the nonrelativistic PWIA the transition matrix element is the matrix element between plane wave states and nuclear ground states of the scattering amplitude II-87. To form a relativistic impulse approximation we want a form for the nucleon-nucleon scattering amplitude which is a Lorentz scalar [Mc83]

$$\Lambda(E,q) = \Lambda_S I_1 I_2 + \Lambda_P \gamma_1^5 \gamma_2^5 + \Lambda_V \gamma_1^\mu \gamma_{2\mu} +$$

$$+ \Lambda_A \gamma_1^5 \gamma_1^\mu \gamma_2^5 \gamma_{2\mu} + \Lambda_T \sigma_1^{\mu\nu} \sigma_{2\mu\nu} \qquad\qquad \text{III-20}$$

where the Λ's are functions of E and q and their subscripts denote their Lorentz transformation properties (scalar, pseudoscalar, vector, axial vector and tensor), also 1 and 2 refer to the incident and the struck nucleons respectivly.

We require that matrix elements of II-87 and III-20 give the same result, i.e. the probability amplitudes for initial and final spin configurations must be preserved, so we get a five-by-five matrix equation relating the nonrelativistic amplitudes A, B, C, D and E to the Lorentz invariant amplitudes Λ_S, Λ_P, Λ_V, Λ_A and Λ_T. The transformation matrix is given explicitly by McNeil et al. [Mc83]. The amplitudes of II-87 can be determined from phase shift analysis [Ar83] and through the kinematic transformation the Lorentz invariant amplitudes can be calculated.

The optical potential is given in terms of the Lorentz invariant scattering amplitude as

$$U = < \Phi_0 \mid \sum_i \Lambda_i(E, q) \mid \Phi_0 > \qquad \text{III-21}$$

where the sum extends over all the nucleons in the nucleus. For even-even nuclei the spins of the nucleons add to zero so the optical potential is left with only scalar and zeroth-component vector terms which can be written as

$$U_V = (2\pi)^{-3} \int \exp(-iq \cdot r) \, \Lambda_V(q) \, \rho_V(q) \, d^3q \qquad \text{III-22a}$$

$$U_S = (2\pi)^{-3} \int \exp(-iq \cdot r) \, \Lambda_S(q) \, \rho_S(q) \, d^3q \qquad \text{III-22b}$$

Note that in general we can write vector and scalar potentials for the neutrons and protons separately so we can use experimental measurements of the neutron and proton charge distribution if we wish. The $\rho(q)$'s are the Fourier transforms of the vector and scalar densities

$$\rho_V(q) = \int \exp(iq \cdot r) \, \rho_V(r) \, d^3r \qquad \text{III-23a}$$

$$\rho_S(q) = \int \exp(iq \cdot r) \, \rho_S(r) \, d^3r \qquad \text{III-23b}$$

and $\rho_V(r)$ and $\rho_S(r)$ can be written in terms of the upper and lower components of the

nuclear wave function:

$$\rho_V(r) = 1/(4\pi) \sum_{n\ell j} (2j+1) [|u_{n\ell j}|^2 + |d_{n\ell j}|^2] \qquad \text{III-24a}$$

$$\rho_S(r) = 1/(4\pi) \sum_{n\ell j} (2j+1) [|u_{n\ell j}|^2 - |d_{n\ell j}|^2] \qquad \text{III-24b}$$

The sums in these densities are over all occupied proton and neutron orbitals in the

nucleus.

Calculations of the scalar and vector potentials based on this theory [Mc83]

agree closely with the potentials that are given by Dirac phenomenology for incident

proton energies above 200 Mev. For protons incident on ^{40}Ca at 200 Mev these potential

depths are approximately:

$$V_V \approx 300 \text{ Mev} \qquad W_V \approx -100 \text{ Mev}$$

$$V_S \approx -400 \text{ Mev} \qquad W_S \approx 100 \text{ Mev}$$

The magnitude of V_V and V_S decrease slowly with increasing energy while W_V and W_S

are fairly constant. For low energies, in this simple model, the magnitudes of V_V and V_S

increase rapidly with decreasing energy. Recently Wallace [Wa85] has related the

relativistic impulse approximation to the conventional meson theory of the N-N force

which decreases the magnitude of the low energy optical potentials so they are in much

better agreement with the phenomenological optical potentials at low energy.

III-3   Elastic Scattering Fits

The fits to the elastic scattering data were done using the program RUNT written by E. D. Cooper [Co81]. This code allows free variation of the twelve optical model parameters of equations III-5 to provide minimum values of the chi-squared for the elastic scattering observables.

The parameter sets of tables III-1 and III-2 vary with both mass number and the energy of the incoming proton. For most cases there are two sets of parameters shown. One set (set A) agrees quite well with the Impulse Approximation calculations of the potential depths mentioned earlier while the other set (B) usually gives a better fit (lower chi-squared) to the elastic scattering data but does not agree so well with the IA calculation. Now we proceed to examine some of the medium energy elastic scattering data which has become available recently.

^{40}Ca at 362 Mev.

The fit to the cross section and analyzing power data are shown in Figures III-5 and III-6. The data are from D. Frickers [Fr86]. The fit to the cross section data is excellent over the entire angular range and the analyzing power is also excellent up to 50°. After 50° the error bars on the analyzing power data get quite large so those points make very little contribution to the chi-squared and therefore will not cause much of a change in the optical model parameters during the search. The parameters here seem to be very well determined as no other sets were found.

^{40}Ca at 500 Mev.

The parameters are shown in table III-1. Note that both sets give identical chi-squared for cross section and analyzing power, and the chi-squared for the Q parameter is very close as well. The data for cross section and analyzing power are from Hoffmann et al. [Ho81] and the Q data are from Rahbar et al. [Ra81]. The fits to data are shown in figures III-7 to III-9. The cross section fits are virtually indistinguishable from each other and fit the data very well except for the last four data points. The analyzing power graphs of figure III-8 are slightly different for the two parameter sets but it is impossible to say which is a "better" fit. The Q parameter is shown in figure III-9 and though there is a small difference it is questionable whether this difference is sufficient to choose one set over the other. The interesting question which arises is whether or not inelastic scattering to collective states is sensitive to this slight difference. We consider this question in chapter IV.

Seth et al. [Se85] have analyzed these data using a nonrelativistic optical potential in which they have included a term which involves the square of a Woods-Saxon function. This "density squared" term arises in the relativistic impulse approximation calculation of the Schrödinger equivalent potential and is included in an attempt to correct for relativistic effects. This gives them fifteen free parameters to search on during the fitting whereas we have only twelve. The fits we get are about the same as theirs.

^{40}Ca at 800 Mev.

The cross section and analyzing power data are from Bleszynski et al. [B182] and the Q data are from Fergerson et al. [Fe86]. Potential set A was obtained by restricting the cross section data to 33° but including all data for analyzing power and Q parameter in the search. Note that the fit to the cross section (figure III-10) continues to oscillate with a period of approximately 6.5° after 33° but the experimental data departs from this trend. Parameter set B was obtained by searching on all the data. The fit obtained to the cross section with this set is much better for large angles although we still can not get the maximum at 38°. The analyzing power shown in figure III-11 is quite good for both sets but it does seem easier to fit when the large angle data are ignored. The Q data shown in figure III-12 are also fit better when the large angle cross section data are ignored, and we do not seem able to fit all the data simultaneously [Ko86].

Bleszynski et al. have analyzed these data using the Glauber multiple scattering approach. Their cross section minima tend to underestimate the data slightly and the two minima at 27° an 34° are shifted to smaller angles from the data which is in agreement with our calculation. This shift away from a periodic diffraction pattern is indicative of another process becoming important. The fits to the analyzing power are very similar and agree well with the data except that we do better at describing the peak at 21°.

^{20}Ne at 800 Mev.

The cross section and analyzing power fits are shown in figures III-13 and III-14. The data are from Blanpied et al. [B184]. Only one parameter set is shown in

table III-2 because every starting set that was tried converged to the set shown. This uniqueness could be due to the small angular range of the data since for small angles only the direct reaction is important. Also the small number of data points and the small error bars help to uniquely determine the parameters.

Blanpied et al. have analyzed these data using both nonrelativistic optical model and coupled channels techniques. Both of these calculations result in fits which are about the same as ours.

There has been some discussion of the existence of unconventional potential shapes [Me81] which lead to better fits of the data for proton scattering from light nuclei. ^{20}Ne seems to be heavy enough not to suffer the problem since the parameter set shown in table III-2 gives effective potentials with the same general characteristics as those shown in figures III-1 to III-4 for ^{40}Ca. This again, could be a result of the small angular range. When we try to analyze ^{12}C, though, a good fit to the data is obtained only if the real central potential has the form shown in figure III-15. The odd wiggle in the center of the nucleus seems to have no physical justification and is possibly an artifact of some important process other than elastic scattering.

^{48}Ca at 500 Mev.

Figures III-16 and III-17 show fits to data for protons scattered elastically from ^{48}Ca at a proton energy of 500 Mev. The data are from Hoffmann et al. [Ho81]. The cross section fits are excellent except at the last minimum where both fits miss a little. Parameter set B does a slightly better job than set A for the analyzing power(see figure III-13) for angles above 18°.

Seth et al. [Se85] have analyzed these data the same way they analyzed the ^{40}Ca data at 500 Mev. and their analysis is outlined in that section. The fit they get is very similar to the one we get using parameter set B.

^{90}Zr at 800 Mev.

The fits are shown in figures III-18 and III-19. The data are from Gazzaly et al. [Ga82]. Both parameter sets give good fits to the data but set B's total chi-squared is almost half that of set A. Set B is not able to describe the first minimum of the analyzing power at 5° but does a better job than A of describing the rest of the angular range.

Gazzaly et al. have analyzed the cross section data using a Schrödinger optical model but with relativistic kinematics and they get a fit very similar to ours.

IV - INELASTIC SCATTERING

We have seen that a relativistic description of the incoming proton gives a good description of the elastic scattering data. It has been shown [Pi83] that scattering observables for low-lying collective states can be related to the elastic scattering amplitude so with our elastic scattering model we should be able to do a good job of predicting collective excitations. Sawafta [Sa84] has examined the importance of the "wine-bottle-bottom" shape of the effective potential in inelastic scattering. Using the relativistically based potential improves inelastic scattering predictions above 200 Mev. Relativistic impulse approximation calculations [Ro84, Ro85] of inelastic scattering have also been done with reasonable success. In this chapter we extend the relativistic optical model to inelastic scattering to collective states. The incident proton is described relativistically by a Dirac spinor but the nucleons bound in the nucleus have an average energy of less than 20 Mev. each so we describe the nucleus nonrelativistically [Ja70].

IV-1 Extension of the Optical Model

The extension of the optical model to inelastic scattering to collective states can be accomplished by writing [Bl64] the previously spherical optical potential as a function of the displacement of the nuclear surface

$$U(\, r,\, R\,) \rightarrow U(\, r\, ,\, R + \alpha(\hat{r})\,)$$
IV-1

where R is the range of the potential and $\alpha\, (\, \hat{r}\,)$ is the displacement of the nuclear

42

surface, which we can write as

$$\alpha(\hat{r}) = R \sum_{\ell m} a_{\ell m} Y_{\ell m} \qquad \text{IV-2}$$

If we assume the displacement of the surface is small we can expand the potential in powers of $\alpha(\hat{r})$ and keep terms to first order only

$$U(r , R + \alpha(\hat{r})) = U(r, R) + \alpha(\hat{r})\, \partial/\partial R\, [\, U(r, R)\,] \qquad \text{IV-3}$$

The distorted wave matrix element is, from II-80

$$T_{fi} = \langle \chi_f^{(-)} \Phi_f \mid \omega \mid \Phi_i \chi_i^{(+)} \rangle \qquad \text{IV-4}$$

where we have approximated the total wave functions as the products of the projectile distorted waves, χ, and the target nuclear wave functions, Φ. We need to find the form of the residual interaction II-76

$$\omega = V - U$$

where U is the spherical optical potential. We approximate the matrix element of V between the ground state and an excited state by the matrix element of the deformed optical potential [Sa65]

$$\langle \Phi_f \mid V \mid \Phi_i \rangle \approx \langle \Phi_f \mid U_d \mid \Phi_i \rangle \qquad \text{IV-5}$$

where U_d is given by IV-3. The T-matrix element for inelastic scattering is then

$$T_{fi} = \langle \chi_f^{(-)} \mid \langle \Phi_f \mid \alpha(\hat{r})\, \partial/\partial R\, [\, U(r, R)\,] \mid \Phi_i \rangle \mid \chi_i^{(+)} \rangle\, . \qquad \text{IV-6}$$

The matrix element between the nuclear states plays the role of the transition operator between the initial and final elastic scattering states. It contains all of the information about the nuclear structure and any angular momentum selection rules. The integration over nuclear coordinates can be done quite easily since we only need to consider symmetry (eg. rotational) properties of the nuclear wave function. The ground state

wave function of an even-even nucleus with $J^\pi = 0^+$ can be written as [Ja70]

$$\Phi_i = (1 / 8\pi^2)^{1/2} D^0_{00}(\epsilon) \, \phi_{INT} \qquad \text{IV-7a}$$

and the final state with spin I and projection M is

$$\Phi_f = [(2I+1) / 8\pi^2]^{1/2} D^I_{0M}(\epsilon) \, \phi_{INT} \qquad \text{IV-7b}$$

where D is a rotation matrix, ϵ denotes the orientation of the body fixed axes with respect to the space fixed axes, and ϕ_{INT} is the intrinsic nuclear wave function. For an axially symmetric deformation IV-2 is independent of the projection of the spin. We can then write

$$\alpha(\hat{r}) = R \sum_{\ell} a_{\ell 0} Y_{\ell 0}(\hat{r}') \qquad \text{IV-8}$$

where $\hat{r}'$ gives the angle in the body fixed frame. To transform to the space fixed frame we use

$$Y_{\ell 0}(\hat{r}') = \sum_\mu D^\ell_{0\mu} Y^*_{\ell\mu}(\hat{r}) \qquad \text{IV-9}$$

The matrix element over nuclear coordinates is then

$$< \Phi_f | \alpha(\hat{r}) \, \partial/\partial R [V(r, R)] | \Phi_i > = <\Phi_f | \alpha(\hat{r}) | \Phi_i > \partial/\partial R [V(r, R)]$$

$$= (2I+1)^{1/2} / 8\pi^2 \sum_{\ell\mu} < D^I_{0M} | D^\ell_{0\mu} | D^0_{00} >$$

$$< \Phi_{INT} | R a_{\ell 0} | \Phi_{INT} > Y^*_{\ell\mu} \, \partial/\partial R [V(r, R)]$$

The matrix element of the intrinsic wave functions contains the radius parameter, R, which is a constant so that matrix element can be written as

$$\delta_\ell = R < \Phi_{INT} | a_{\ell 0} | \Phi_{INT} > = R\beta_\ell \qquad \text{IV-10}$$

where β_λ is the deformation parameter of the state, and δ_λ is the deformation length. The matrix element of the rotation matrices is [Ro57],

$$< D^l_{0M} \mid D^l_{0\mu} \mid D^0_{00} > = 8\pi^2 (2I + 1)^{-1} \delta_{l\lambda} \delta_{M\mu} \qquad \text{IV-11}$$

so we get

$$< \Phi_f \mid \alpha \; \partial/\partial R \; V \mid \Phi_i > = \delta_\lambda (2I+1)^{-1/2} Y^*_{lM}(\hat{r}) \; \partial/\partial R \; [V(r, R)] \qquad \text{IV-12}$$

and the T-matrix element for inelastic scattering is then

$$T_{fi} = \delta_l (2I+1)^{-1/2} < \chi_f^{(-)} \mid Y^*_{lM}(\hat{r}) \; \partial/\partial R \; [V(r, R)] \mid \chi_i^{(+)} > \qquad \text{IV-13}$$

That this is the correct form of the matrix element when we change from the nonrelativistic distorted waves and transition operator to the relativistic versions, has been shown by Cooper et al. [Co85b]. The derivation of this result is outlined in Appendix A.

The optical potential we deform involves the scalar and vector terms of the Dirac equation III-9

$$\Delta U = \Delta[U_v + \gamma^0 U_S] \qquad \text{IV-14}$$

These potentials are parameterized as in III-11 and the deformation is done with respect to the range of the potential, R. We make this optical potential nonspherical as in IV-1. As in IV-3 the deformed part of the potential is really just the derivative of each Woods-Saxon function in the potential with respect to the range of that function. We write the matrix elements of the deformed potentials between initial and final nuclear states as

$$< \Delta U_S > = \delta_l / (2I+1)^{1/2} Y^*_{IM} [V_S \, \partial/\partial R_{S1} \, f(r, R_{S1}) +$$

$$i W_S \, \partial/\partial R_{S2} \, f(r, R_{S2})] \qquad \text{IV-15a}$$

$$< \Delta U_V > = \delta_l / (2I+1)^{1/2} Y^*_{IM} [V_V \, \partial/\partial R_{V1} \, f(r, R_{V1}) +$$

$$i W_V \, \partial/\partial R_{V2} \, f(r, R_{V2})] \qquad \text{IV-15b}$$

Here we keep the deformation lengths (βR) equal for each term rather than having equal deformation parameters since it has been shown [In73,Sa84] that the choice of equal deformation lengths gives a better prediction for inelastic polarization than equal deformation parameters.

IV-2   Calculation of the T-Matrix Element

All we need now to calculate the T-matrix IV-13 are the initial and final distorted waves. These distorted waves are solutions of III-9, and are four component spinors which we can write as III-12. The matrix element is then

$$T_{fi} = \int (u^\dagger_f, d^\dagger_f) (<\Delta U_V> + \gamma^0 <\Delta U_S>) (u^\dagger_i, d^\dagger_i)^\dagger \, d^3r$$

$$= \int [u^\dagger_f (<\Delta U_V> + <\Delta U_S>) u_i + d^\dagger_f (<\Delta U_V> - <\Delta U_S>) d_i] \, d^3r \qquad \text{IV-16}$$

The sum of the deformed potentials is associated only with the upper components of the wave functions and the difference of the deformed potentials is associated with the lower components. Recall from chapter III that the potentials have opposite signs and typically $<\Delta U_V> - <\Delta U_S>$ is from five to ten times larger than $<\Delta U_V> + <\Delta U_S>$. This means that unless the lower components of the wave functions are much smaller than the upper

components this difference term will be critical to the calculation, but Cooper [Co81] has

shown that the upper and lower components can have close to the same magnitude at

high momenta. Moreover this difference term contains the spin-orbit dependence of the

T-matrix and we shall discuss the importance this term is in the following chapter.

We write the upper component of the incoming Dirac spinor in a partial wave

sum

$$u^\mu(k_i, r) = 4\pi \left[(E_i+m)/2m\right]^{1/2} \sum_{\ell j} i^\ell \exp(i\sigma_{\ell j}) (2\ell+1)^{1/2} / (4\pi)^{1/2}$$

$$<\ell, 1/2 ; 0, \mu \mid j, \mu > f_{\ell j}(k_i r)/(k_i r) \, \mathcal{Y}^\mu_{\ell 1/2 j} \qquad \text{IV-17}$$

where we have chosen the incoming wave vector k_i to point along the z-axis. Here we

denote the Clebsh-Gordan (C-G) coefficient by $<\ell, s ; m_\ell, m_s \mid j m_j >$. Note that in the

absence of a potential this wave function is normalized to a plane wave. The generalized

spherical harmonic $\mathcal{Y}^\mu_{\ell 1/2 j}$ is given by coupling an orbital angular momentum wave

function to a spin wave function

$$\mathcal{Y}^\mu_{\ell 1/2 j} = \sum_\gamma <\ell, 1/2 ; \mu\text{-}\gamma, \gamma \mid j \mu > Y_\ell^{\mu\text{-}\gamma} \mid 1/2, \gamma > . \qquad \text{IV-18}$$

Also in IV-17 we have:

μ - the spin projection of the incoming particle.

E_i - the total energy of the incoming particle (kinetic plus mass)

m - the rest mass of the projectile

$\sigma_{\ell j}$ - the coulomb phase shift of the ℓth partial wave with $j = \ell \pm 1/2$

$f_{\ell j}$ - the radial Dirac wave function

The upper component of the outgoing distorted wave can be written in a similar way as

$$u^\lambda(k_f, r) = 4\pi \, [(E_f+m)/2m]^{1/2} \sum_{\ell' j' \nu} i^{\ell'} \exp(i\sigma_{\ell' j'}) \, Y_{\ell'}^{\nu-\lambda}(\hat{k}_f)$$

$$<\ell', 1/2 \, ; \, \nu-\lambda, \lambda \mid j', \nu > f_{\ell' j'}(k_f)/(k_f) \, \mathcal{Y}^\nu_{\ell' \, 1/2 \, j'} \qquad\qquad \text{IV-19}$$

Note that we have labelled these distorted waves with the projection of their spin so we see that the T-matrix element depends on incoming and outgoing spin projections as well as the spin and projection of the final state of the nucleus.

We can also write an expression for the lower component for the Dirac wave function using III-14 and IV-19

$$d^\lambda = (E - U_V - V_C + m + U_S)^{-1} \, \sigma \cdot p \, u^\lambda$$

$$= (E - U_V - V_C + m + U_S)^{-1} \, 4\pi[(E_f+m)/2m]^{1/2} \sum_{\ell' j' \nu} i^{\ell'} \exp(i\sigma_{\ell' j'})$$

$$Y_{\ell'}^{\nu-\lambda}(\hat{k}_f) <\ell', 1/2 \, ; \, \nu-\lambda, \lambda \mid j', \nu > \sigma \cdot p \, f_{\ell' j'}(k_f)/(k_f) \, \mathcal{Y}^\nu_{\ell' \, 1/2 \, j'}$$

The operator $\sigma \cdot p$ can be written as

$$\sigma \cdot p = - i \, \sigma \cdot \hat{r} \, (\partial/\partial r - 1/r \, \sigma \cdot L) \qquad\qquad \text{IV-20}$$

and since the generalized spherical harmonic is an eigenfunction of J^2, L^2 and S^2 the operator $\sigma \cdot L$ can be evaluated as

$$\sigma \cdot L = J^2 - L^2 - S^2 = j(j+1) - \ell(\ell+1) - s(s+1) \qquad\qquad \text{IV-21}$$

so the lower component of the outgoing Dirac wave function is

$$d^\lambda = (E - U_V - V_C + m + U_S)^{-1} \, 4\pi[(E_f+m)/2m]^{1/2} \sum_{\ell' j' \nu}$$

$$i^{\ell'} \exp(i\sigma_{\ell' j'}) Y_{\ell'}^{\nu-\lambda}(\hat{k}_f) <\ell', 1/2 \, ; \, \nu-\lambda, \lambda \mid j', \nu >$$

$$(-i) \, (\partial/\partial r - 1/r \, \sigma \cdot l') \, f_{\ell' j'}(k_f)/(k_f) \, \sigma \cdot \hat{r} \, \mathcal{Y}^\nu_{\ell' \, 1/2 \, j'} \qquad\qquad \text{IV-22}$$

where $\sigma \cdot l'$ is just the function

$$\sigma \cdot l' = j'(j'+1) - \ell'(\ell'+1) - 3/4 \qquad \text{IV-23}$$

The lower component for the incoming wave function is handled in exactly the same way. Now put all the pieces together into IV-15. The angle integral for the term involving the lower components is

$$\int [\sigma \cdot \hat{r} \, \mathcal{Y}^{\nu}_{\ell' \, 1/2 \, j'}]^{\dagger} [\, Y^{*}_{IM}(\hat{r}) \,]^{*} \, \sigma \cdot \hat{r} \, \mathcal{Y}^{\mu}_{\ell \, 1/2 \, j} \, d\Omega$$

$$= \int [\mathcal{Y}^{\nu}_{\ell' \, 1/2 \, j'}]^{\dagger} [\, Y^{*}_{IM}(\hat{r}) \,]^{*} \, \mathcal{Y}^{\mu}_{\ell \, 1/2 \, j} \, d\Omega \qquad \text{IV-24}$$

where we have used

$$\sigma \cdot \hat{r} \, \sigma \cdot \hat{r} = 1 \qquad \text{IV-25}$$

and we see that the angular integral is the same for both terms.

We need two results to be able to put the angular integral into the form we want. First a sum of three C-G coefficients [Ro57]

$$\sum_{\gamma} < \ell, 1/2 ; \mu_i - \gamma, \gamma \mid j, \mu_i > < \ell', 1/2 ; \nu - \gamma, \gamma \mid j', \nu >$$

$$< \ell', I ; \nu - \gamma, M \mid \ell, \mu_i - \gamma >$$

$$= (-)^{j + \ell' - I - 1/2} [(2\ell + 1)(2j'+1)]^{1/2} < j', I ; \nu, M \mid j, \mu_i >$$

$$W(\ell, j, \ell', j'; 1/2, I) \qquad \text{IV-26}$$

and second we want to get rid of the 6-j coefficient by using [Ma58]

$$< \ell, \ell' ; 0, 0 \mid I, 0 > W(\ell, j, \ell', j'; 1/2, I)$$

$$= 1/2 \, [\, 1 + (-)^{\ell + \ell' + I} \,][\, (2\ell + 1) \, (2\ell'+1) \,]^{-1/2}$$

$$< j, j'; 1/2, -1/2 \mid I, 0 > \qquad . \qquad \text{IV-27}$$

The integration over angle then gives

$$\int [\mathcal{Y}^{\nu}_{\ell' \, 1/2 \, j'}]^{\dagger} [\, Y^{*}_{IM}(\hat{r}) \,]^{*} \, \mathcal{Y}^{\mu}_{\ell \, 1/2 \, j} \, d\Omega = (16\pi)^{-1/2} \, [2j'+1]^{1/2} \, (-)^{j-1/2}$$

$$[1 + (-)^{\ell + \ell' + I}] < j', I; \nu, M \mid j, \mu > < j, j'; 1/2, -1/2 \mid I, 0 > \qquad \text{IV-28}$$

The T-matrix is then

$$T^{IM}_{\lambda\mu} = \delta_1 (4\pi)^2 [(E_i+m) (E_f+m)]^{1/2} (16m\pi)^{-1} \sum_{\ell j \ell' j'} [1+(-1)^{\ell+\ell'+1}] i^{\ell-\ell'}$$

$$\exp[i(\sigma_{\ell j} + \sigma_{\ell' j'})] [(2j'+1)(2\ell+1) / (2j+1)]^{1/2} Y^*_{\ell}{}^{\mu-M-\lambda}(\theta,0)$$

$$< \ell, 1/2 ; 0, \mu \, | \, j\,\mu > \; < j', I ; -1/2, 0 \, | \, j\, -1/2 > \; < \ell', 1/2 ; \mu-M-\lambda, \lambda \, | \, j' \, \mu-M >$$

$$< j', I ; \mu-M, M \, | \, j\,\mu > \; \{ \int f_{\ell' j'}(k_f r)/(k_f r) \; F \; f_{\ell j}(k_i r)/(k_i r) \; r^2 \, dr \; +$$

$$+ \int [(\partial/\partial r - 1/r \; \sigma\cdot 1') f_{\ell' j'}(k_f r)/(k_f r)] \; G \; [(\partial/\partial r - 1/r \; \sigma\cdot 1) f_{\ell j}(k_i r)/(k_i r)] \; r^2 \, dr \; \}$$

$$\text{IV-29}$$

where the radial form factors F and G are

$$F = V_V \, \partial/\partial R_{V1} \, f(R_{V1}) + iW_V \, \partial/\partial R_{V2} \, f(R_{V2})$$

$$+ V_S \, \partial/\partial R_{S1} \, f(R_{S1}) + iW_S \, \partial/\partial R_{S2} \, f(R_{S2}) \qquad \text{IV-30}$$

$$G = [\, V_V \, \partial/\partial R_{V1} \, f(R_{V1}) + iW_V \, \partial/\partial R_{V2} \, f(R_{V2})$$

$$- V_S \, \partial/\partial R_{S1} \, f(R_{S1}) - iW_S \, \partial/\partial R_{S2} \, f(R_{S2}) \,]$$

$$/ [(E_f - U_v - V_c + m + U_S) (E_i - U_v - V_c + m + U_S)] \qquad \text{IV-31}$$

IV-3 Dirac Equation Based (DEB) Calculation

This calculation uses the usual Schrödinger equation formalism [Sh68], but the optical potential which generates the distorted wave is the effective potential III-18. This optical potential is deformed by making the substitution of IV-1 and saving terms to first order in $\alpha(\hat{r})$ as in IV-3. The resulting transition density is quite a complicated function [Sh86]

$$\Delta U_{DEB} = \Delta U_C + \Delta U_{S.O.} \qquad\qquad \text{IV-32}$$

where

$$\Delta U_C \approx \Delta U_S + E/m\,\Delta U_V + 1/m\,[\,U_S\,(\,\Delta U_S\,) - U_V\,(\,\Delta U_V\,)\,]$$

$$+ 3/(4m)\,[\,S'/S\,(\,\Delta U_S - \Delta U_V\,)' - (S''/S)^2\,(\,\Delta U_S - \Delta U_V\,)/S\,]$$

$$+ [(E+m)4m]^{-1}\,[\,\nabla^2 S\,/\,S^2\,(\,\Delta U_S - \Delta U_V\,) - \nabla^2\,(\,\Delta U_S - \Delta U_V\,)\,/\,S\,] \qquad \text{IV-33}$$

$$\Delta U_{S.O.} \approx - [(E+m)2mS]^{-1}\,\sigma\cdot\nabla\,(\,\Delta U_S - \Delta U_V\,)\times\nabla/i \qquad\qquad \text{IV-34}$$

and S is defined in III-16. The terms which include the Coulomb potential have been

dropped and a small term proportional to $\sigma\cdot L$ has been left out of the expression for

$\Delta U_{S.O.}$, which then has the "full Thomas" form [Sh68]. This transition density is used

with the Schrödinger distorted waves to calculate the T-matrix. A comparison between

the DEB calculation and the full relativistic calculation will be done in the following

chapter.

IV-4   Inelastic Scattering in DWIA

Rost et al. [Ro84] have done a calculation of inelastic scattering which is based

on the relativistic impulse approximation. In their calculation the vector and scalar

potentials are calculated through equation III-21. The nucleon-nucleon invariant

amplitudes, Λ, are obtained in the impulse approximation from the N-N interactions as

determined from phase shift analysis [Ar83]. The collective excitations are assumed to

result in a deformation of the density so

$$\rho(\,r, R\,) \rightarrow \rho(\,r\,,\,R + \alpha(\Omega)\,) \qquad\qquad \text{IV-35}$$

just as we did in IV-1, where we assumed the potential follows the density. The density

is then expanded in powers of α and only terms to first order in α are kept so the density

is

$$\rho(r, R) = \rho_0 + \Delta\rho \qquad\qquad \text{IV-36}$$

The scalar term of the transition density is then

$$< \Phi_f \mid \Delta U_S(r,R) \mid \Phi_i >$$

$$= \delta_I / (2I+1)^{1/2} \int \Lambda_S(r - r') \, \partial/\partial R \, [\, \rho(r', R) \,] \, d^3r' \qquad \text{IV-37}$$

and there is a similar vector term. This transition density is integrated between initial and final distorted wave states. The optical potential used to calculate the distorted waves is calculated from the impulse approximation but the spirit of the calculation is very similar to that of our own.

This impulse approximation calculation was compared to measured cross sections and analyzing powers for the reaction ^{54}Fe(p,p')^{54}Fe* at 800 Mev. Excellent agreement was found with the cross section and fair ageement with the analyzing powers for the $J^{\pi}=2^+$ and 3^- states. Similar quality was found for the calculation of the elastic scattering observables. The shape of the potentials used in this DWIA calculation is fixed by the knowledge of the free amplitudes and this limits the agreement with the data that can be obtained. The freedom of a phenomenological determination of the optical potential allows us to do a better job of calculating the elastic observables and therefore (hopefully) the inelastic observables.

V - INELASTIC SCATTERING PREDICTIONS

A program, PROM, has been written to do the full relativistic optical model calculation for proton inelastic scattering outlined in chapter IV. We use the distorted waves obtained from the elastic scattering fits of chapter III for our initial and final state wave functions. The transition operator has one adjustable parameter, the deformation parameter β, which is determined by fitting the peak of the calculated cross section to that of the experimental cross section.

We compare our calculations to experimental data and to the analyses of other authors as well as calculating some observables for which there is no experimental data available. We start by considering the inelastic scattering of protons on ^{40}Ca where a lot of experimental effort has been concentrated. In ^{40}Ca we consider three different energies of the incident proton (362 Mev., 500 Mev., 800 Mev.) and three excited states. The $J^{\pi} = 3^{-}$ state with $E_x = 3.7364$ Mev. is a good collective state, the $J^{\pi} = 2^{+}$ state with $E_x = 3.9041$ Mev. is a slightly collective state and the $J^{\pi} = 5^{-}$ state with $E_x =$ 4.4915 Mev. is almost a pure single particle - single hole ($d^{-1}_{3/2}$ - $f^{1}_{7/2}$) state [Kä84, Se85]. We also consider levels in ^{20}Ne at an incident proton energy of 800 Mev., ^{48}Ca at 500 Mev. and ^{90}Zr at 800 Mev.

^{40}Ca at 362 Mev.

Figures V-1 and V-2 show the cross section and analyzing power for the 3^{-} state calculated from the parameter set in table III-1. The data are from Frekers [Fr86]. The

dashed curve is calculated by ignoring the term involving lower components in the T-matrix element IV-16. The contributions of the lower component wave function are clearly significant since not only is the peak of the cross section overestimated by a factor of five but the minima and maxima of the diffraction pattern are shifted towards smaller angles. A similar shift is also seen in the analyzing power so we see that the spin dependent part of the T-matrix is critical to correctly describing the data.

The dotted curves of figures V-1 to V-3 show the DEB calculation, described in section IV-3, using the same parameter set as the RDWBA calculation. The DEB calculation gives a smaller deformation parameter (β_{DEB} = 0.34) than the RDWBA (β_{RDWBA} = 0.36) and the deformation lengths are just 3.46 times larger for both. The quality of the predictions for the cross section are very similar. The two calculations for analyzing power and polarization transfer show similar features but the two calculations start to differ quite a bit at about 48°. The full calculation for the 3⁻ state gives a fairly good prediction, as we expect.

The calculation for the 5⁻ state, shown in figures V-4 and V-5, is as we expect not as good as the calculation for the 3⁻ state since the 5⁻ is not as collective a state as the 3⁻ [Kä84]. The cross section calculation shows the general trend of the data up to about 45° then remains above the data while the analyzing power calculation does not position the maxima and minima correctly or get the magnitudes right.

^{40}Ca at 500 Mev.

The inelastic scattering predictions calculated from the parameter sets in table

III-1 are shown in figures V-6 to V-17. The cross section and analyzing power data are from Seth et al. [Se85] and the polarization transfer data are from Aas et al. [Aa82].

Figures V-6 and V-7 show cross section and analyzing power for the 2^+ state. The predictions from the two parameter sets are very similar. The minimum at $14°$ in both cross section and analyzing power is underestimated but the position of the minimum is correct. The prediction is reasonable since this state is only partly collective [Se85]. Also the data set extends to only $25°$ and as for the 5^- state at 362 Mev, the prediction would probably get worse at larger angles.

Predictions for the 3^- state are shown in figures V-8 to V-13. We have also included the DEB calculation of Sawafta [Sa84] for which parameter set A was used. The three predictions for cross section and analyzing power are very close and in good agreement with the data. The deformation parameter extracted from the DEB calculation (β_{DEB}=0.36) is slightly smaller than that obtained from the RDWBA calculation (β_{RDWBA}=0.39).

Figures V-10 to V-13 show the spin rotation parameters which are defined in appendix B. Note that as discussed in appendix B $D_{SS'}$, which is shown in figure V-11, is very similar to $D_{LL'}$, shown in figure V-10, for a collective natural parity state, and $D_{LS'}$ (figure V-12) is the negative of $D_{SL'}$ (figure V-13) in the adiabatic approximation, so the full analysis has been included for $D_{LL'}$ and $D_{LS'}$ only. The three predictions for $D_{LL'}$ are very close and decribe the data well. The predictions for $D_{LS'}$ calculated from the two parameter sets are also very similar but the DEB calculation does not give as large a change from maximum to minimum around $17°$ as the full calculation does.

Figures V-14 to V-17 show predictions for the 5⁻ state. The two parameter sets give similar predictions of the observables but the agreement with the data is not very good. However over the range of the data the quality of the prediction is comparable the the prediction of the 5⁻ state at 362 Mev. For angles less than 3° the analyzing power predictions have different signs and a measurement of analyzing power at 2° could distiguish between these sets. Note that these optical potentials give essentially the same elastic scattering and also the same inelastic. Previous work [Au65,Am80] has shown that the inelastic observables can be calc⬛⬛d in terms of the elastic observables. This is reflected in the insensitivity of the inelastic calculation to the different parameter sets.

The elastic analysis of Seth et al. [Se85] which is discussed in chapter III is extended to inelastic scattering by the method outlined in section IV-1. We underestimate the minima for cross section and analyzing power for the 2⁺ state at 14° more than Seth et al. do. For the 3⁻ state the behaviour of our cross section calculation is very similar to theirs but we calculate the analyzing power better. RDWBA slightly overestimates the maxima at 12° and 21° while DWBA underestimates the first maximum badly and places the maximum in the wrong place while the second maximum is correctly predicted.

· ·The cross section for the 5⁻ state is described slightly better by RDWBA for angles less than 15° and by DWBA for angles larger than 15°. The analyzing power is again overestimated by RDWBA and underestimated by DWBA for angles less than 23°.

٧° Generally Seth et al. do a little better at predicting the cross sections but we do better at predicting the analyzing power, particularly at small angles.

Barlett et al. [Ba85] have analyzed the polarization transfer data in the nonrelativistic DWBA framework using both phenomenology and impulse

approximation to generate potentials and transition densities. Their phenomenological calculation gives a better representation of the data than the impulse approximation and also agrees better with our RDWBA. Barletts' calculation of D_{LL} is very close to the RDWBA prediction and is in good agreement with the data. D_{LS} is slightly overestimated by the DWBA calculation and the change from a maximum of 0.8 to a minimum of -0.8 at about 17° is very slight while the RDWBA calculation gives a very good representation of the data.

Our RDWBA analysis is at least as good as these DWBA analyses and is definitly better at calculating analyzing powers at forward angles.

The extracted deformation parameters are shown in table V-1 as are the parameters of Seth et al. The agreement is very good for all three states.

^{40}Ca at 800 Mev.

Figures V-18 to V-23 show cross section and analyzing power predictions for proton inelastic scattering from ^{40}Ca at 800 Mev. The data are from Blezynski et al. [Bl82].

The calculations of the cross sections for the three states using parameter set B all match the data better for large angles than the predictions due to set A. The analyzing power data does not extend as far in angle as the cross section data for the 3⁻ state, and the two parameter sets give similar predictions over the smaller angular range. Fitting the large angle elastic cross section data brings the inelastic scattering prediction for the cross section down closer to the data for all three states.

Blezynski et al. [Bl82] have analyzed these data in the Glauber approximation

framework and their prediction for the cross section of the 3^- state is very close to that given by parameter set B but they come closer to getting the last minimum at $42°$.

Gazzaly et al. [Ga82] have done a nonrelativistic DWBA analysis in order to extract the deformation parameters. These are shown in table V-1 along with the results of the analyses of Blezynski et al. and of this work. The deformation parameters of Blezynski et al. are in better agreement with this work than those of Gazzaly et al. but for the 3^- state there is a fairly large spread between the deformation parameters and lengths.

Other parameter sets were found for this nucleus and energy by ignoring both the Q data and the large angle cross section data but the predictions of cross section and analyzing power from any of these sets are not as good as those from the sets shown.

^{20}Ne at 800 Mev.

Predictions for inelastic proton scattering are shown in figures V-24 to V-29. The data are from Blanpied et al. [B184]. RDWBA decribes the 3^- state much better than the 2^+ or the 4^+. The cross section is very close to the data except that the minimum at $18°$ is slightly underestimated. The DEB calculation overestimates this minimum by about the same amount that RDWBA underestimates it. The analyzing power prediction from RDWBA shift the maxima and minima to smaller angles by about $1°$ and overestimates the data while the DEB calculation is much closer to the data.

The predictions for the 2^+ and 4^+ states give maxima and minima which are shifted towards larger angles by two to three degrees. The shape of the analyzing power curve for the 2^+ state agrees well with the data except for the shift in angle. The shapes

of the differential cross section for the 2^+ state and both curves for the 4^+ state are inconsistent with the data.

Blanpied et al. [Bl84] have analyzed the data for the 0^+, 2^+ and 4^+ states in both the DWBA and coupled channels frameworks. The coupled channels calculation does a much better job of describing the data than DWBA or RDWBA.

The deformation parameters are shown in table V-1. The parameters from [Bl84] were obtained from their DWBA analysis and are in reasonable agreement with the RDWBA values. The coupled channels method gives deformation parameters which are much smaller than the RDWBA values [$\beta_{2\,CC} = 0.47$ and $\beta_{4\,CC} = 0.25$].

We have also analyzed ^{12}C and find the same type of problems with this nucleus, i.e. the predicted observables having the wrong shape and the maxima and minima being shifted in angle.

Some deformation parameters for the 2^+ state have been included in table V-1. Jones et al. [Jo86] have done a coupled channel analysis of ^{12}C data over a wide range of energies and find that the deformation parameter for the 2^+ state remains almost constant at approximately $\beta_2 = 0.66$. We give a range of parameters for each energy because we found several parameter sets which gave different deformation parameters. Simply letting the search program find a minimum chi-squarsd gave excellent fits to the elastic observables but the potentials had the odd wiggles in the nuclear interior as shown in figure III-15. These potentials consistently result in the largest deformation parameters and lengths at all energies. Parameter sets without the interior wiggles did not give chi-squared minima but gave extracted deformation parameters near the lower end of the ranges given and in better agreement with the results of [Jo86]. The coupled channels

calculations describe the data much better than RDWBA does.

^{48}Ca at 500 Mev.

Figures V-30 to V-33 show predictions for protons, with an incident energy of 500 Mev., scattering inelastically from ^{48}Ca to the 2$^+$ and 3$^-$ states using the parameters from table III-2. The data are from Seth et al. [Se85].

. The parameter sets give similar predictions even though the chi-squared for the elastic scattering observables is twice as large for set A as for set B. The agreement with the data is good except that the first minimum in the 2$^+$ state, at 13°, is underestimated in both cross section and analyzing power and for the 3$^-$ state the cross section minima are shifted by about 1°.

The analysis of Seth et al. gives predictions for the cross section for both states which are quite close to the RDWBA predictions. Figure V-33 shows Seth's DWBA calculation of the analyzing power for the 3$^-$ state as the long-dashed curve. For small angles the analyzing power is badly underestimated. This effect is even larger in their ^{40}Ca analysis for the 3$^-$ and 5$^-$ states. The 2$^+$ states of both ^{40}Ca and ^{48}Ca are only slightly underestimated at small angles while RDWBA overestimates these data slightly.

The extracted deformation parameters are shown in table V-1 with those of Seth et al. and they are in good agreement. .

^{90}Zr at 800 Mev.

Figures V-34 to V-38 show predictions calculated from the two parameter sets

in table III-2. The data are from Gazzaly et al. [Ga82].

The two parameter sets give very similar predictions for all four states and the agreement with data is excellent in all cases. Parameter set A seems to give slightly better predictions for the inelastic cross section even though this set does not give the lowest chi-squared for the elastic observables. The difference between the two pedictions is small and it is doubtful whether this calculation could decide if a parameter set is "correct". There are no analyzing power data available but figure V-36 shows a comparison for the 3^- state predictions. DEB calculations using parameter set A have been included for the 3^- state in figures V-35 and V-36. This calculation agrees very closely with the RDWBA calculation.

Table IV-1 shows the deformation parameters and deformation lengths obtained by Gazzaly et al. [Ga82] for ^{90}Zr to compare with the results of this work. The agreement between the extracted deformation parameters and lengths is excellent. The RDWBA calculation does as good a job of predicting the observables as the DWBA analysis of Gazzaly et al. and the curves are too close to pick one set over the other.

Figure V-39 shows a plot of deformation length verses proton energy for the 3^- state in ^{40}Ca. The triangles are from various nonrelativistic analyses [Gr72, Sh68, Sa83,Se85,Bl82,Ga82], the squares are from DEB [Sa84] calculations and the circles are the results of this work. There is no clear energy dependence of the deformation length. The value of the deformation length is approximately 1.3 Fm. and varies with the type of analysis done.

VI - CONCLUSION

We have extended the phenomenological Dirac optical model to describe proton inelastic scattering to collective states. These calculations have been compared with experimental data and with the analyses of other authors. The predictions due to different fits of the elastic scattering data have also been compared.

The two parameter sets for ^{40}Ca at 500 Mev. give almost the same elastic scattering and also give almost the same inelastic scattering, while for ^{40}Ca at 800 Mev. an improvement of the fit to the large angle elastic cross section data resulted in an improvement in the predicted inelastic cross section over the same angular range. The slight differences in the elastic scattering fits for ^{48}Ca and ^{90}Zr produced similar differences in the inelastic scattering predictions. The biggest differences in these parameter sets are in the imaginary parts of the potential and the inelastic scattering to collective states does not seem to be very sensitive to these differences. This is in agreement with the result [Au65, Am80] that the excitation to collective states is related to elastic scattering.

The DEB calculation is very close to the RDWBA calculation for all the observables. The approximations made in this calculation leave the essentials of the relativistic calculation and the DEB calculation has the advantage that it can be done with only minor modifications to existing Schrödinger codes. The differences between the calculations do not seem to be important except for large angles (greater than 45°).

When a transition is described in the coupled channels formalism (appendix A) the states are connected through a set of coupled equations, and the coupling between the

states is proportional to the transition density, ΔV_{IM}. The transition density is proportional to the deformation parameter so if β is small enough the channel coupling is not very important, and for large β's a proper coupled channels description becomes necessary to describe the data. This is what we have seen in this work. For ^{90}Zr the deformation parameters are all very small and the predictions for inelastic scattering are excellent. On the other hand ^{12}C and ^{20}Ne have very large deformation parameters and the predictions are quite bad. Nonrelativistic coupled channel analyses for these nuclei do better than RDWBA at describing the data. J. Raynal [Ra86] is currently working on a program to do relativistic coupled channels calculations, which should be able to explain the ^{12}C and ^{20}Ne data better than the nonrelativistic calculations.

The deformation parameters extracted from RDWBA calculations are in good agreement with deformation parameters determined by other analyses, for the good collective states.

The RDWBA calculation of inelastic scattering to collective states does at least as well and usually better than the nonrelativistic calculations that have been considered in the cases where channel coupling is not very important. The spin observables particularly are improved by the relativistic description. The inclusion by Seth et al. [Se85] of a "density squared" term in their optical potential is not enough of a modification to enable their calculation to do as well as the full Dirac calculation.

The term of the T-matrix containing the lower components of the Dirac wave functions is seen to be critical to obtaining a good prediction of the scattering observables. This term contains the spin-orbit dependence of the T-matrix and the data cannot be explained without it.

	^{40}Ca 362 Mev.	^{40}Ca 500 Mev. (A)	^{40}Ca 500 Mev. (B)	^{40}Ca 800 Mev. (A)	^{40}Ca 800 Mev. (B)
V_V	292.27	198.12	189.50	182.68	242.49
R_{V1}	1.0115	1.0541	1.0370	1.0162	0.9814
A_{V1}	0.6421	0.6180	0.7257	0.6733	0.6658
W_V	-94.677	-84.164	-135.77	-87.439	-128.81
R_{V2}	1.1253	1.0580	1.0560	1.0652	1.0756
A_{V2}	0.5509	0.6411	0.5388	0.5886	0.6294
V_S	-414.68	-287.95	-289.53	-312.79	-457.90
R_{S1}	1.0044	1.0583	1.0413	1.0072	0.9419
A_{S1}	0.6690	0.6517	0.7337	0.7176	0.7215
W_S	95.739	71.110	148.95	57.084	155.88
R_{S2}	1.1279	1.0450	1.0538	1.0862	1.0593
A_{S2}	0.5361	0.6967	0.5339	0.5968	0.6431
N_σ	150	153	153	196	196
N_A	150	153	153	193	193
N_Q	--	32	32	33	33
χ^2_σ	2600	1700	1700	39,000	6700
χ^2_P	870	610	610	830	1600
χ^2_Q	--	240	280	110	1100

TABLE III-1. Relativistic optical model parameters for protons incident on ^{40}Ca at various energies.

	^{20}Ne 800 Mev.	^{48}Ca 500 Mev. (A)	^{48}Ca 500 Mev. (B)	^{90}Zr 800 Mev. (A)	^{90}Zr 800 Mev. (B)
V_V	158.45	149.23	136.48	145.94	127.53
R_{V1}	0.9380	1.0813	1.0981	1.0716	1.0925
A_{V1}	0.7032	0.5314	0.5284	0.8042	0.7653
W_V	-97.978	-49.108	-130.70	-96.310	-143.84
R_{V2}	0.8842	1.1023	1.0392	1.0730	1.0354
A_{V2}	0.6839	0.6260	0.7014	0.5466	0.6458
V_S	-257.84	-221.60	-200.39	-301.70	-229.24
R_{S1}	0.9380	1.0666	1.0955	1.0356	1.0892
A_{S1}	0.7370	0.5867	0.5620	0.8231	0.7624
W_S	58.687	51.151	193.40	62.205	252.56
R_{S2}	0.8254	0.9924	0.9734	1.0724	0.8973
A_{S2}	0.7113	0.7086	0.7591	0.4873	0.7487
N_σ	30	117	117	131	131
N_A	30	118	118	129	129
χ^2_σ	80	2100	1200	2200	1200
χ^2_P	40	1200	400	600	410

TABLE III-2. Relativistic optical model parameters for protons incident on various nuclei at various energies.
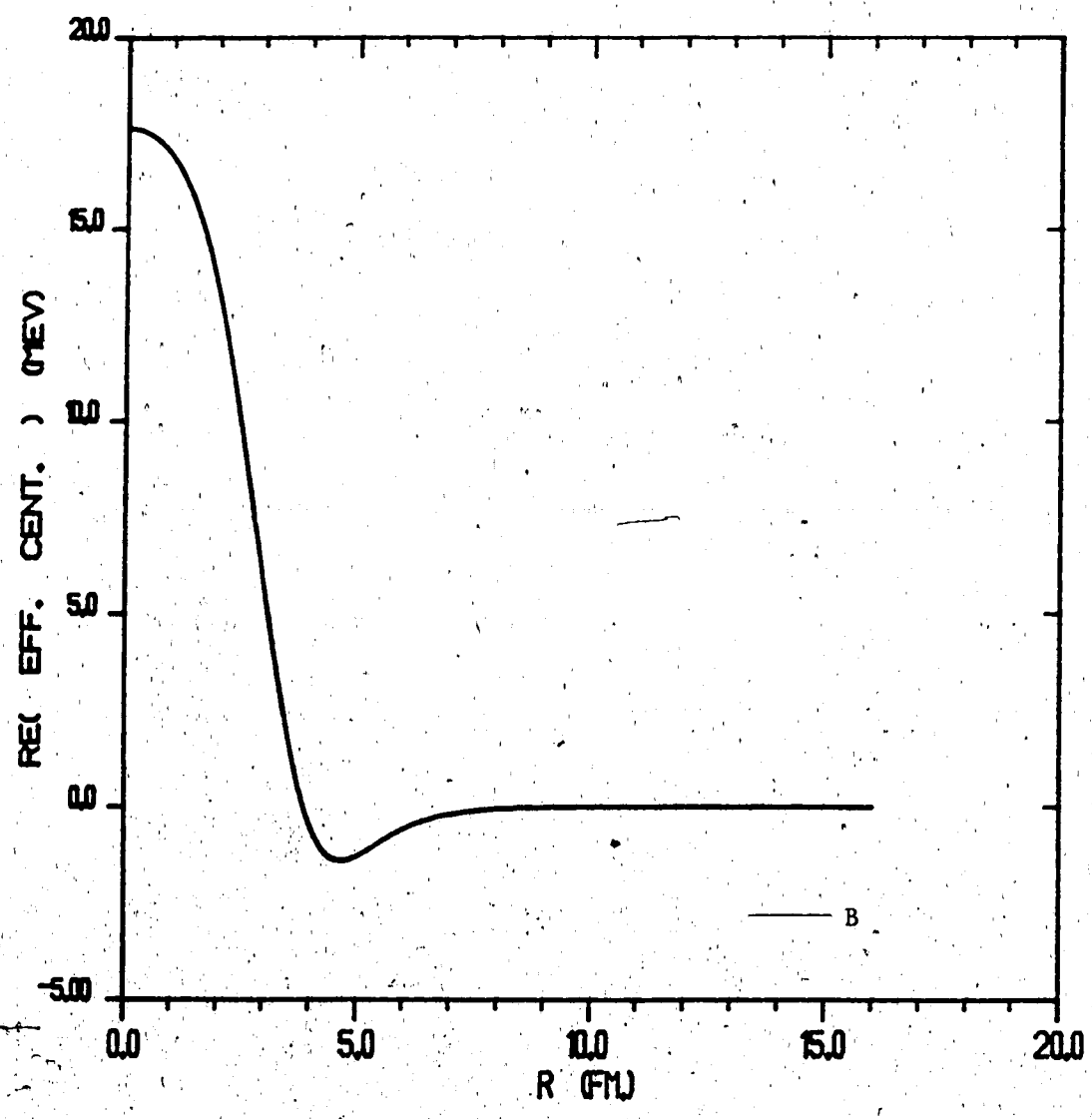
Figure III-1.   The real part of the effective central
                potential for p + ^{40}Ca at E_p = 500 Mev.

                The curve is calculated using parameter
                set B of table III-1.

IM EFF. CENT.) (MEV)

0.0

-20.0

-40.0

-60.0

-80.0

—— B

0.0   5.0   10.0   15.0   20.0

R (FM)
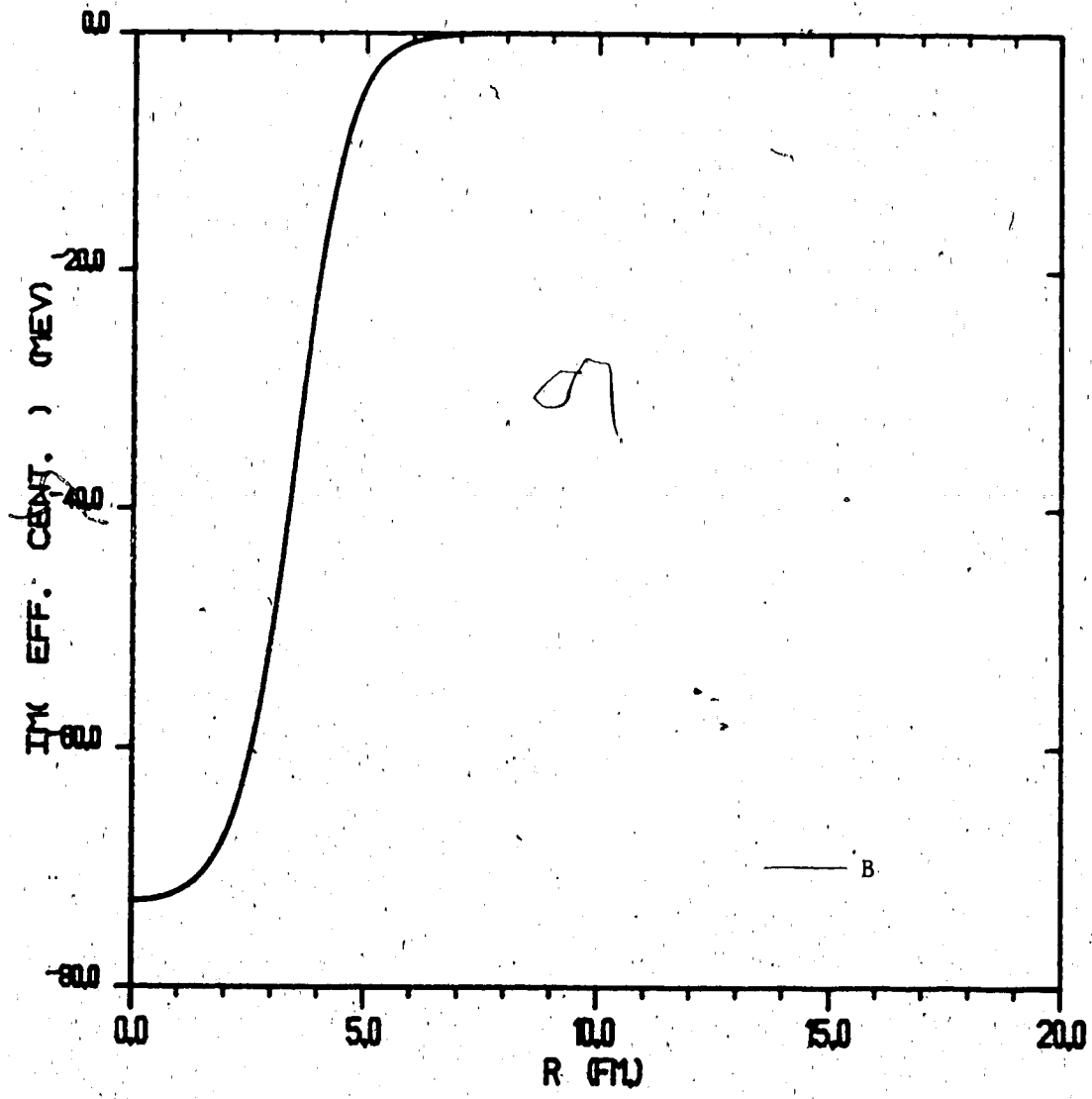
Figure III-2. The imaginary part of the effective central
potential for p + ^{40}Ca at E_p = 500 Mev.

The curve is calculated using parameter set
B of table III-1.
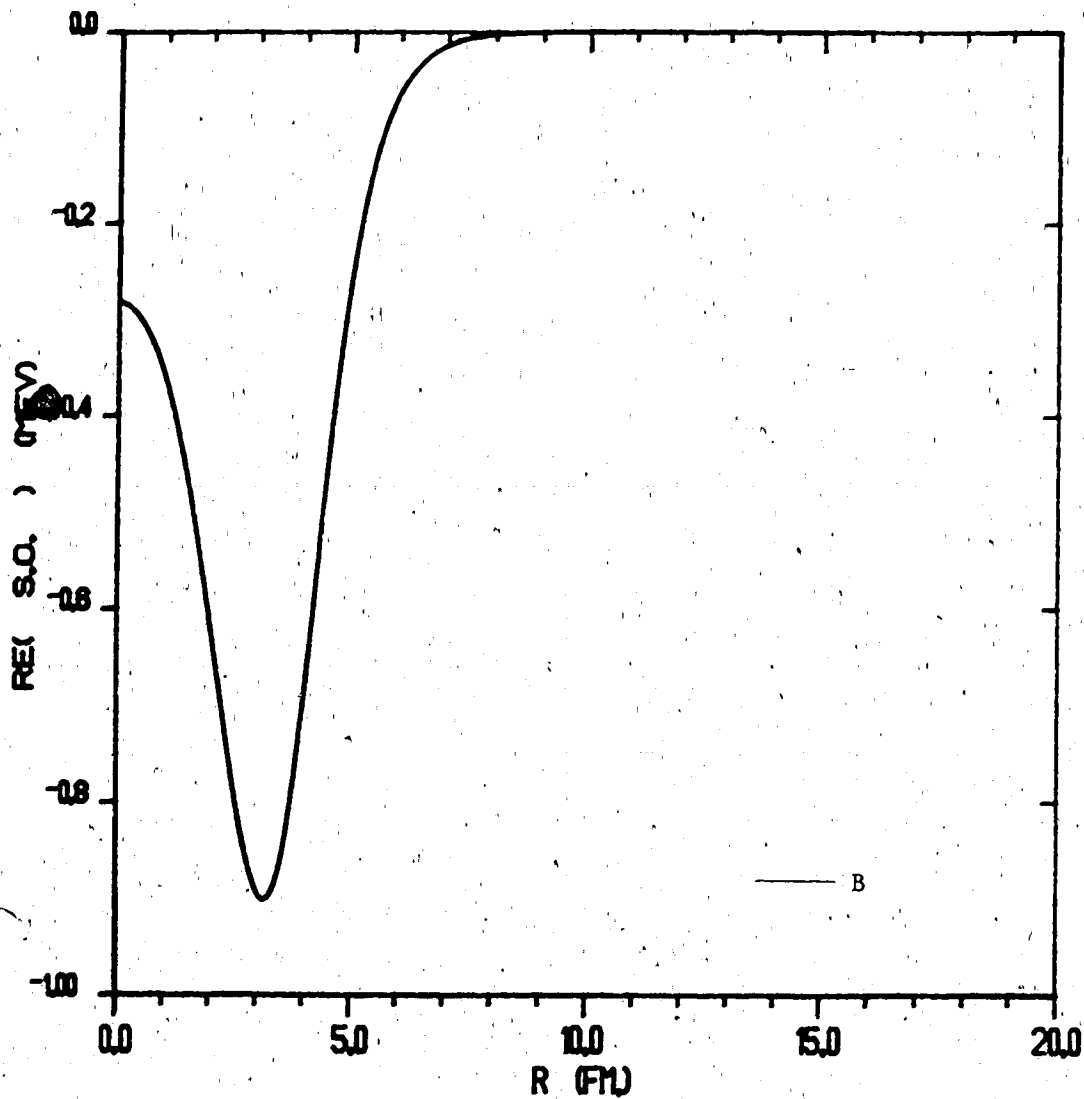
Figure III-3.　The real part of the effective spin-orbit potential for p + ^{40}Ca at E_p = 500 Mev.

The curve is calculated using parameter set B of table III-1.
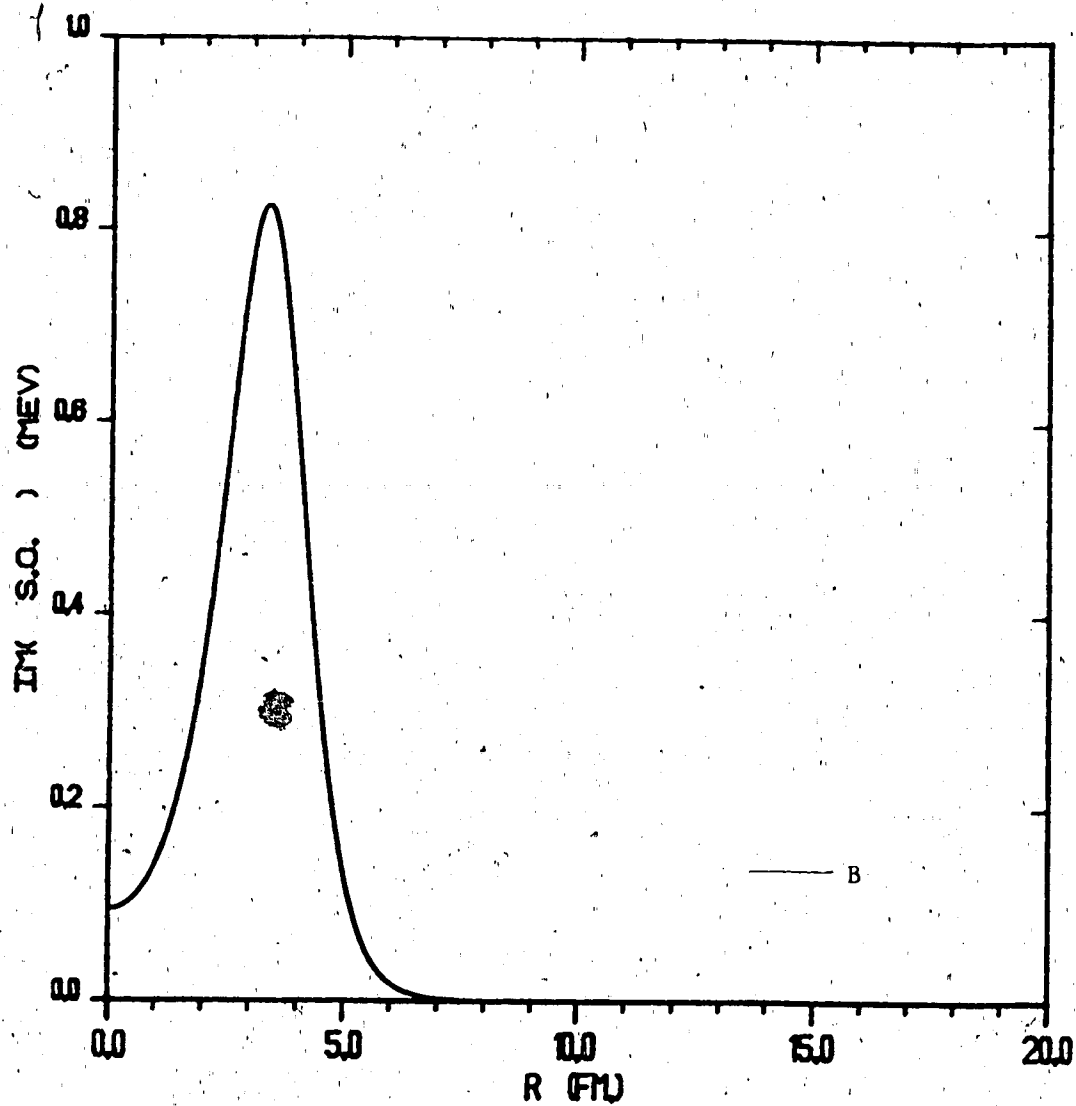
Figure III-4.   The imaginary part of the effective spin-orbit
                 potential for p + ^{40}Ca at E_p = 500 Mev.

                 The curves are calculated using parameter
                 set B of table III-1.
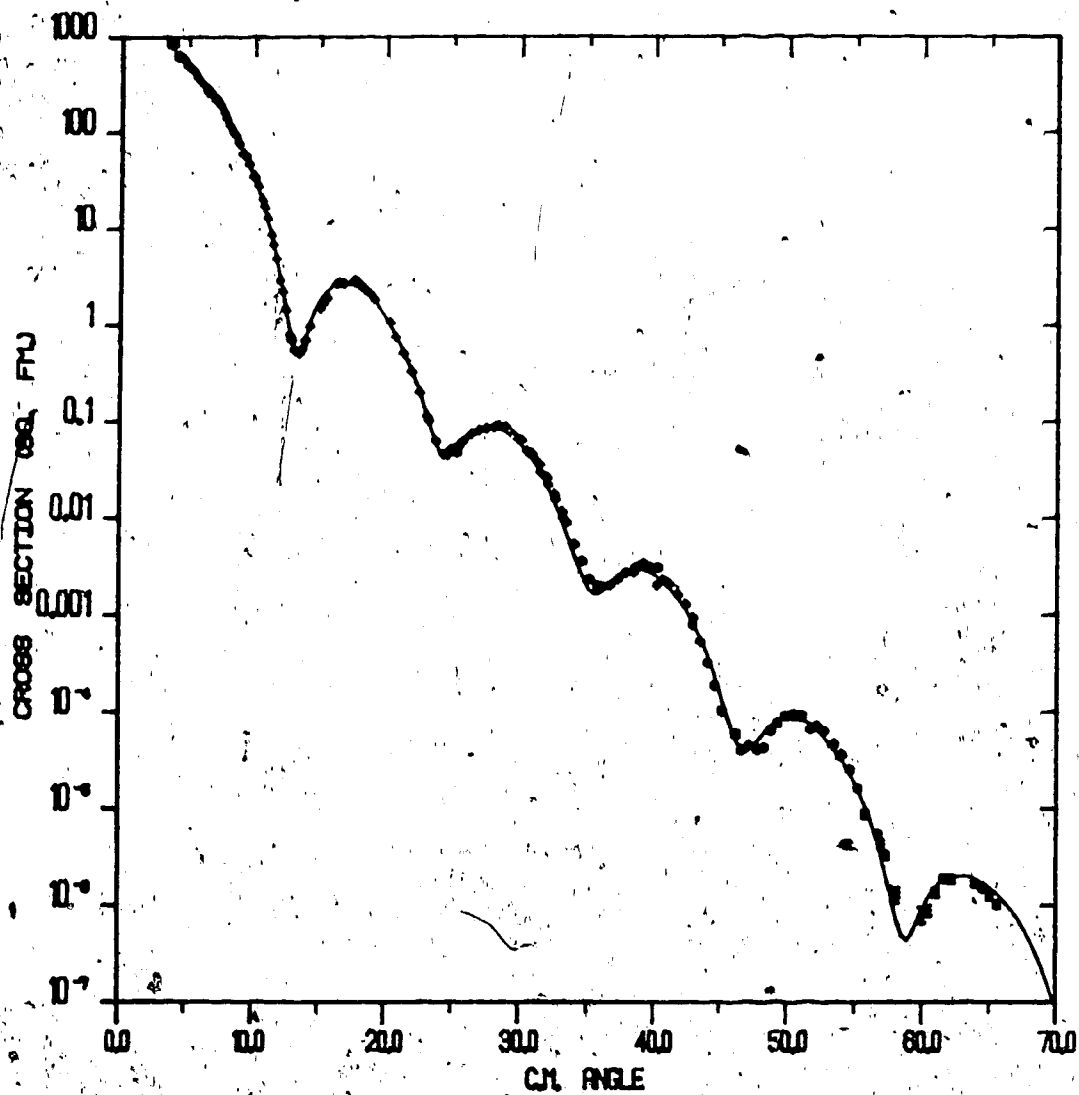
Figure III-5. Differential cross section for p + ^{40}Ca elastic scattering at E_p = 362 Mev.

The curve is an optical model fit calculated from the parameters of table III-1.
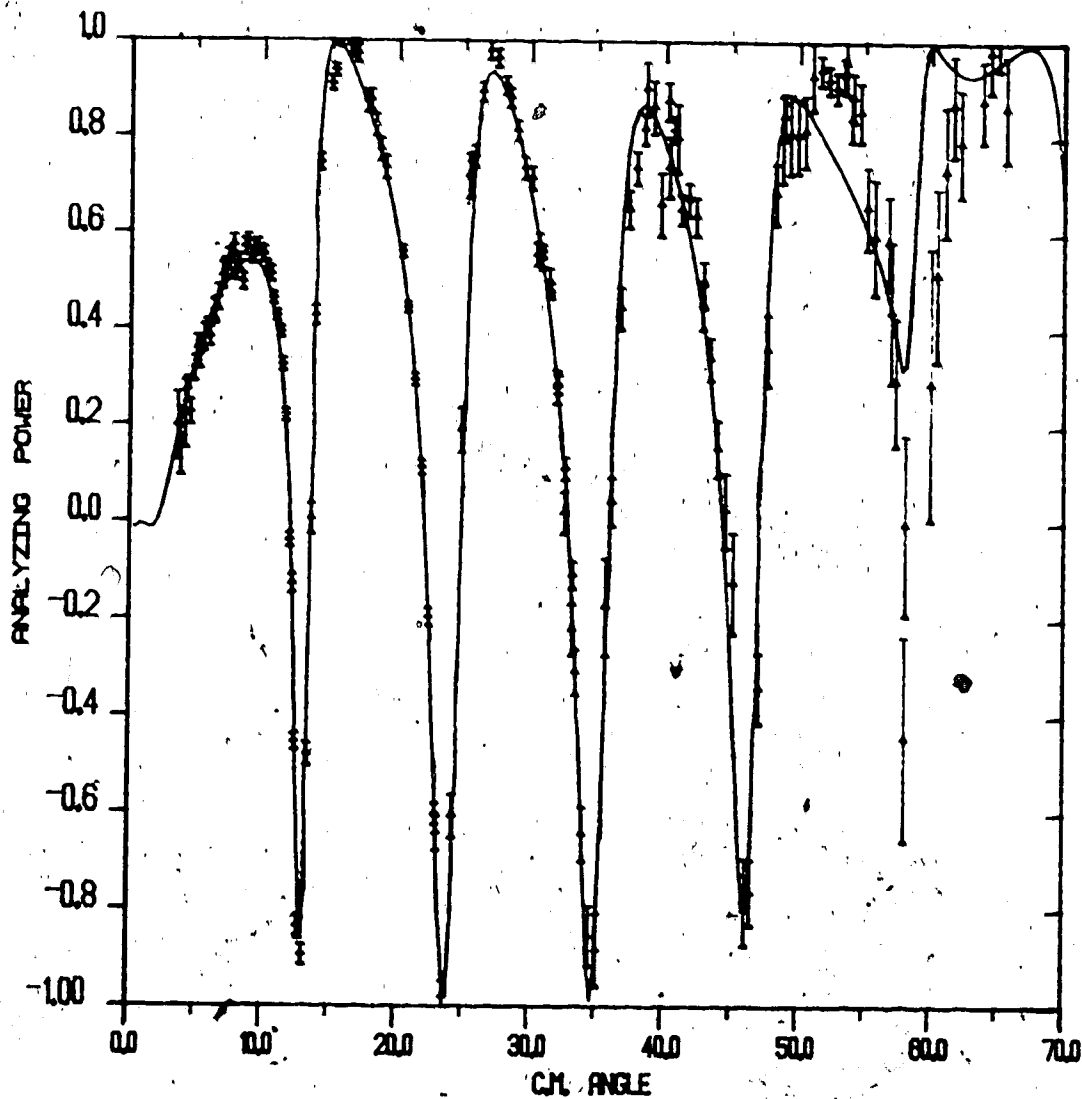
Figure III-6. Analyzing power for p + ^{40}Ca elastic scattering at E_p = 362 Mev.

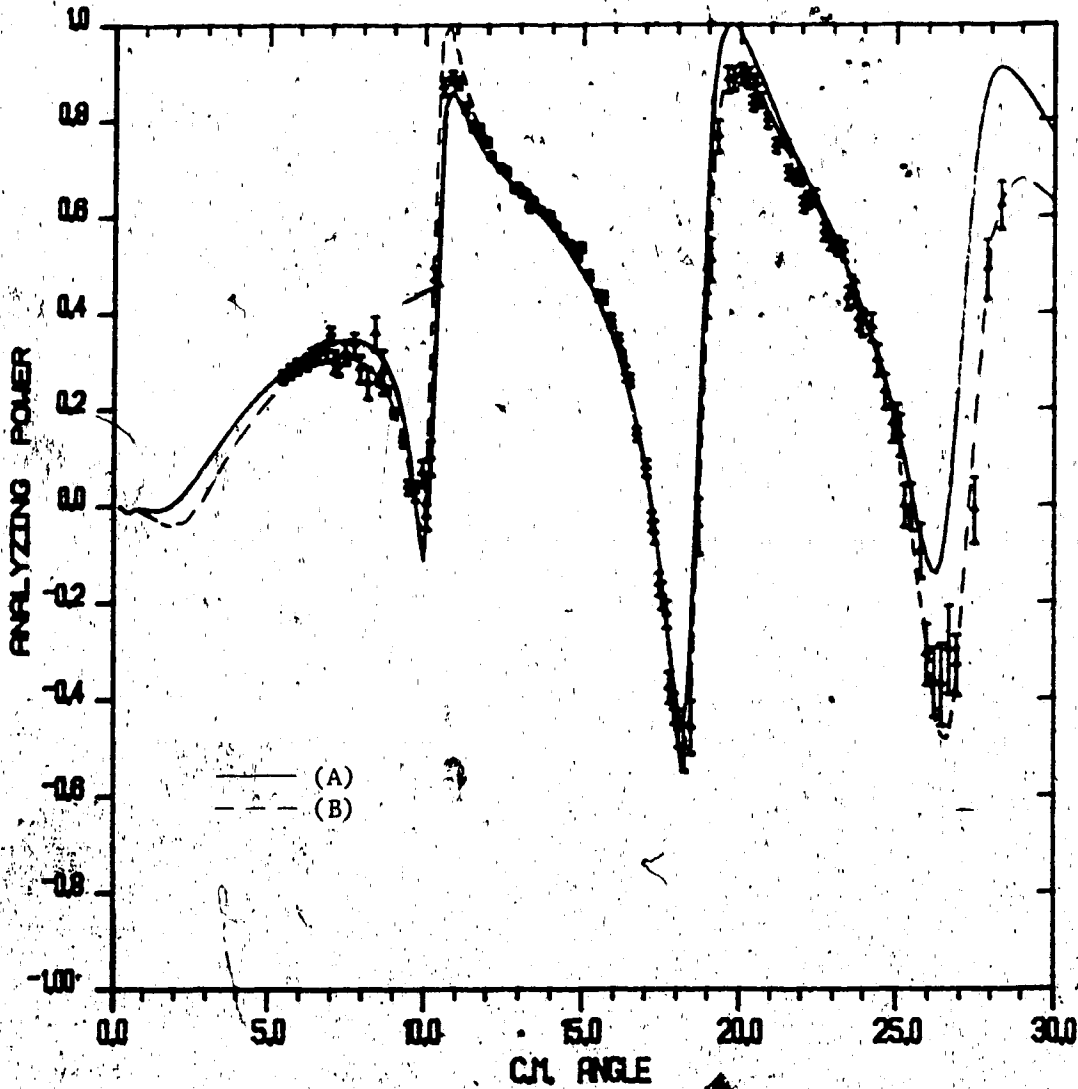The curve is a Dirac optical model fit calculated from the parameter set of table III-1.
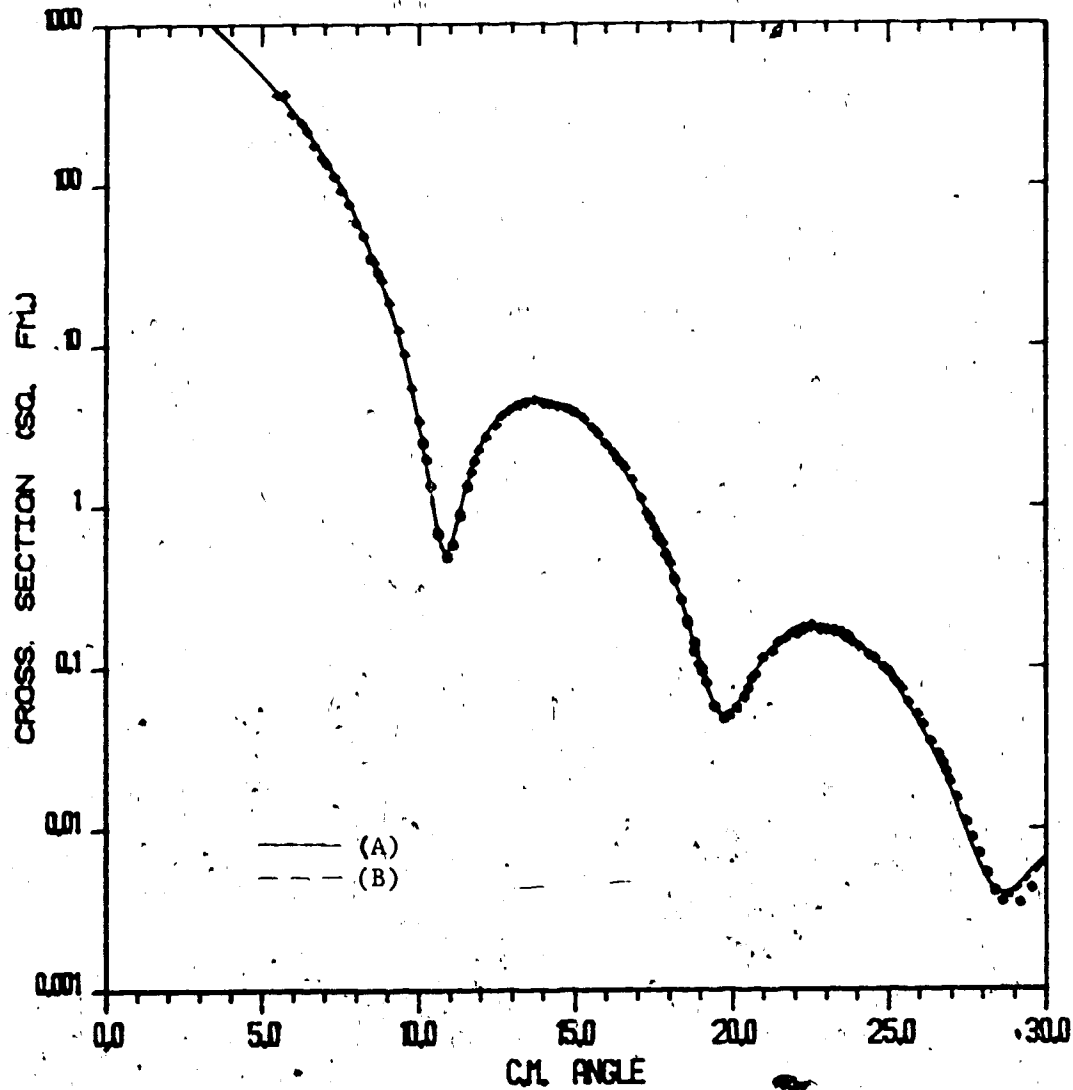
Figure III-7.   Differential cross section for p + ^{40}Ca
elastic scattering at E_p = 500 Mev.

The curves are Dirac optical model fits
calculated from the parameter sets of
table III-1.
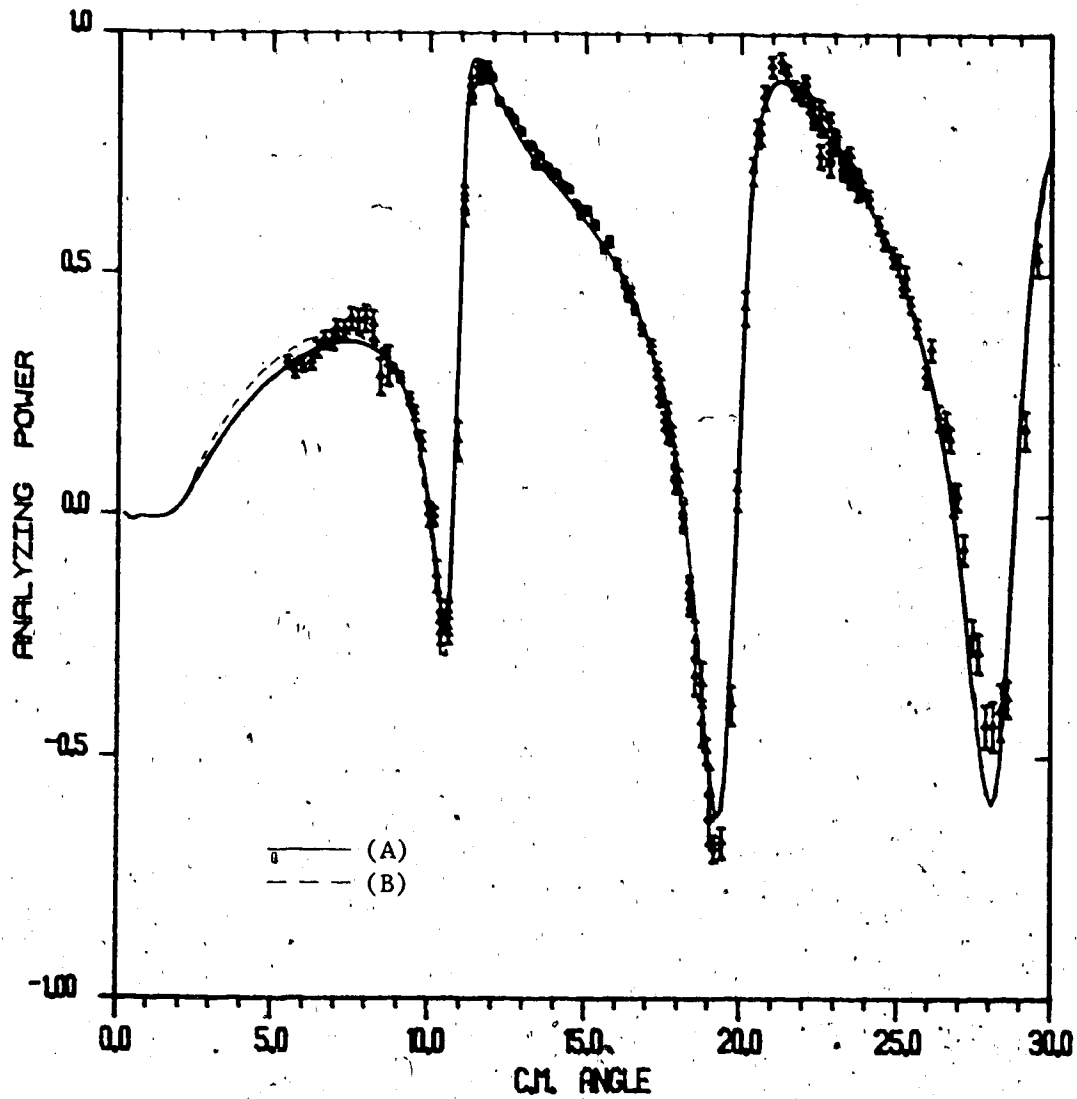
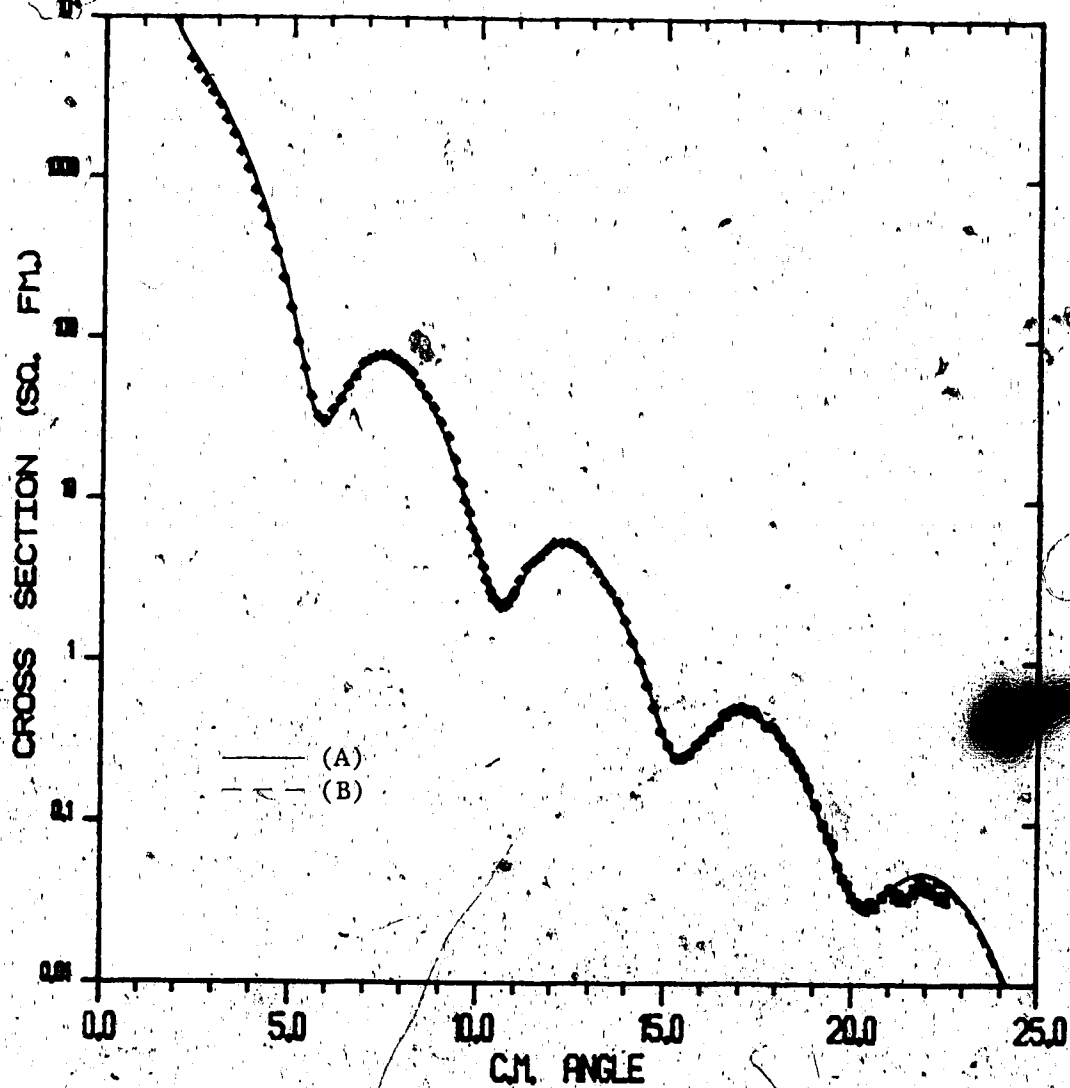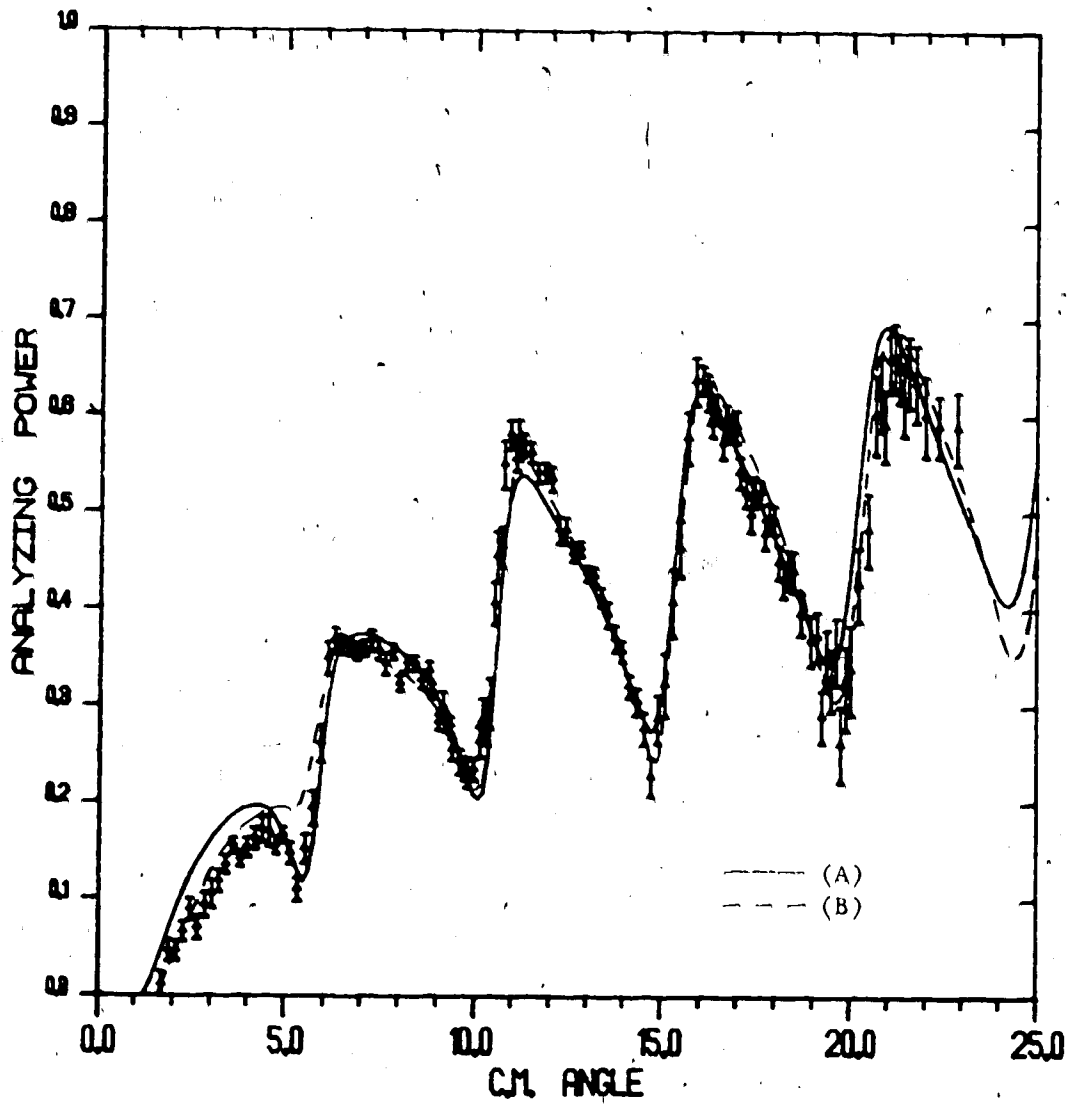Figure III-8. Analyzing power for p + ^{40}Ca elastic
scattering at E_p = 500 Mev.

The curves are Dirac optical model fits
calculated from the parameter sets of
table III-1.
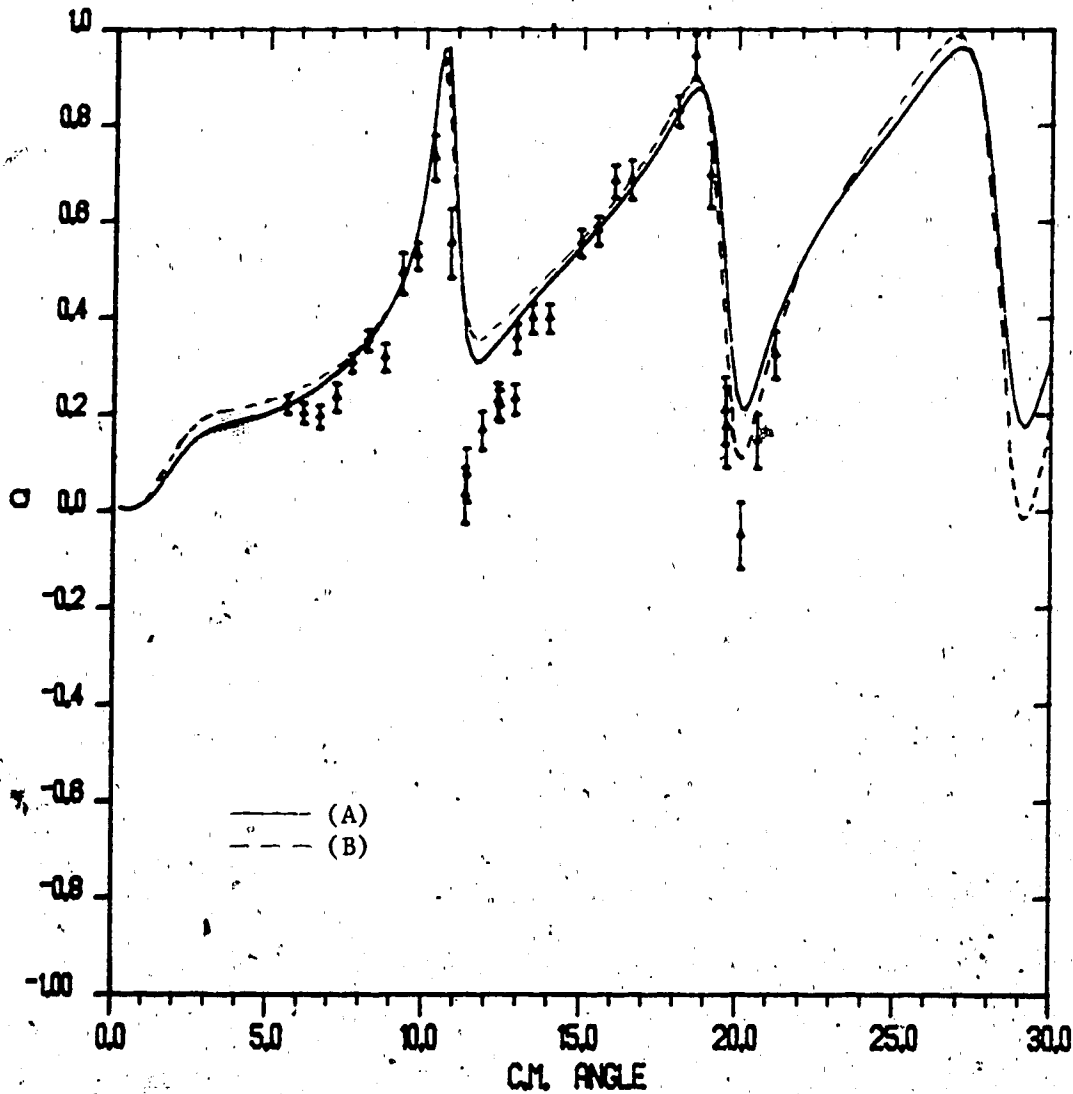
Figure III-9.   Spin, rotation parameter (Q) for p + ^{40}Ca
elastic scattering at E_p = 500 Mev.

The curves are Dirac optical model fits
calculated from the parameter sets of
table III-1.
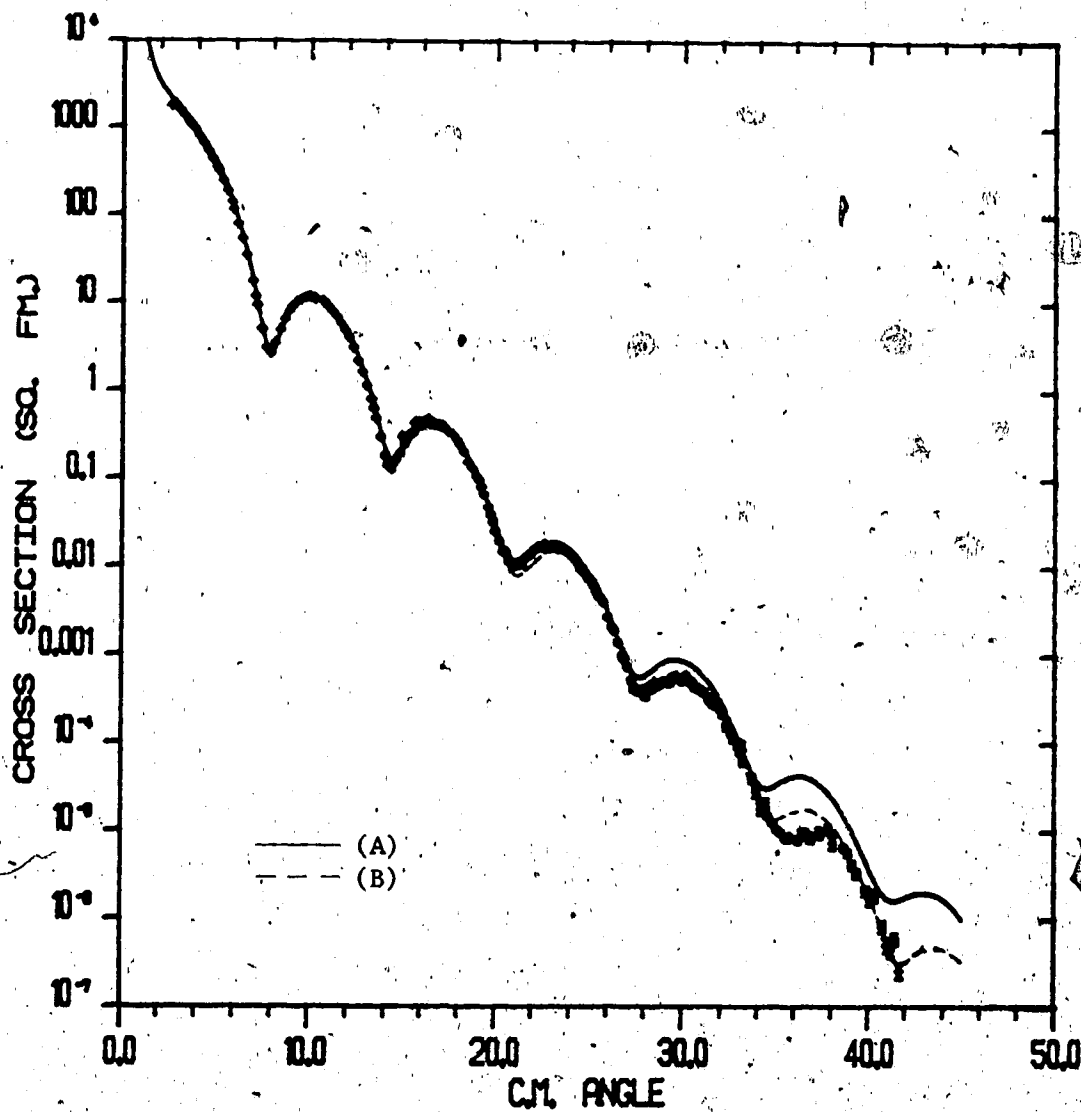
Figure III-10. Differential cross section for p + ^{40}Ca elastic scattering at E_p = 800 Mev.

The curves are Dirac optical model fits calculated from the parameter sets of table III-1.
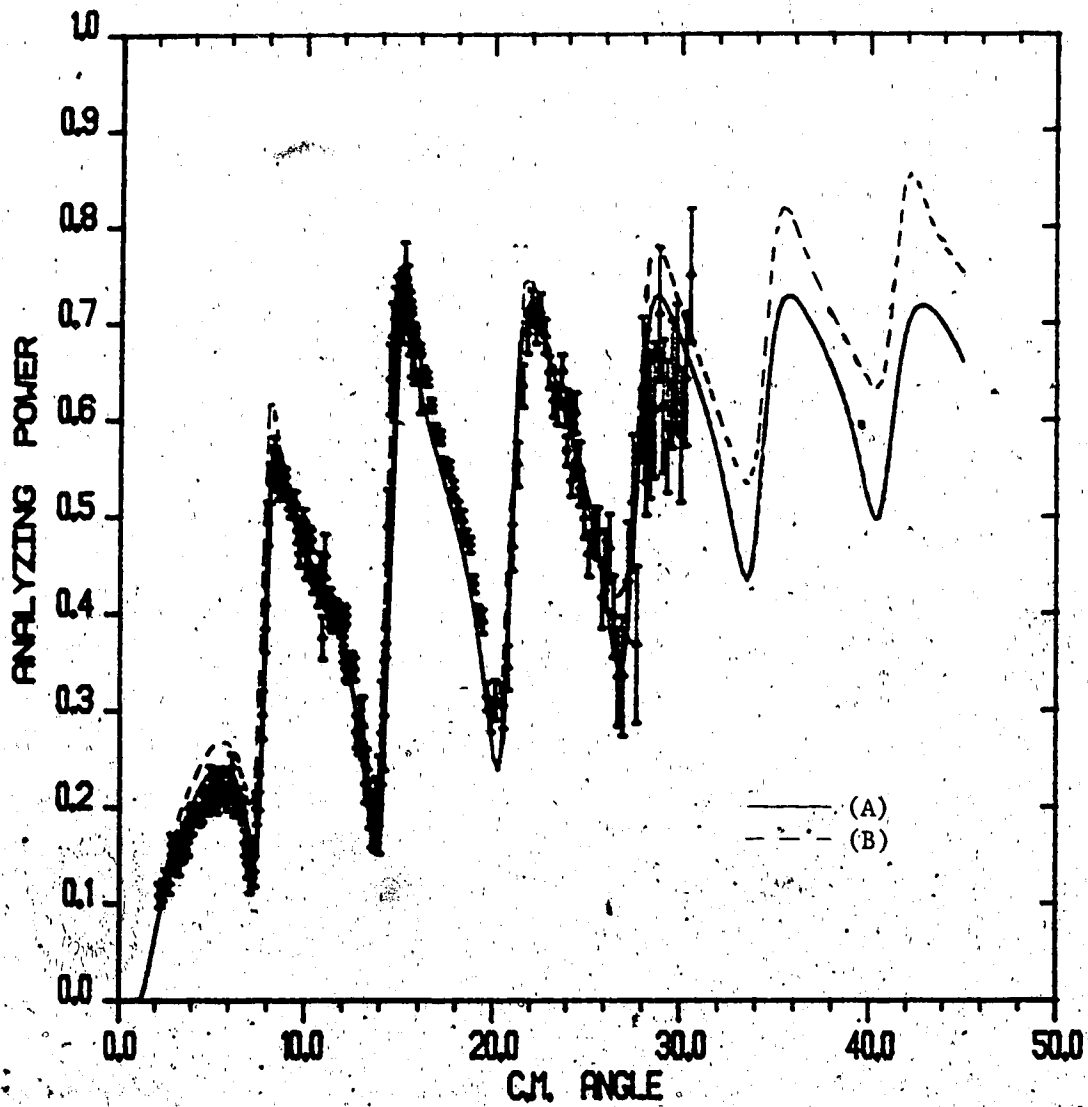
Figure III-11. Analyzing power for p + ^{40}Ca elastic scattering at E_p = 800 Mev.

The curves are Dirac optical model fits calculated from the parameter sets of table III-1.
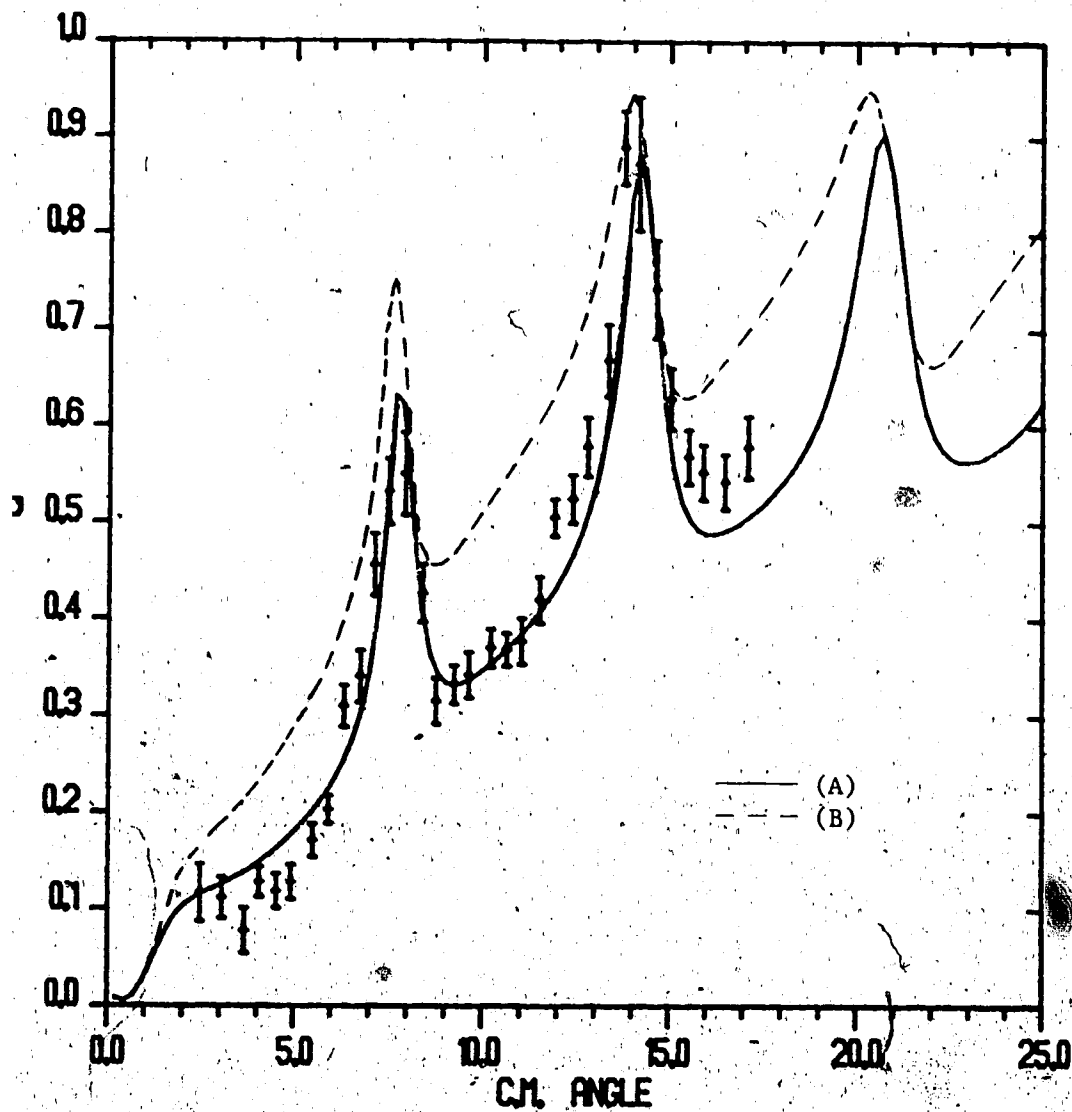
Figure III-12. Spin rotation parameter (Q) for p + ^{40}Ca
elastic scattering at E_p = 800 Mev.

The curves are Dirac optical model fits
calculated from the parameter sets of
table III-1.
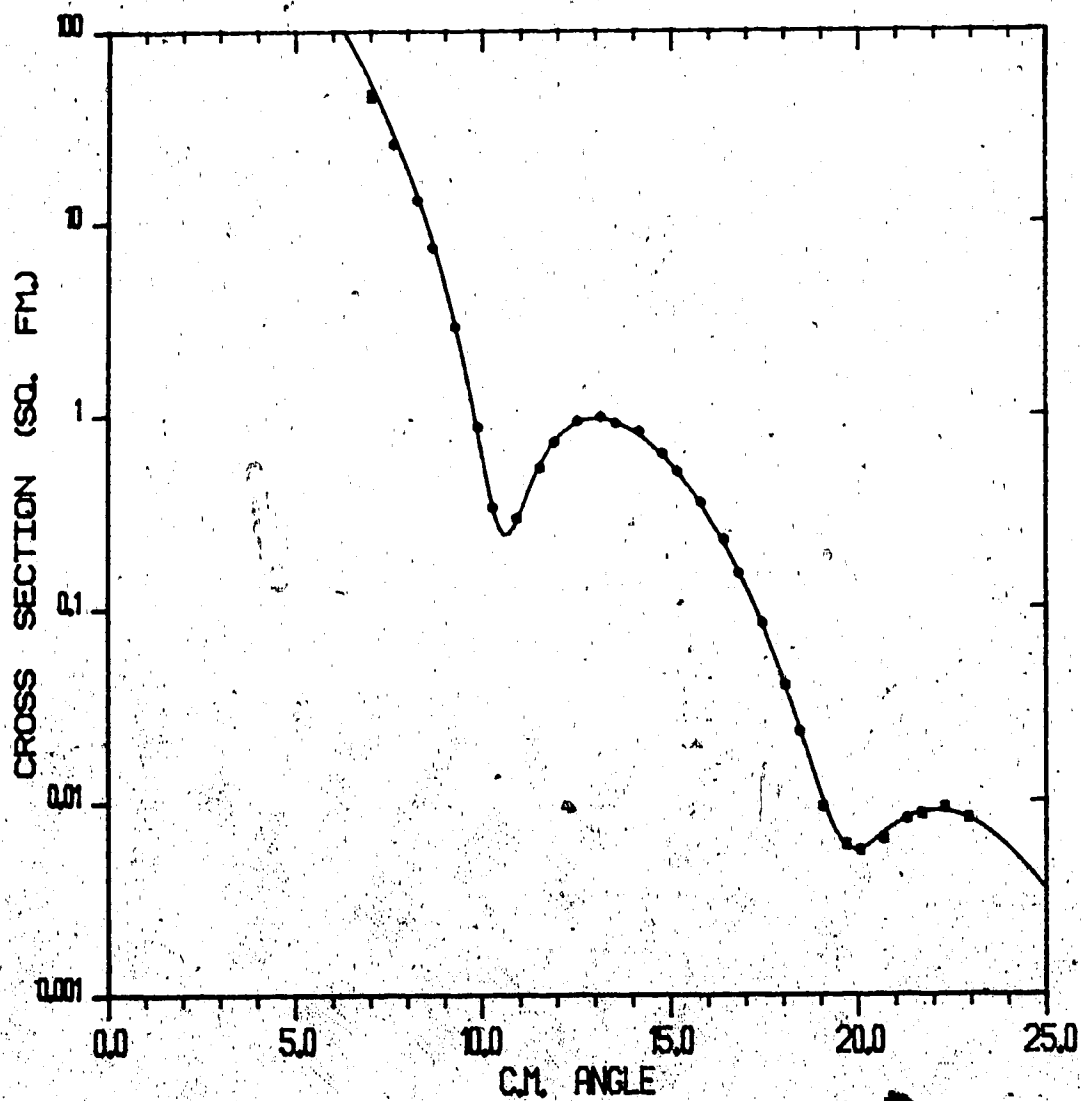
Figure III-13. Differential cross section for p + ^{20}Ne
elastic scattering at E_p = 800 Mev.

The curve is a Dirac optical model fit
calculated from the parameter set of
table III-2.
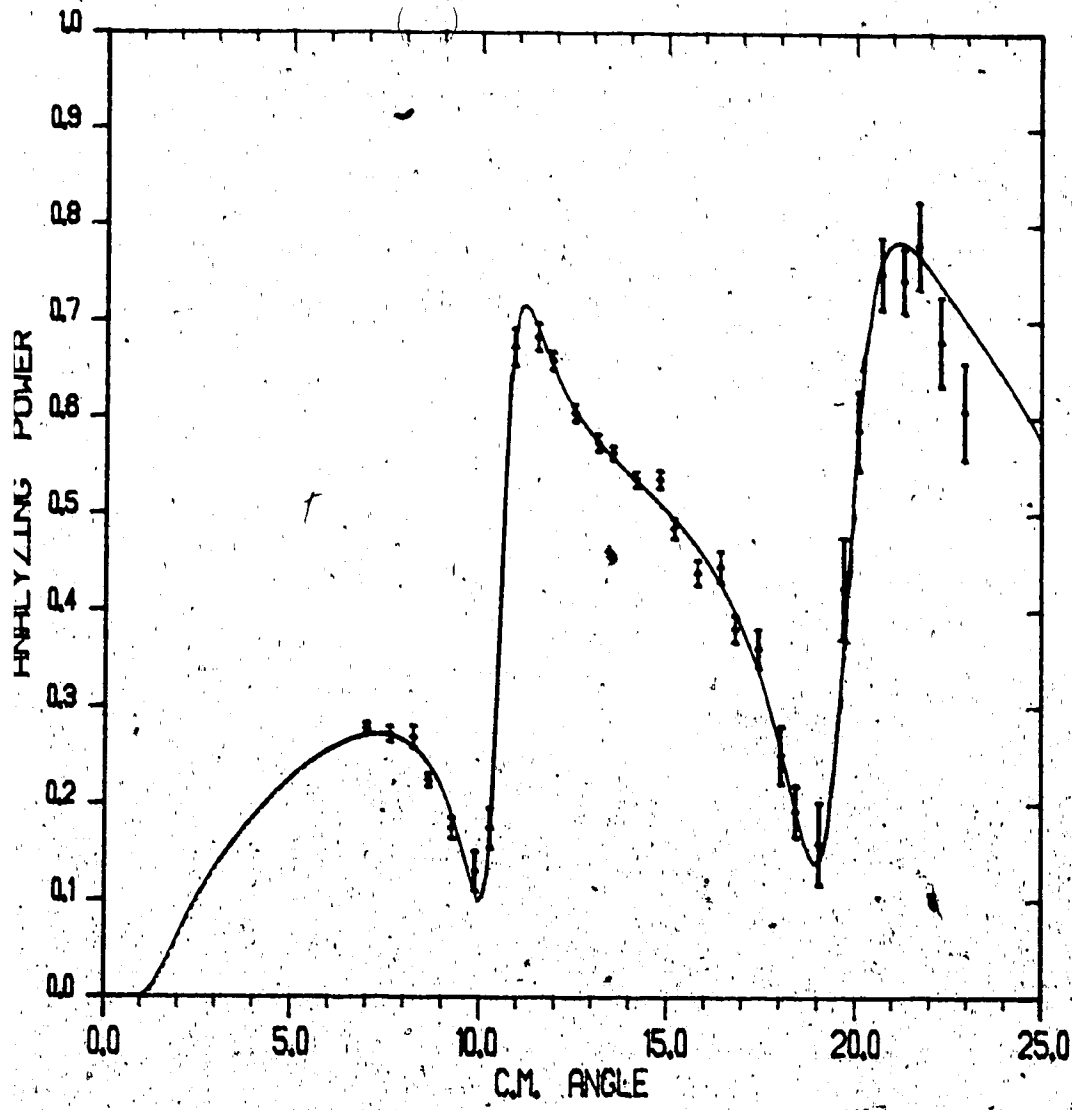
Figure III-14. Analyzing power for p + ^{20}Ne elastic scattering at E_p = 800 Mev.

The curve is a Dirac optical model fit calculated from the parameter set of table III-2.
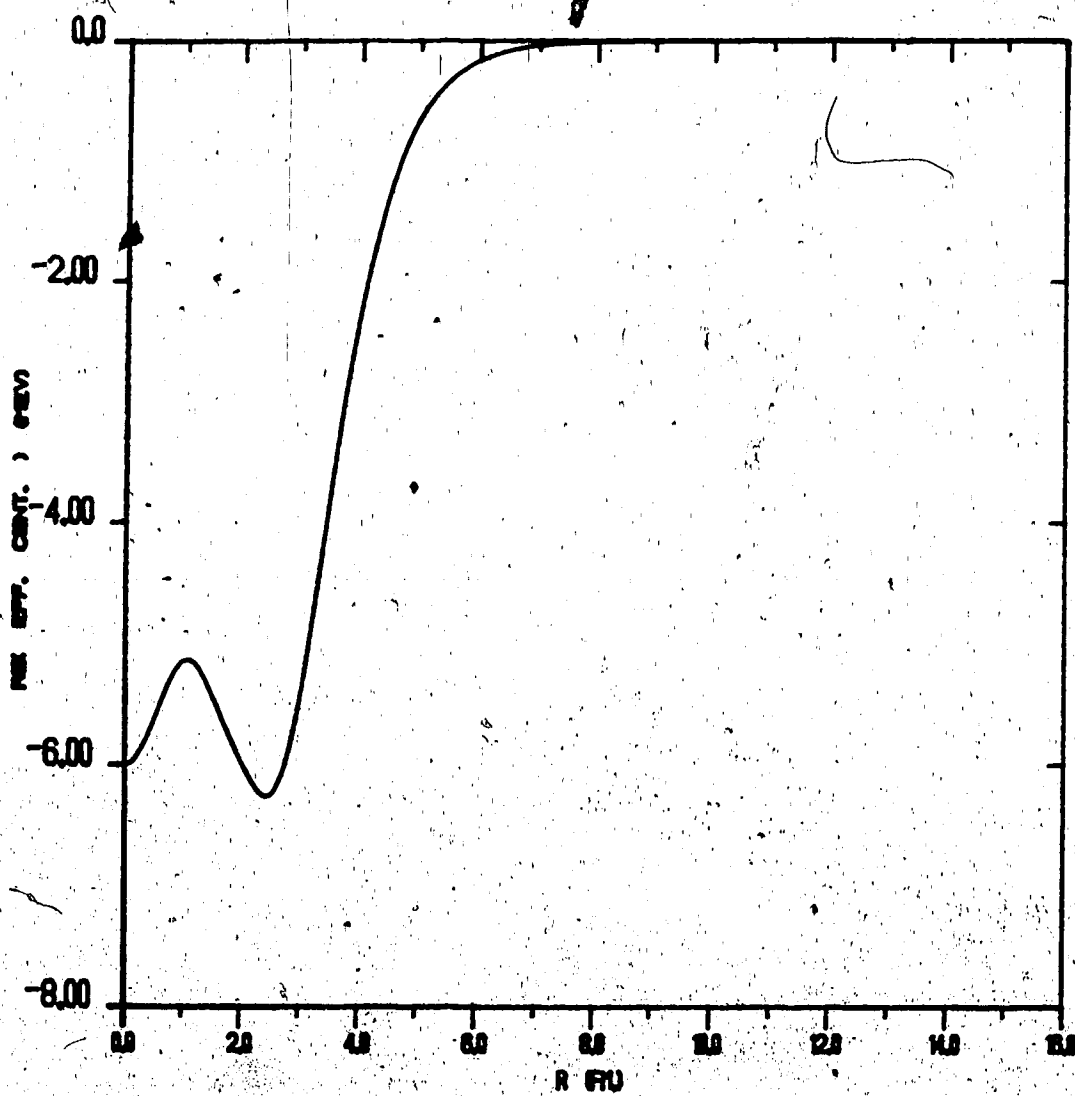
Figure III-15. The real part of the effective central potential for p + ^{12}C at E_p = 200 Mev.

The curve is from parameters obtained by a Dirac optical model fit.
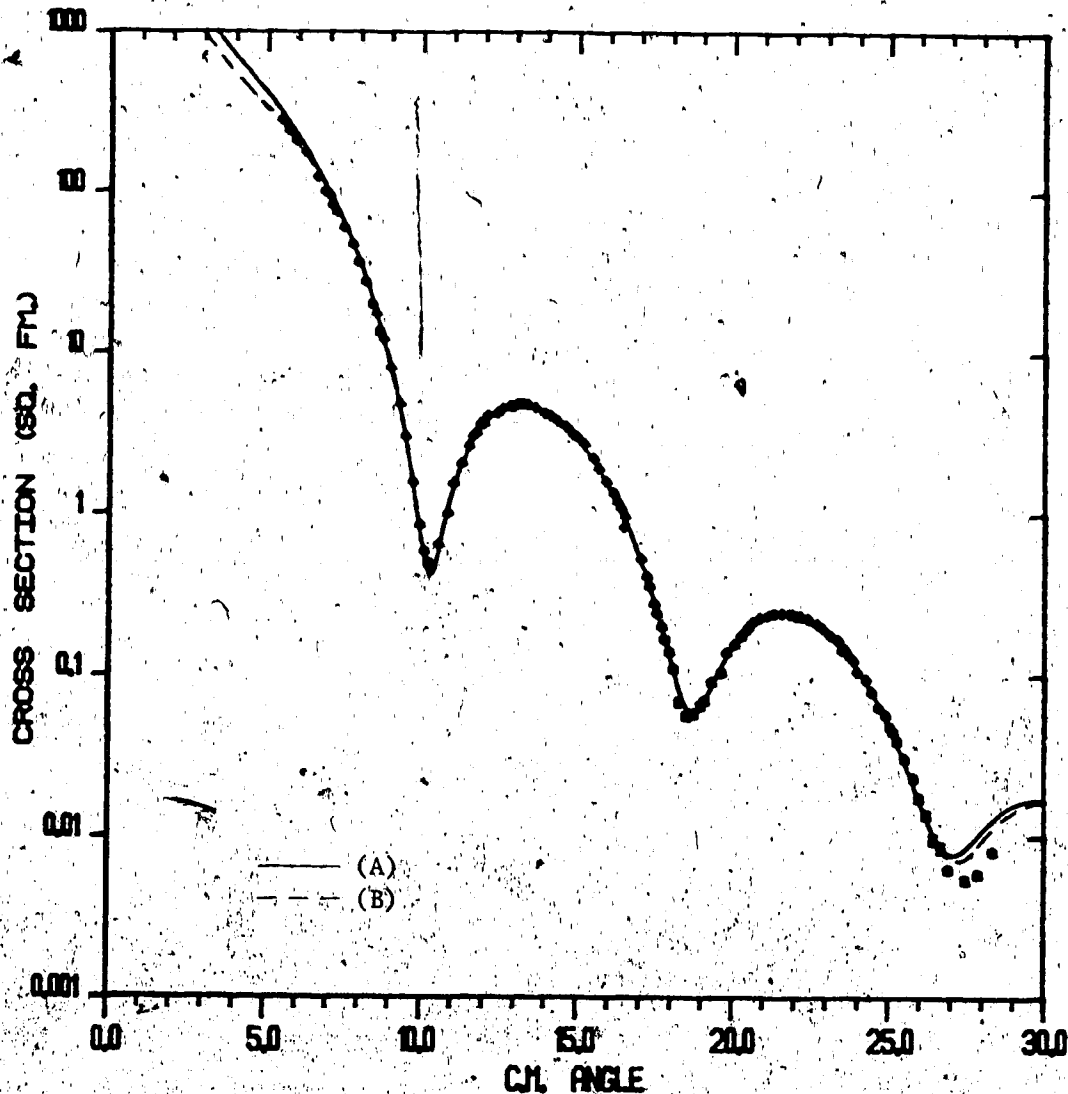
Figure III-16. Differential cross section for p + ^{48}Ca elastic scattering at E_p = 500 Mev.

The curves are Dirac optical model fits calculated from the parameter sets of table III-2.

Figure III-17. Analyzing power for p + ^{48}Ca elastic
scattering at E_p = 500 MeV.

The curves are Dirac optical model fits
calculated from the parameter sets of
table III-2.

Figure III-18. Differential cross section for p + ^{90}Zr
elastic scattering at E_p = 800 Mev.

The curves are Dirac optical model fits
calculated from the parameter sets of
table III-2.

Figure III-19. Analyzing power for p + ^{90}Zr elastic scattering at E_p = 800 Mev.

The curves are Dirac optical model fits calculated from the parameter sets of table III-2.

			This Work		Other Work		
			β	$\delta=\beta R$	β	$\delta=\beta R$	
^{40}Ca	362 Mev.	3⁻	0.36	1.25			
		5⁻	0.21	0.73			
	500 Mev.	2⁺	0.145	0.52	0.14	0.49	[Se85]
		3⁻	0.39	1.41	0.41	1.41	[Se85]
		5⁻	0.225	0.81	0.25	0.86	[Se85]
	800 Mev.	2⁺	0.13	0.45	0.13	0.46	[B182]
					0.17	0.52	[Ga82]
		3⁻	0.38	1.32	0.34	1.19	[B182]
					0.46	1.39	[Ga82]
		5⁻	0.225	0.78	0.22	0.77	[B182]
					0.25	0.76	[Ga82]
^{12}C	160 Mev.	2⁺	0.56 - 1.5	1.21 - 2.66			
	200 Mev.	2⁺	0.49 - 1.1	1.09 - 2.15	.67	1.63	[Jo86]
	400 Mev.	2⁺	0.61 - 1.17	1.36 - 2.30	.65	1.68	[Jo86]
^{20}Ne	800 Mev.	2⁺	0.64	1.63	0.65	1.68	[B184]
		3⁻	0.46	1.17			
		4⁺	0.45	1.15	0.38	0.98	[B184]
^{48}Ca	500 Mev.	2⁺	0.18	0.71	0.17	0.61	[Se85]
		3⁻	0.225	0.88	0.23	0.84	[Se85]
^{90}Zr	800 Mev.	2⁺	0.10	0.48	0.10	0.47	[Ga82]
		3⁻	0.19	0.91	0.19	0.89	[Ga82]
		4⁺	0.06	0.29	0.06	0.28	[Ga82]
		5⁻	0.085	0.41	0.088	0.41	[Ga82]

TABLE V-1. Deformation parameters and deformation lengths for various nuclei and energies.
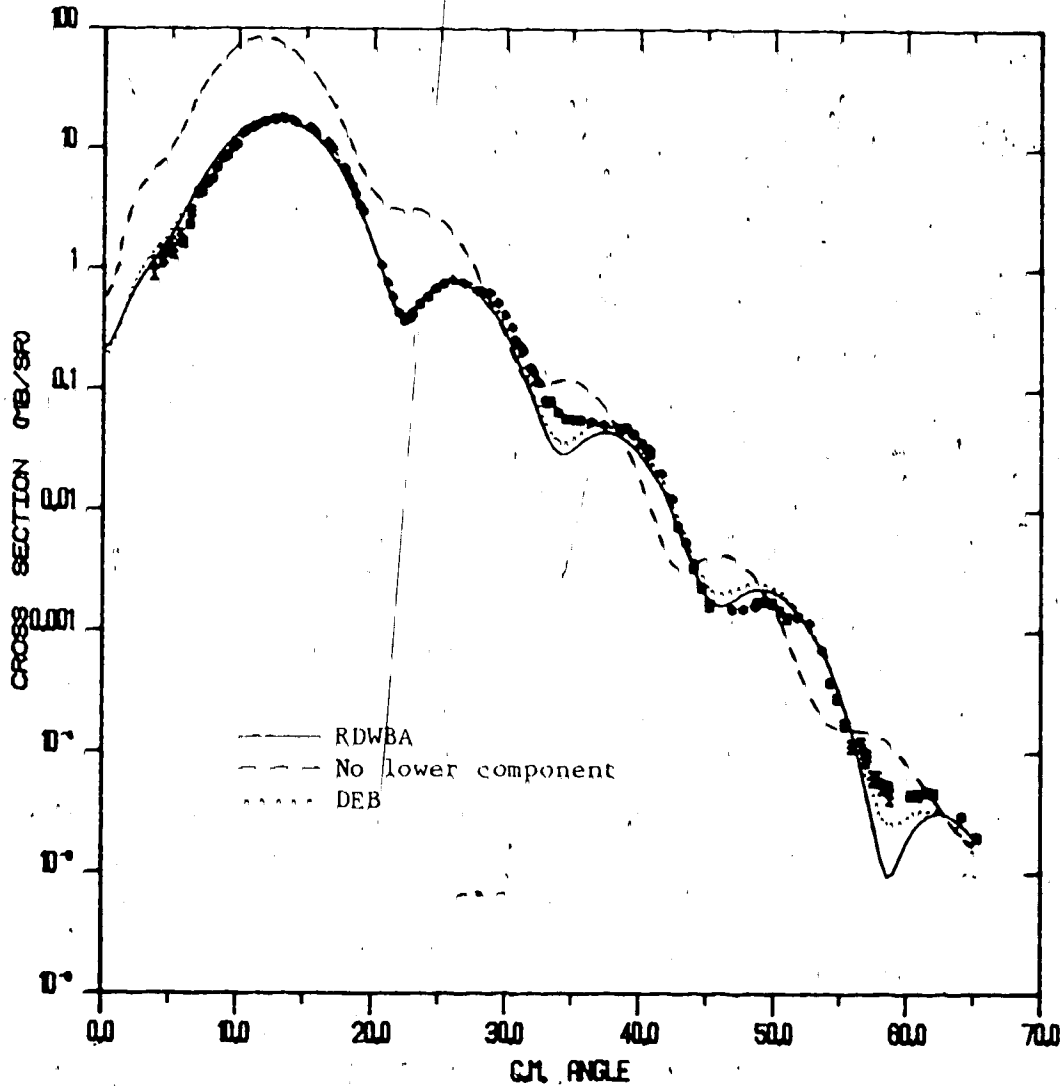
Figure V-1.   ·Differential cross section for p + ^{40}Ca
inelastic scattering to the 3^- state with
E_x = 3.7364 Mev. and E_p = 362 Mev.

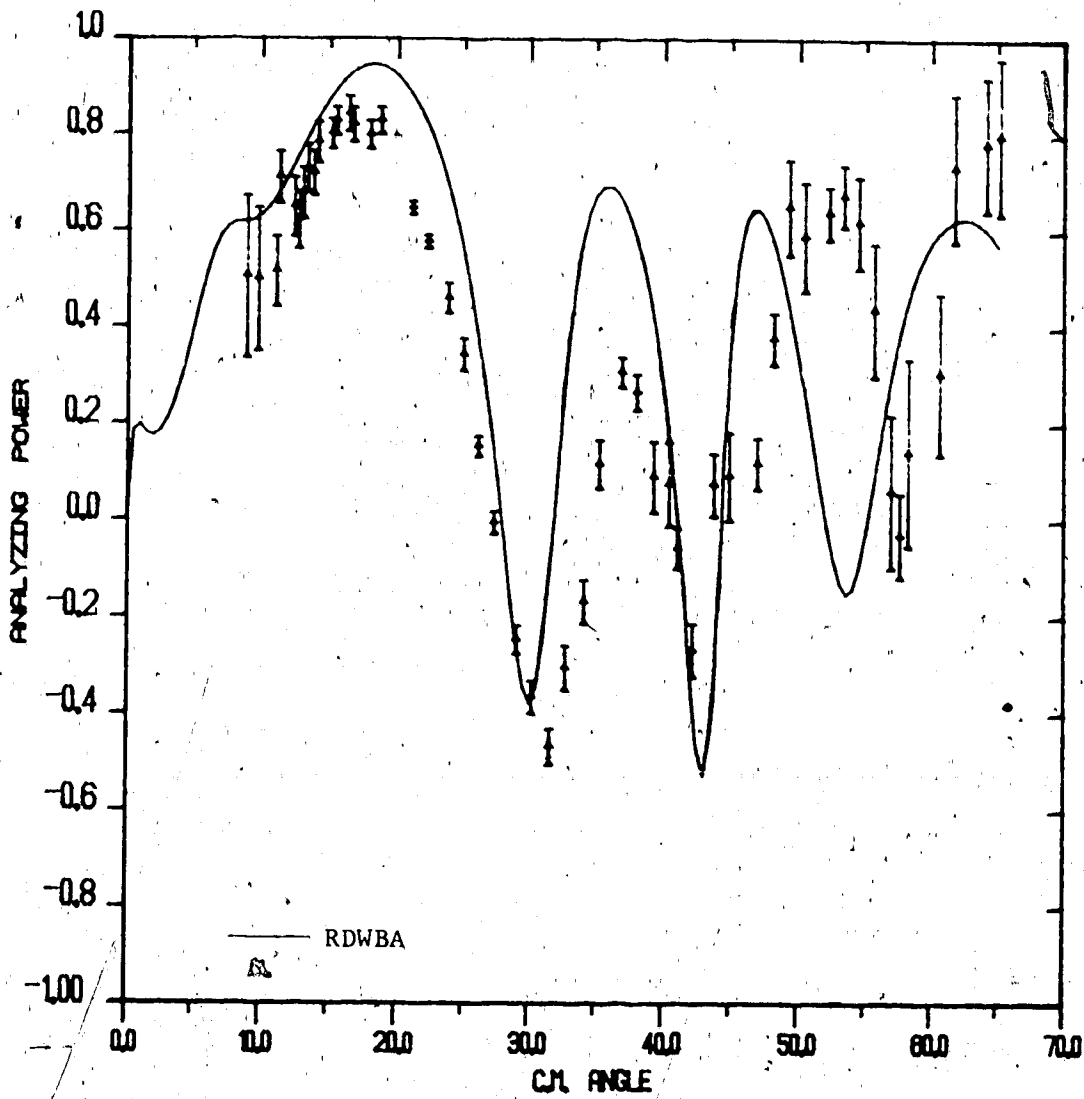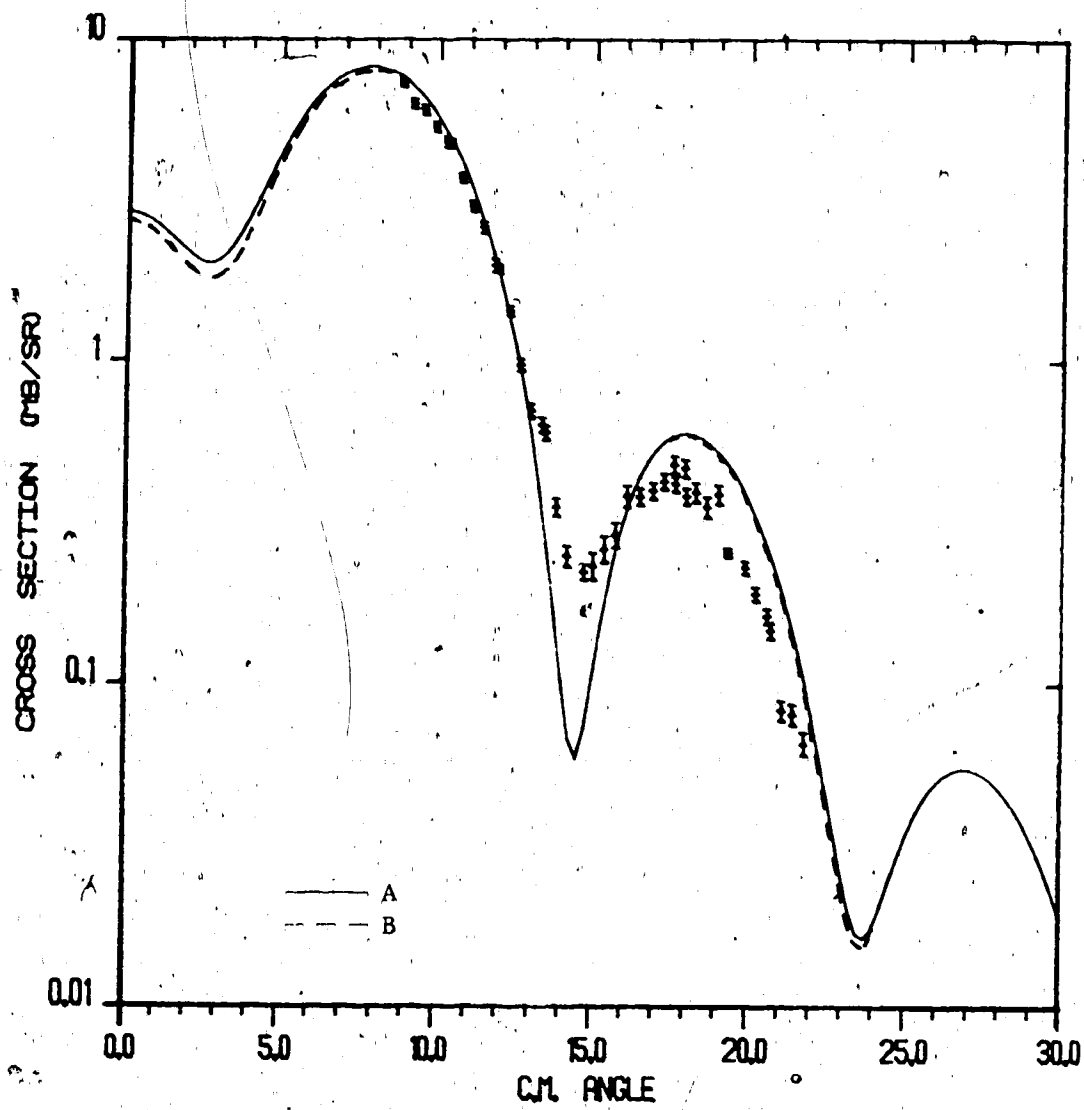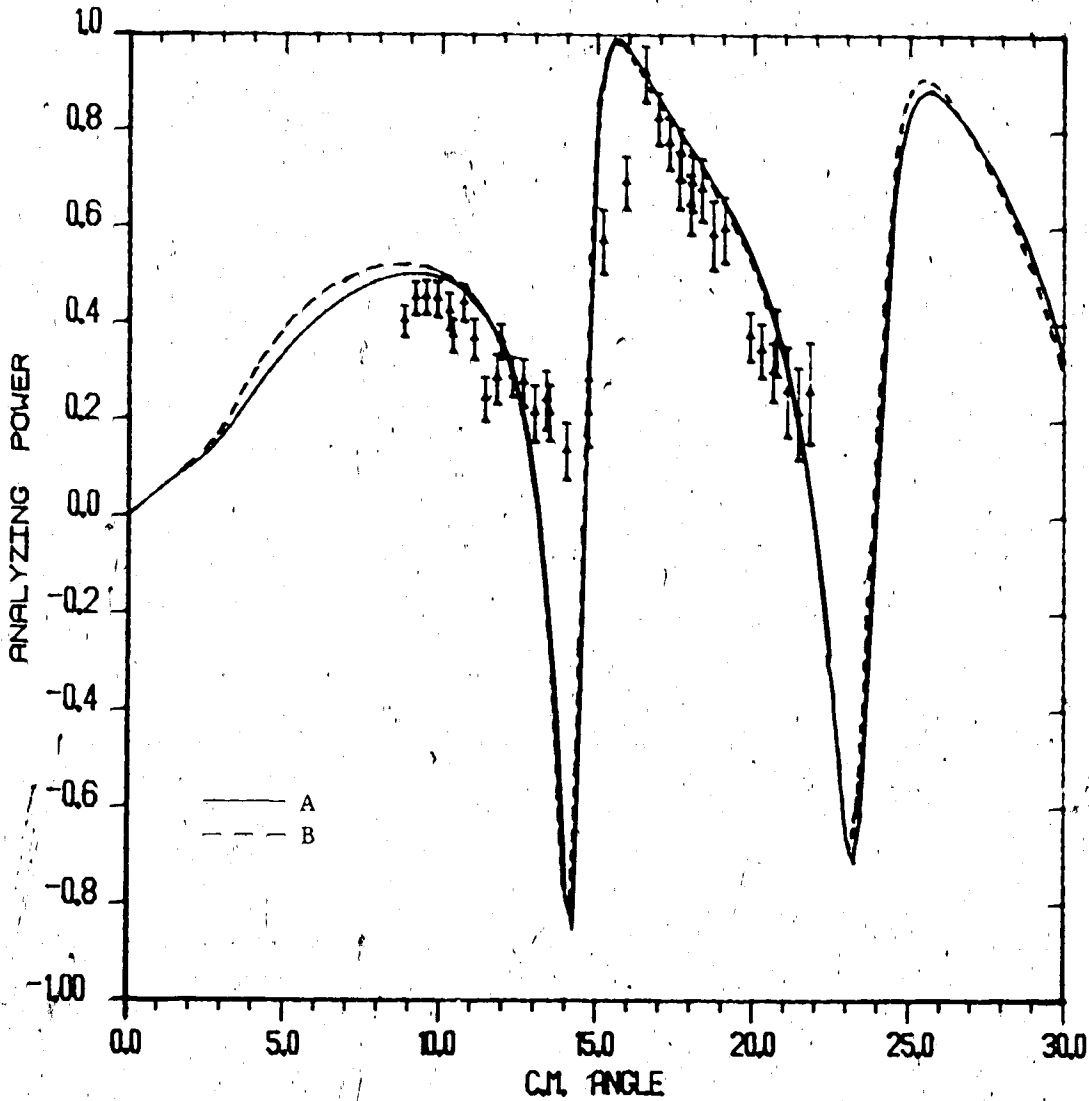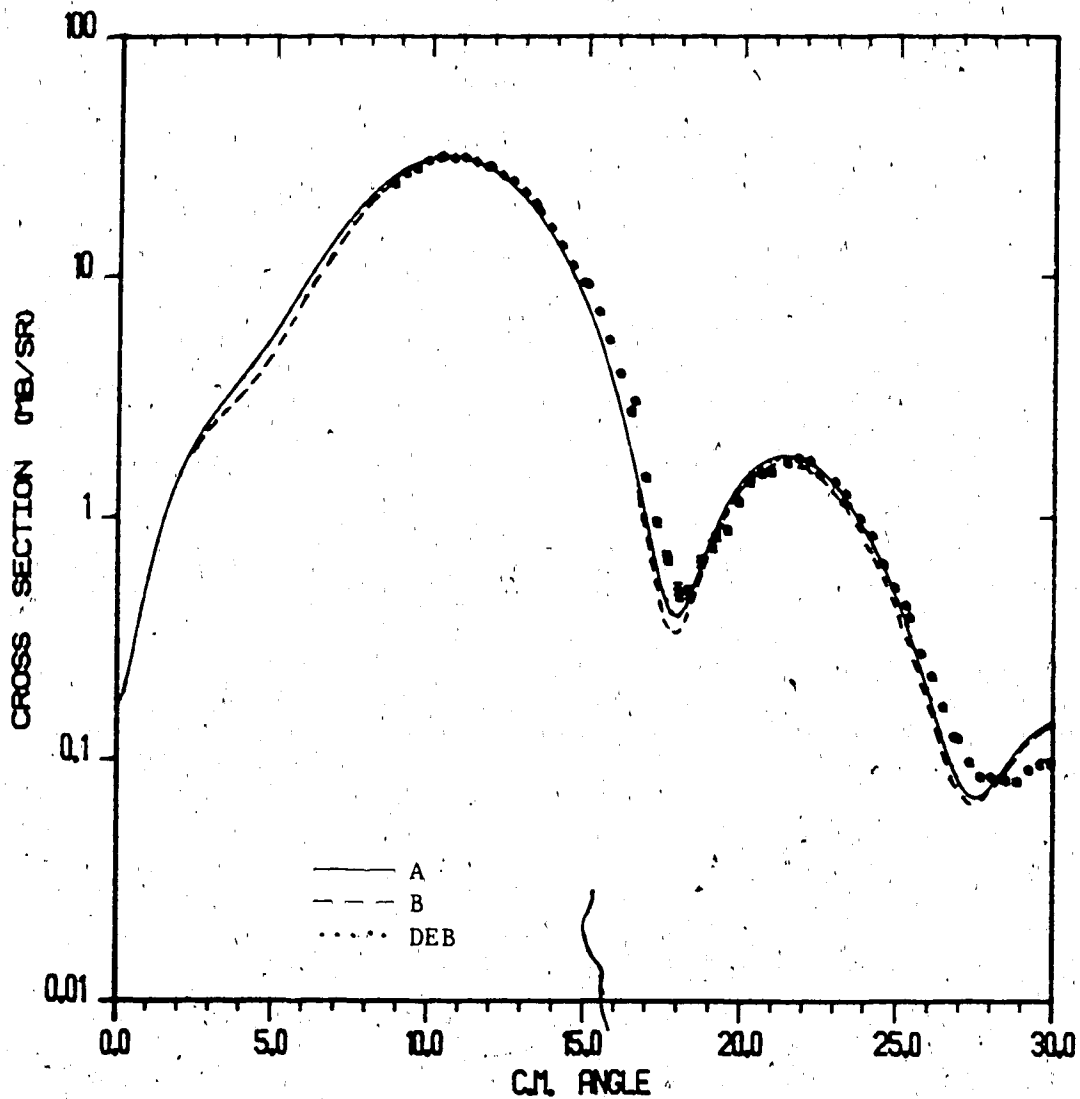The curves are calculated using the parameter
set of table III-1. The solid curve is the
RDWBA calculation, the dashed curve is RDWBA
with the lower component set to zero, and the
dotted curve is the DEB calculation.
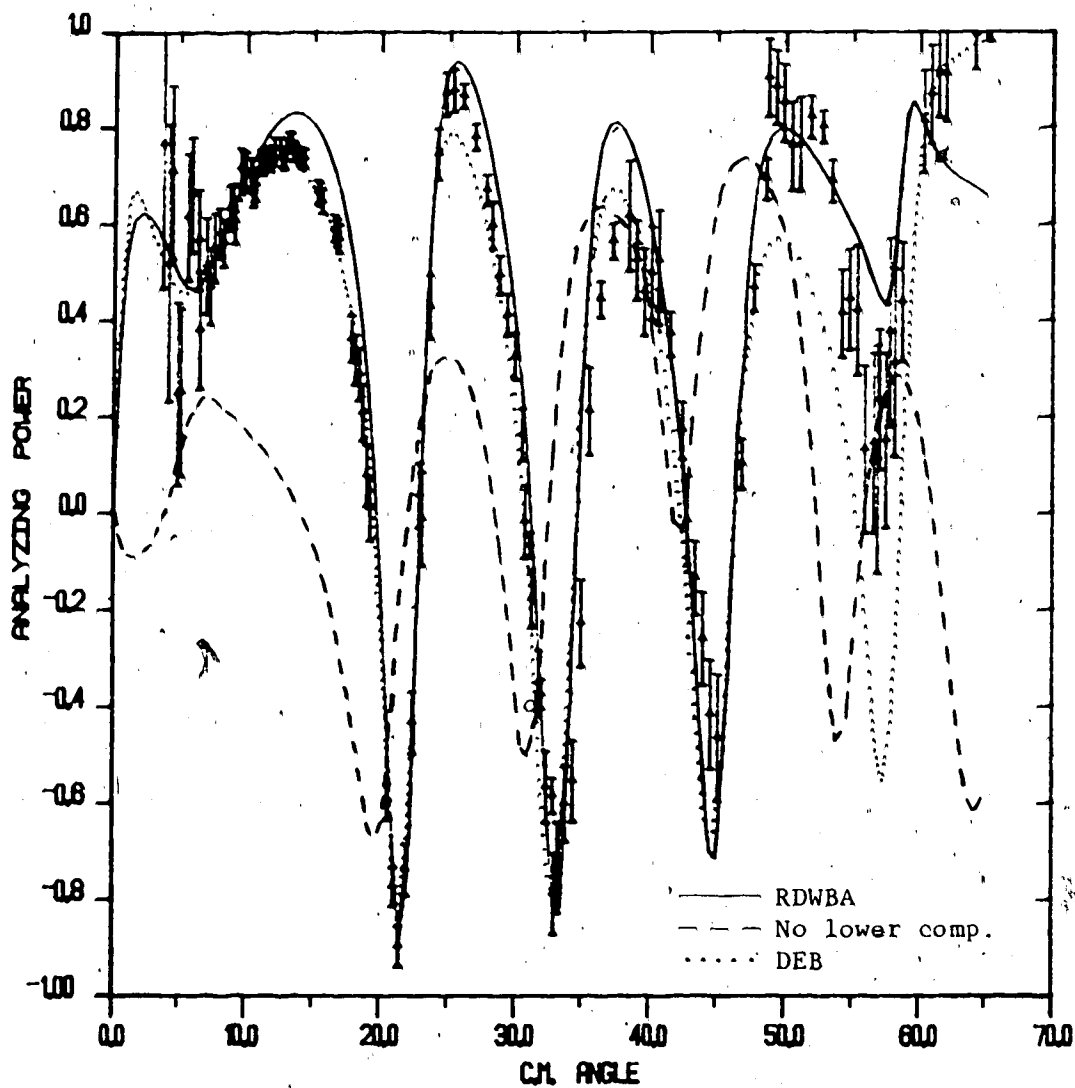
Figure V-2. Analyzing power for p + ^{40}Ca inelastic scattering to the 3$^-$ state with E_x = 3.7364 Mev. and E_p = 362 Mev.

The curves are described in the previous figure.
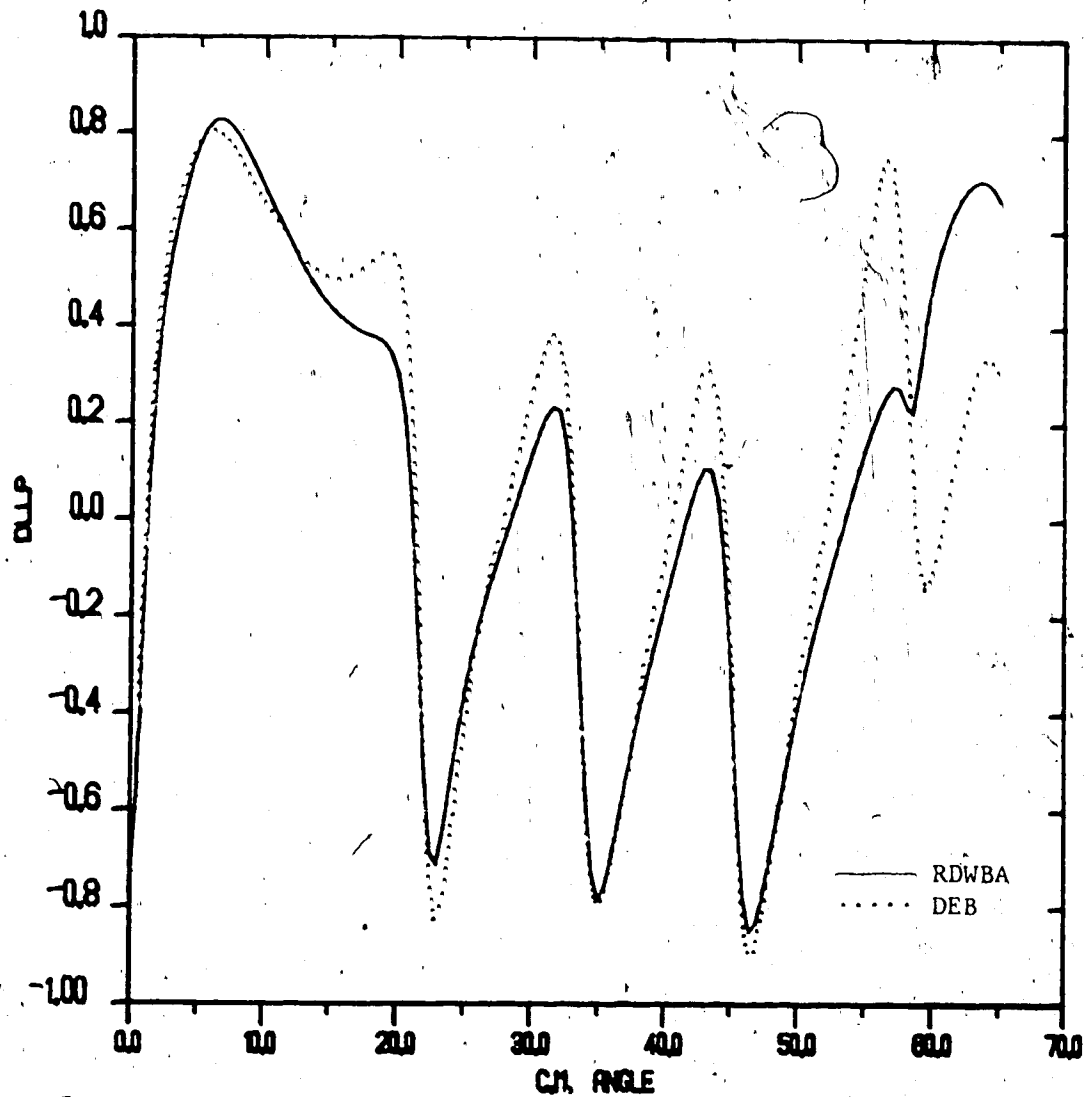
Figure V-3.   A polarization transfer coefficient for
p + ^{40}Ca inelastic scattering to the 3$^-$ state
with E_x = 3.7364 Mev. and E_p = 362 Mev.

The curves are calculated using the parameter
set of table III-1. The solid curve is the
RDWBA calculation and the dotted curve is the
DEB calculation.
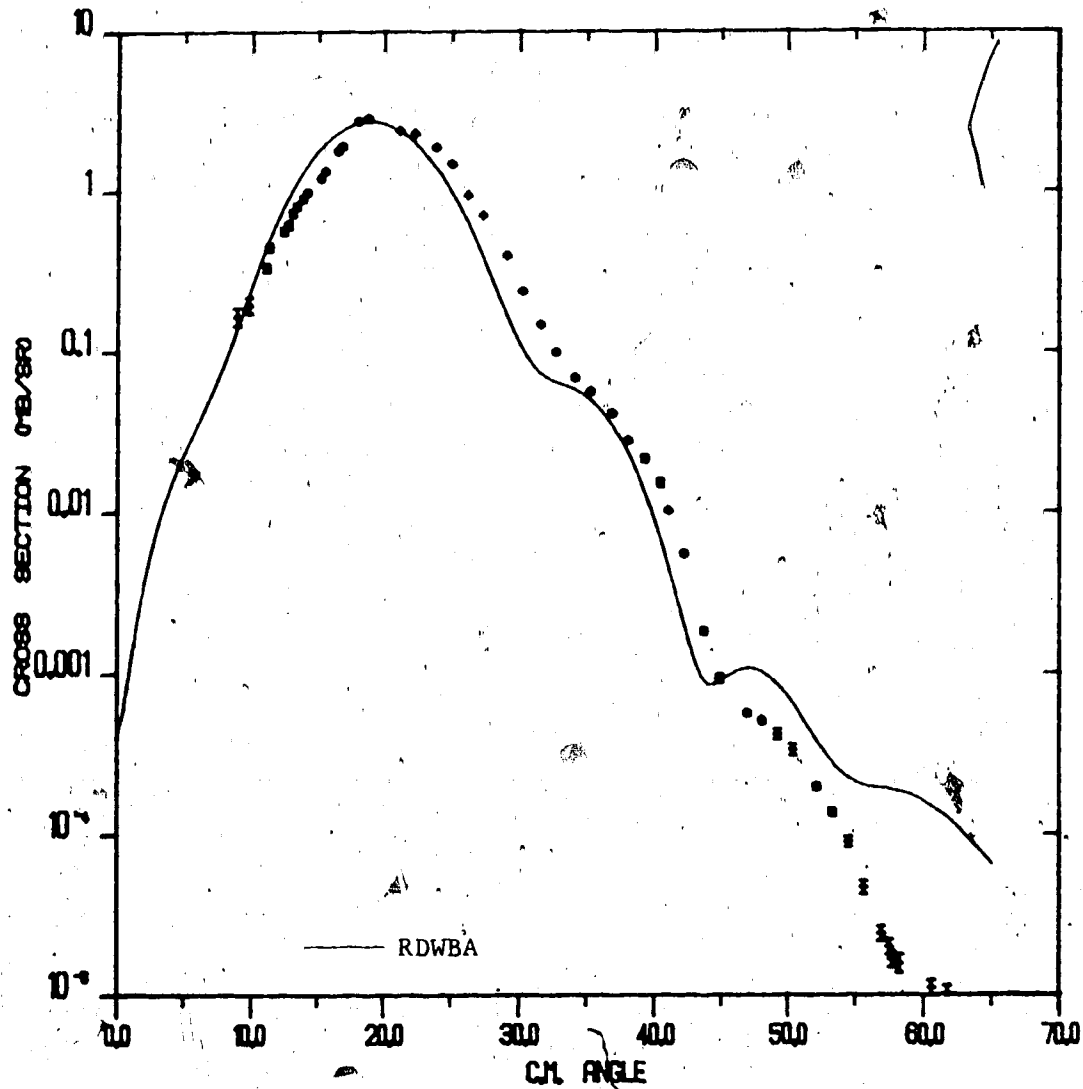
Figure V-4.   Différential cross section for p + ^{40}Ca inelastic scattering to the 5$^-$ state with E_x = 4.4915 Mev. and E_p = 362 Mev.

The curve is the RDWBA calculation using the parameter set of table III-1.
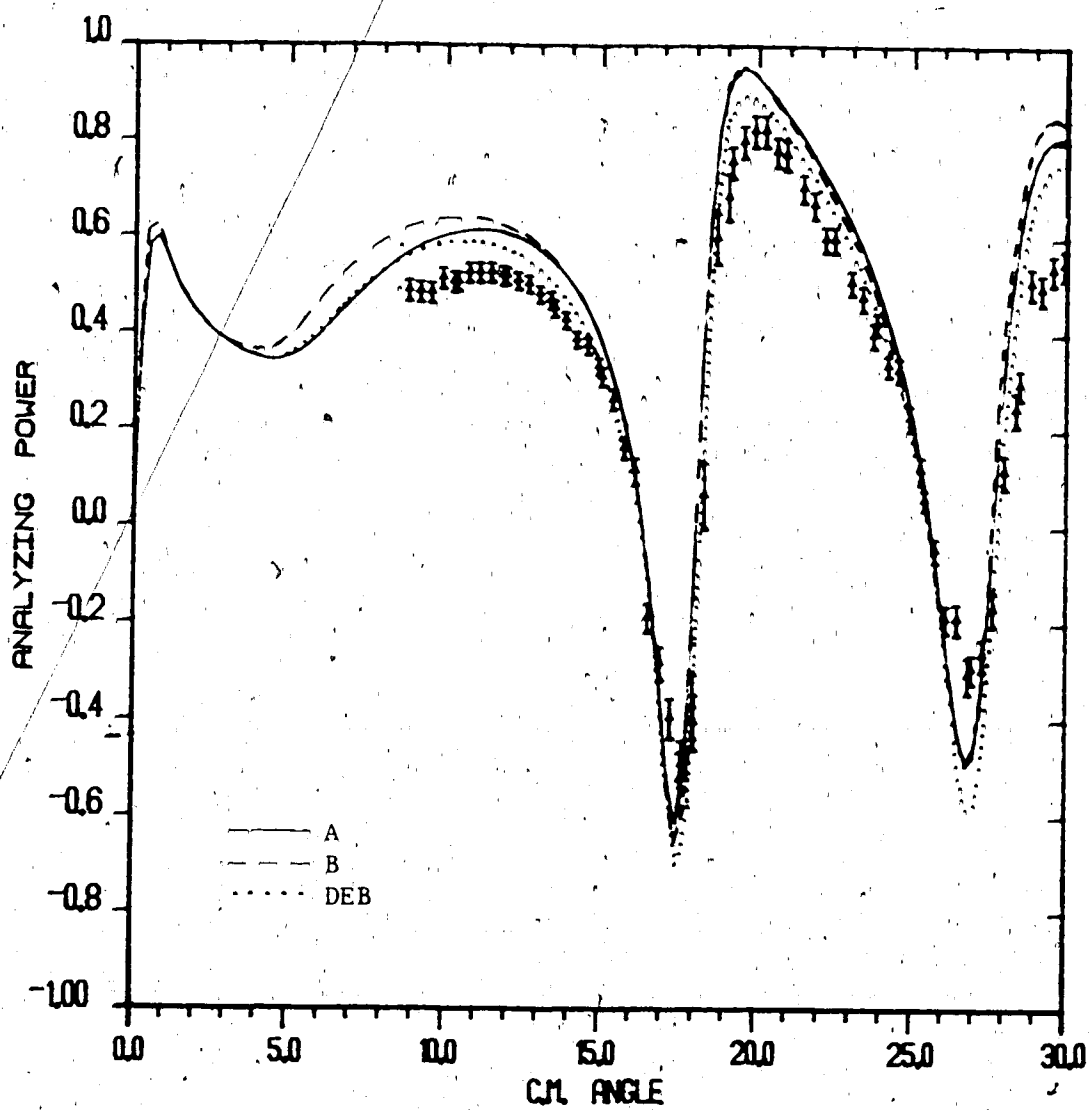
Figure V-5.   Analyzing power for p + ^{40}Ca inelastic
scattering to the 5$^-$ state with E_x = 4.4915 Mev.
and E_p = 362 Mev.

The curve is the RDWBA calculation using the
parameter set of table III-1.

Figure V-6.   Differential cross section for $p + {}^{40}Ca$ inelastic scattering to the 2^+ state with $E_x = 3.9041$ Mev. and $E_p = 500$ Mev.

The curves are RDWBA calculations using the parameter sets of table III-1.

Figure V-7.   Analyzing power for p + ^{40}Ca inelastic
              scattering to the 2^+ state with E_x = 3.9041 Mev.
              and E_p = 500 Mev.

The curves are RDWBA calculations using the
parameter sets of table III-1.

Figure V-8.   Differential cross section for p + ^{40}Ca
inelastic scattering to the 3$^-$ state with
E_x = 3.7364 Mev. and E_p = 500 Mev.

The curves are calculated using the parameter
sets of table III-1. The solid and dashed curves
are RDWBA calculations and the dotted curve is
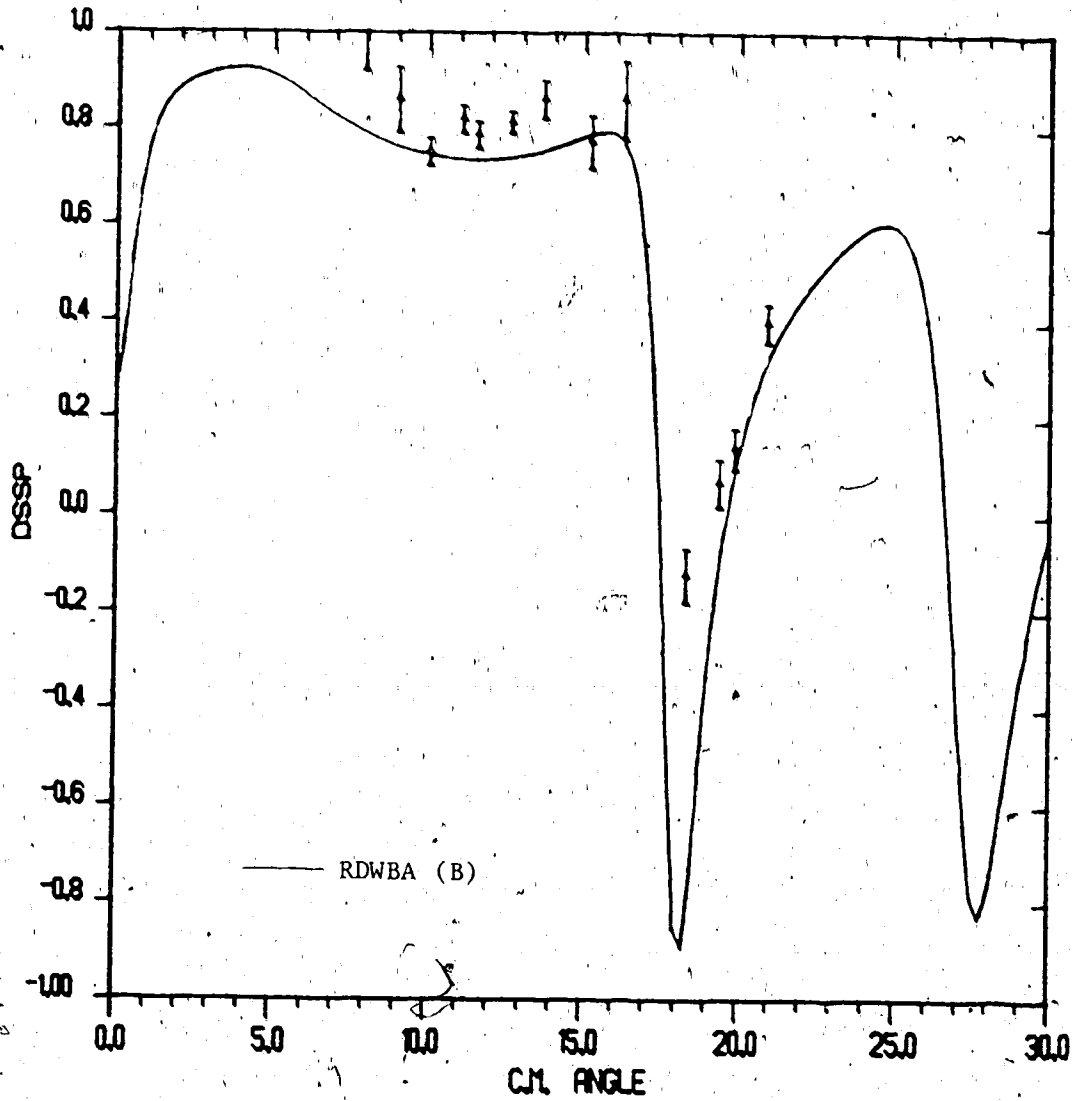a DEB calculation using parameter set A.

Figure V-9.   Analyzing power for p + ^{40}Ca inelastic scattering to the 3$^-$ state with E_x = 3.7364 Mev. and E_p = 500 Mev.
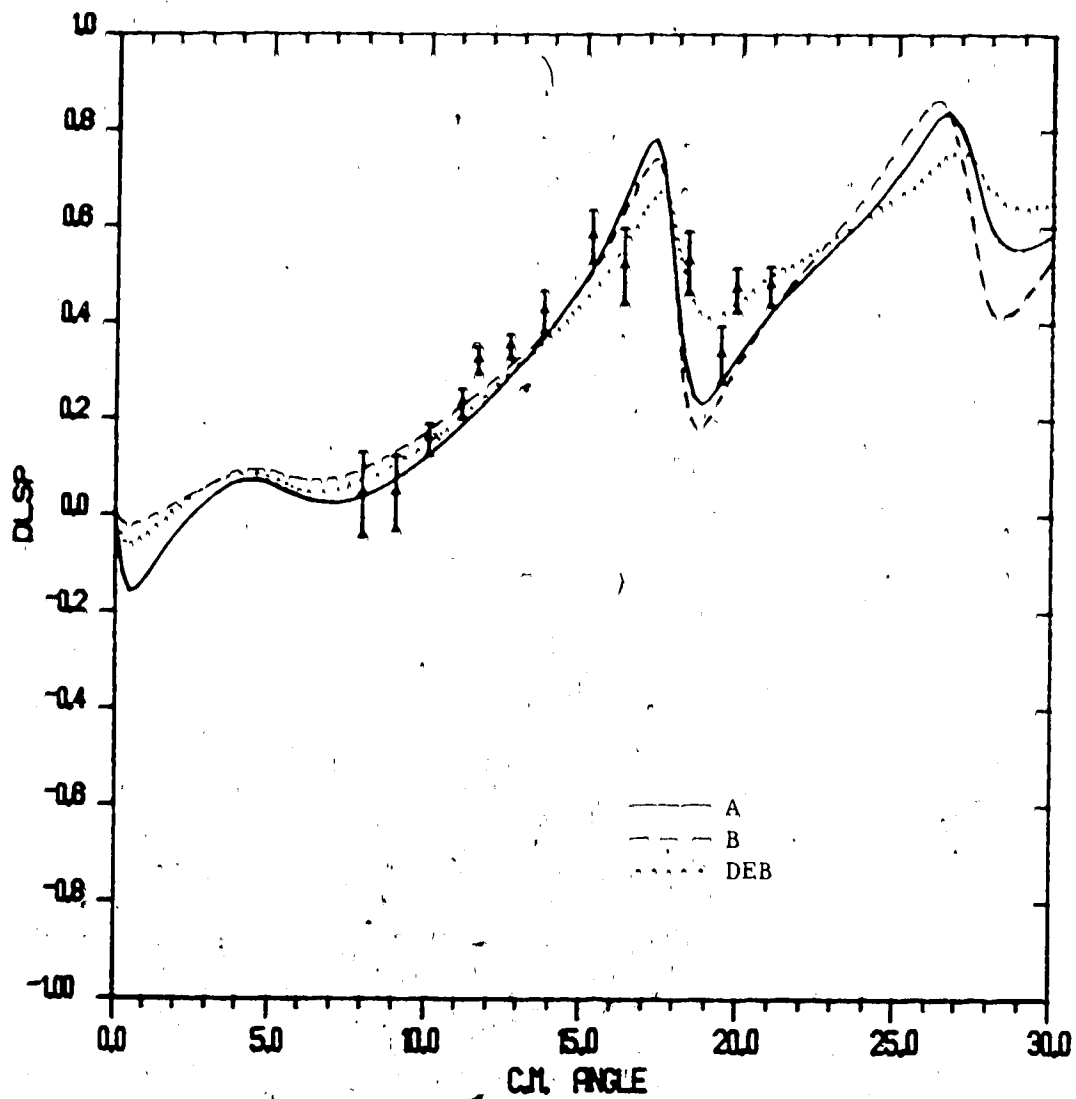
The curves are described in the previous figure.
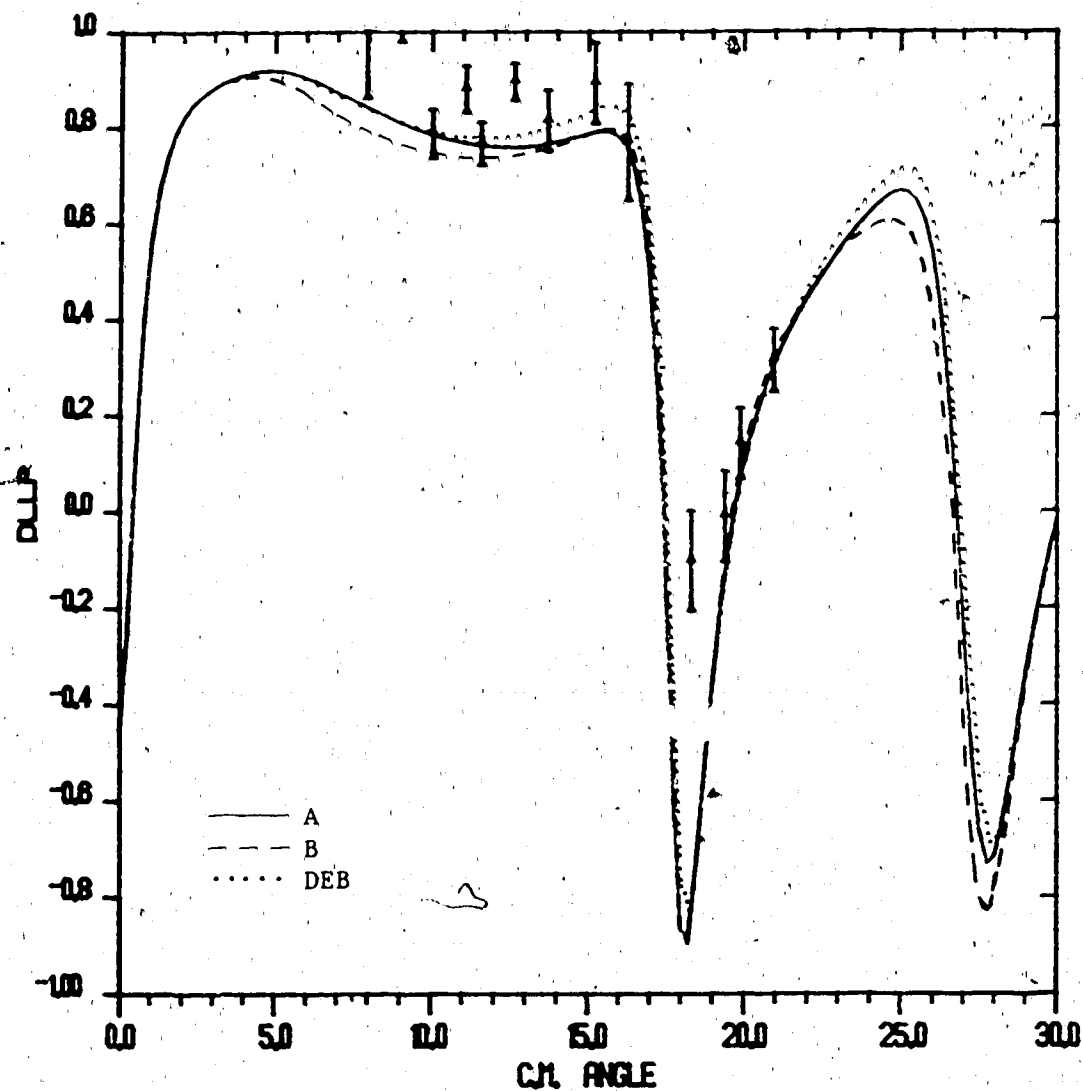
Figure V-10.   Polarization transfer coefficient for
p + ^{40}Ca inelastic scattering to the 3$^-$ state
with E_x = 3.7364 Mev. and E_p = 500 Mev.

The curves are calculated using the parameter
sets of table III-1. The solid and dashed curves
are RDWBA calculations and the dotted curve is
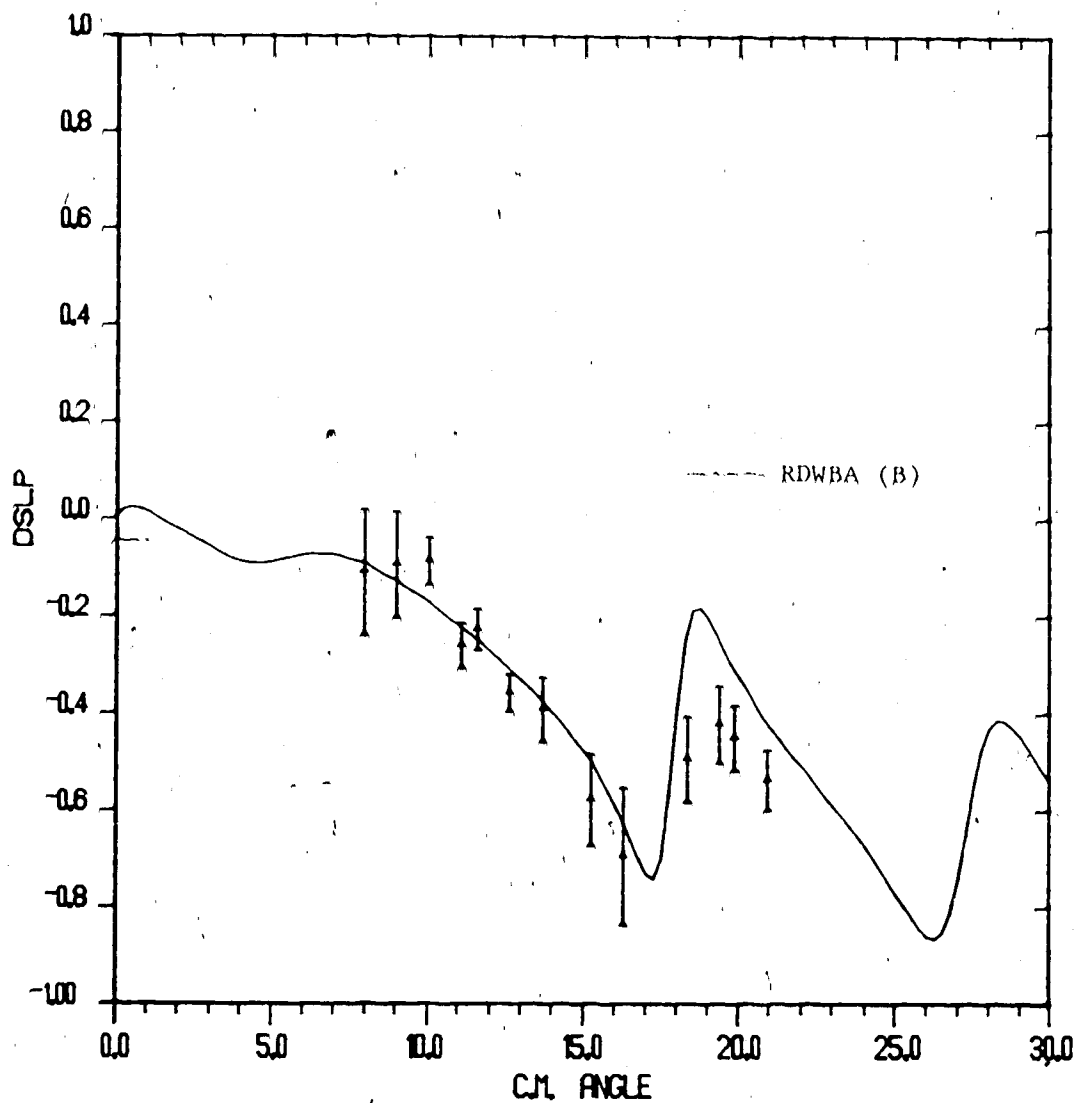a DEB calculation using parameter set A.

Figure V-11. Polarization transfer coefficient for
p + ^{40}Ca inelastic scattering to the 3$^-$ state
with E_x = 3.7364 Mev. and E_p = 500 Mev.

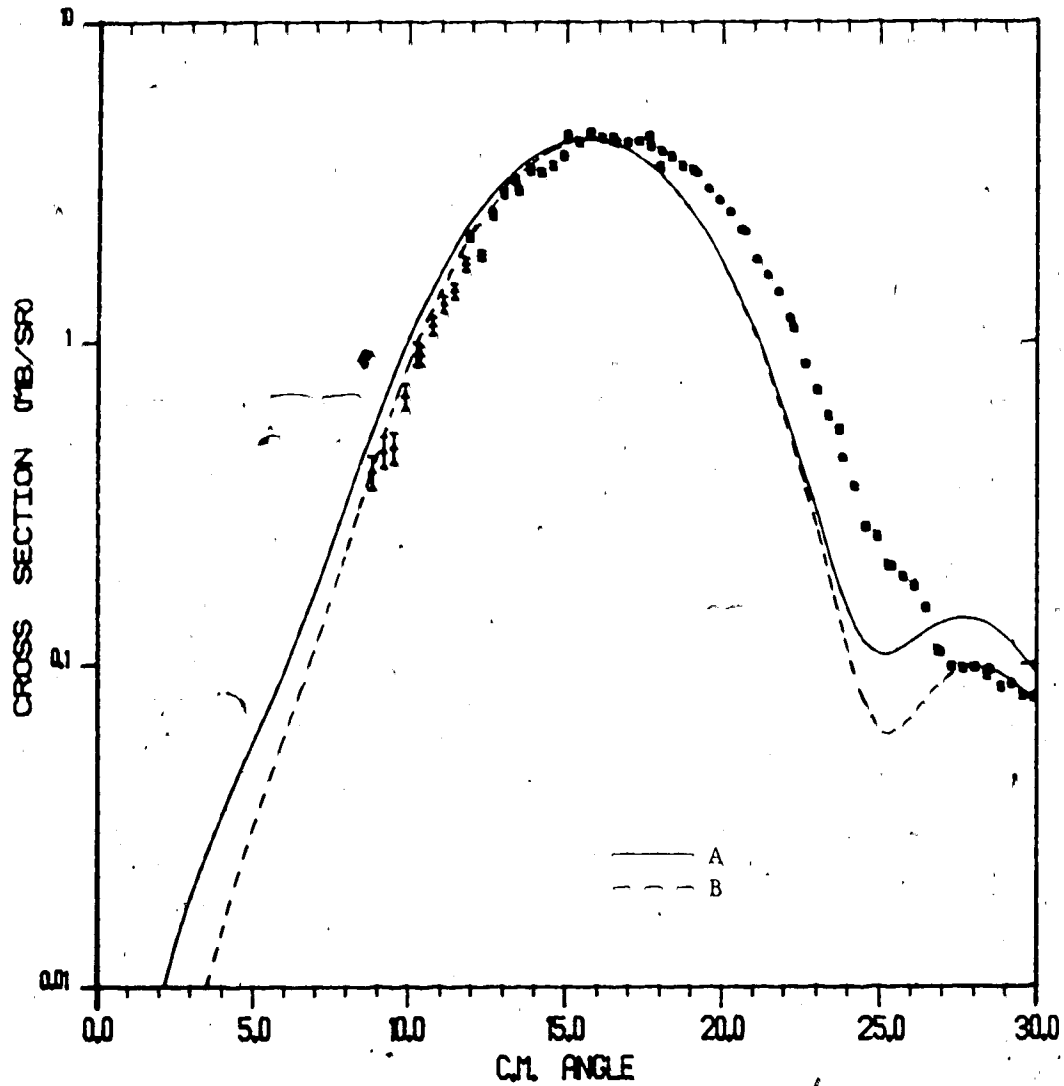The curve is an RDWBA calculation using
parameter set B of table III-1.

Figure V-12.   Polarization transfer coefficient for p + ^{40}Ca inelastic scattering to the 3⁻ state with E_x = 3.7364 Mev. and E_p = 500 Mev.

The curves are calculated using the parameter sets of table III-1. The solid and dashed curves are RDWBA calculations and the dotted curve is a DEB calculation using parameter set A.

Figure V-13.   Polarization transfer coefficient for
p + ^{40}Ca inelastic scattering to the 3^- state
with E_x = 3.7364 Mev. and E_p = 500 Mev.

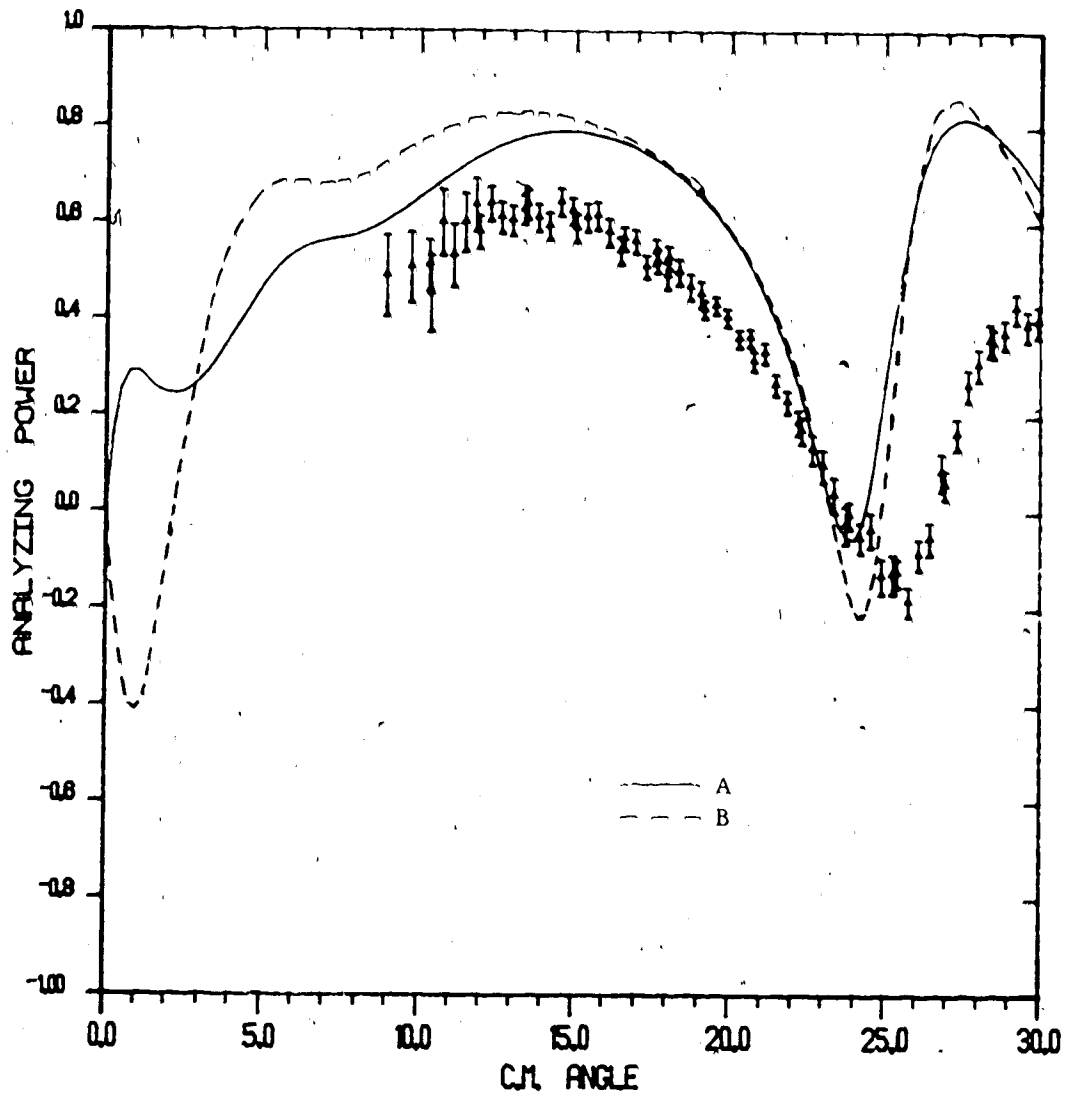The curve is an RDWBA calculation using
parameter set B of table III-1.

Figure V-14.   Differential cross section for $p + {}^{40}Ca$
                inelastic scattering to the 5^- state with
                $E_x = 4.4915$ Mev. and $E_p = 500$ Mev.

                The curves are RDWBA calculations using the
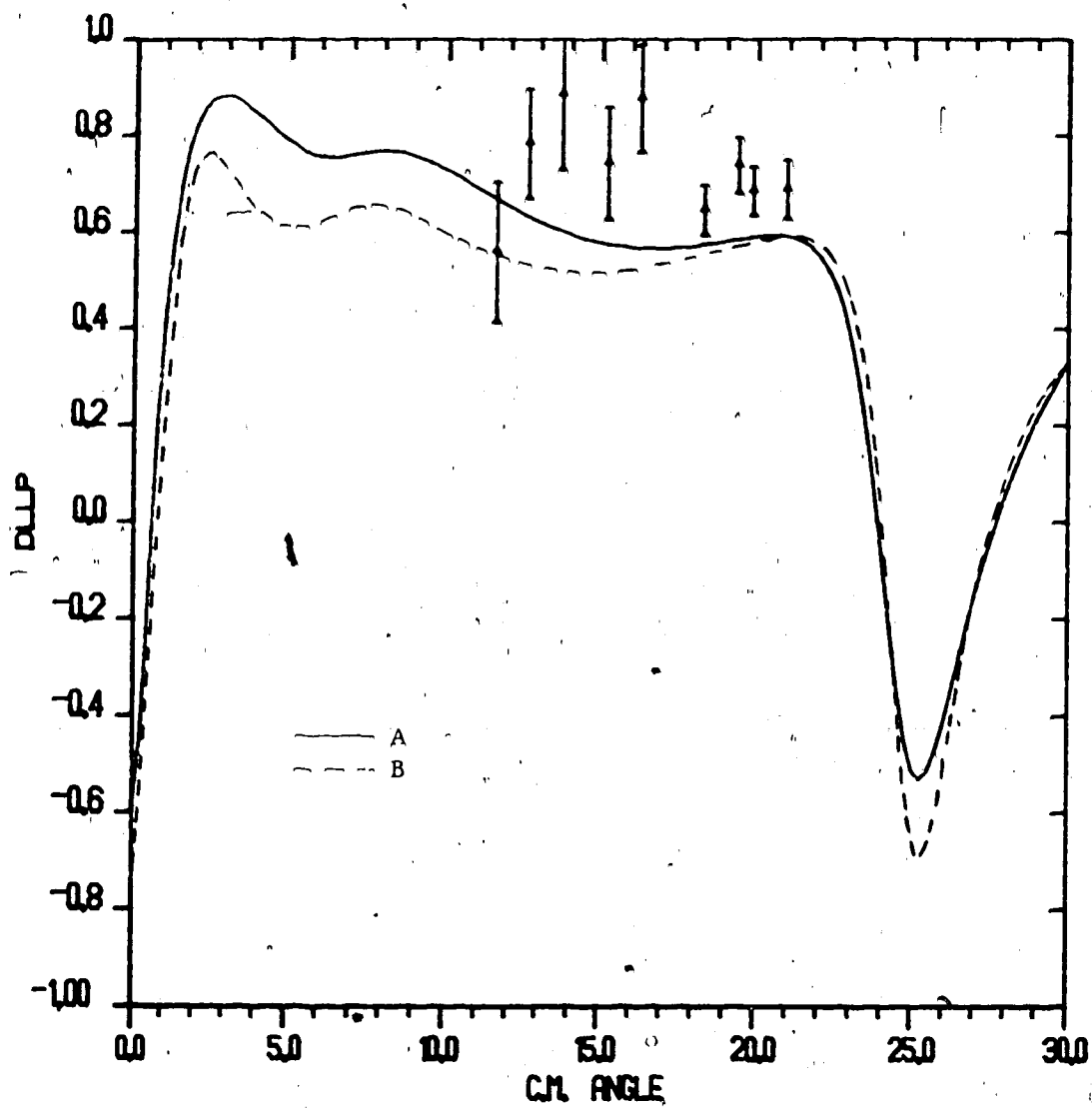   parameter sets of table III-1.

Figure V-15.   Analyzing power for p + ^{40}Ca inelastic
scattering to the 5$^-$ state with $E_x = 4.4915$ Mev.
and $E_p = 500$ Mev.

The curves are RDWBA calculations using the
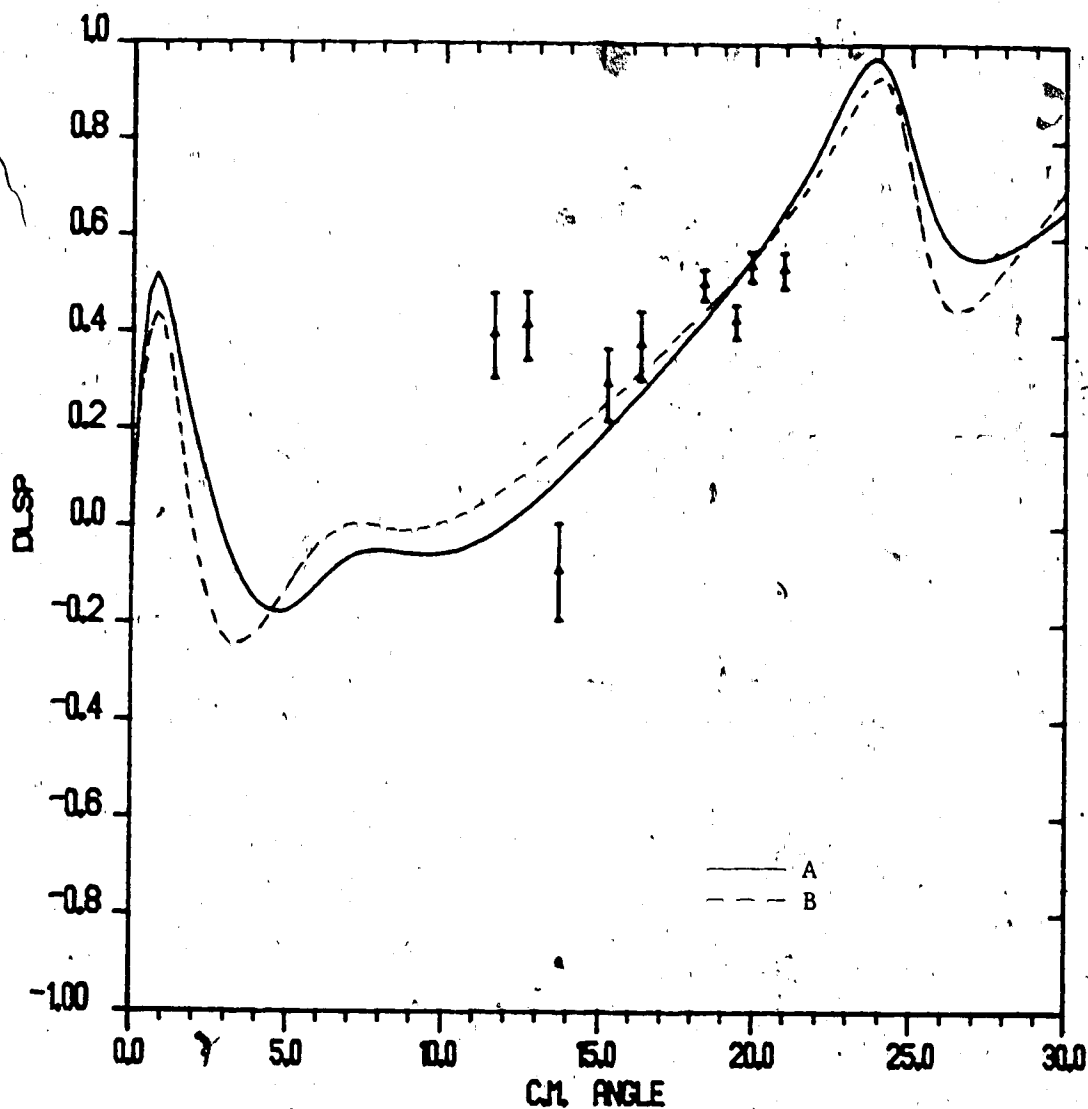parameter sets of table III-1.

Figure V-16.   Polarization transfer coefficient for
p + ^{40}Ca inelastic scattering to the 5$^-$ state
with E_x = 4.4915 Mev. and E_p = 500 Mev.

The curves are RDWBA calculations using the
parameter sets of table III-1.

Figure V-17.   Polarization transfer coefficient for
p + ^{40}Ca inelastic scattering to the 5$^-$ state
with E_x = 4.4915 Mev. and E_p = 500 Mev.

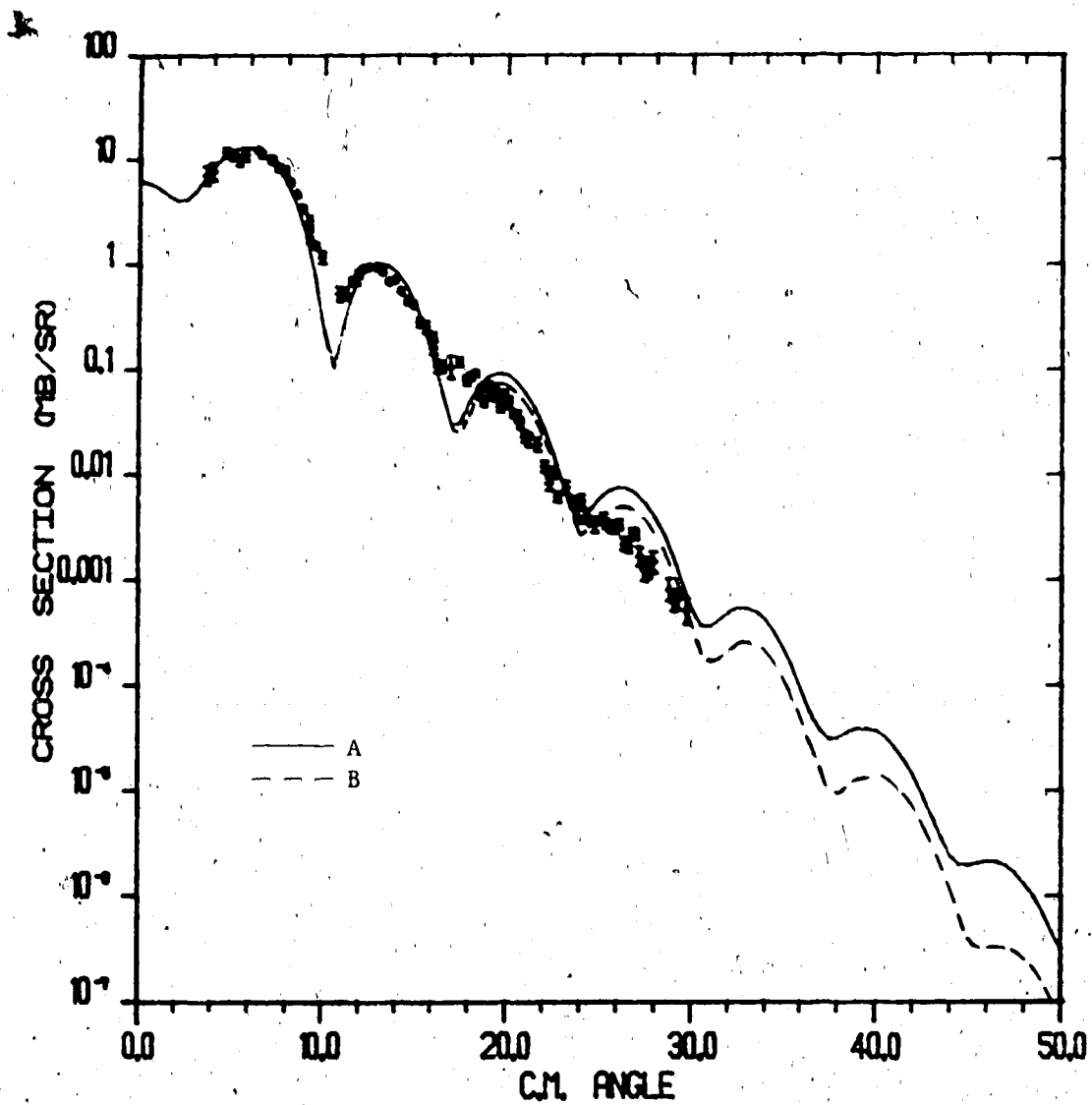The curves are RDWBA calculations using the
parameter sets of table III-1.

Figure V-18.   Differential cross section for p + ^{40}Ca
inelastic scattering to the 2$^+$ state with
E_x = 3.9041 Mev. and E_p = 800 Mev.

The curves are RDWBA calculations using
the parameters of table III-1.

Figure V-19.   Analyzing power for p + ^{40}Ca inelastic
scattering to the 2^+ state with E_x = 3.9041 Mev.
and E_p = 800 Mev.

The curves are RDWBA calculations using the
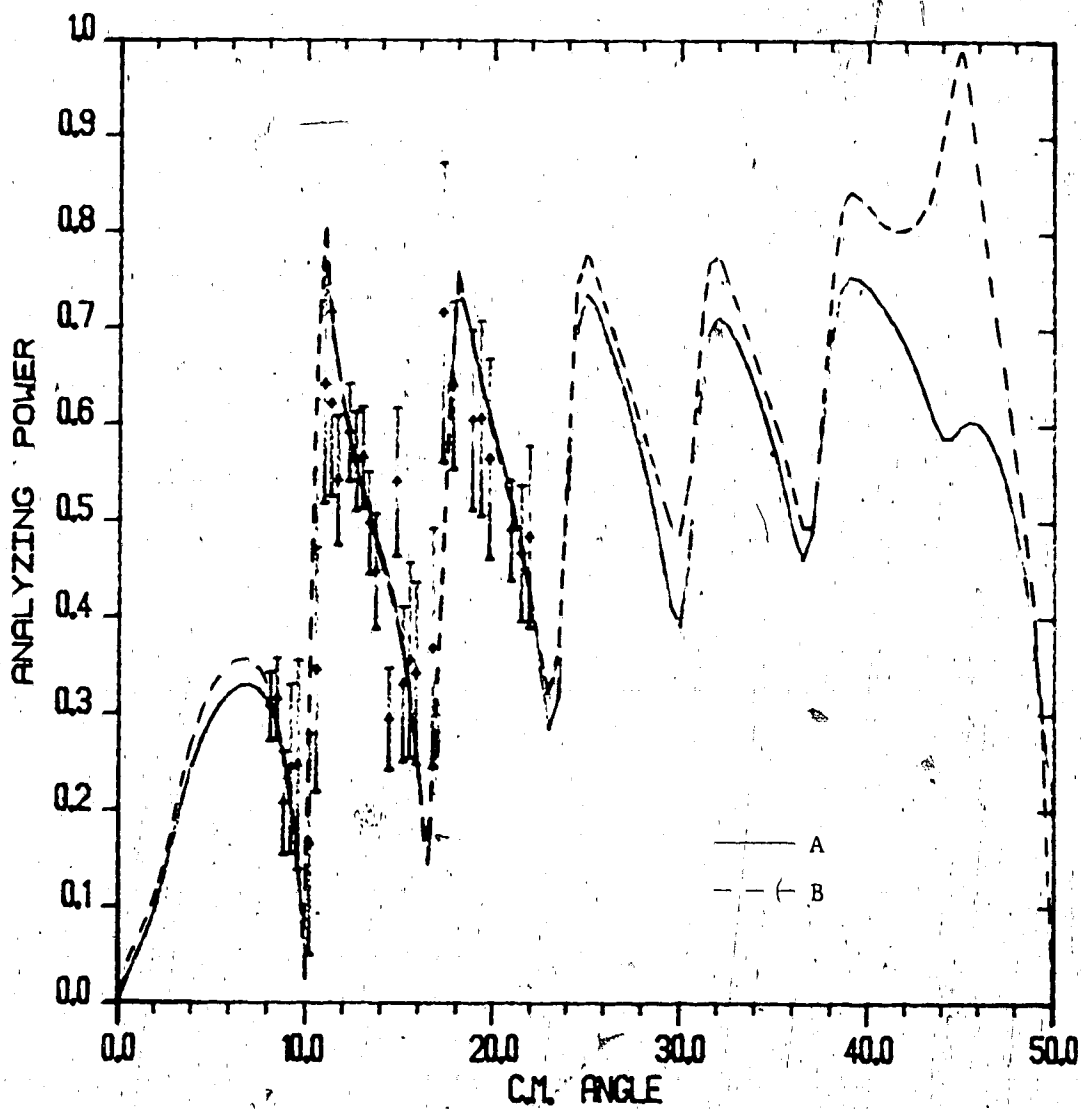parameters of table III-1.

Figure V-20.   Differential cross section for p + ^{40}Ca inelastic scattering to the 3$^-$ state with E_x = 3.7364 Mev and E_p = 800 Mev.

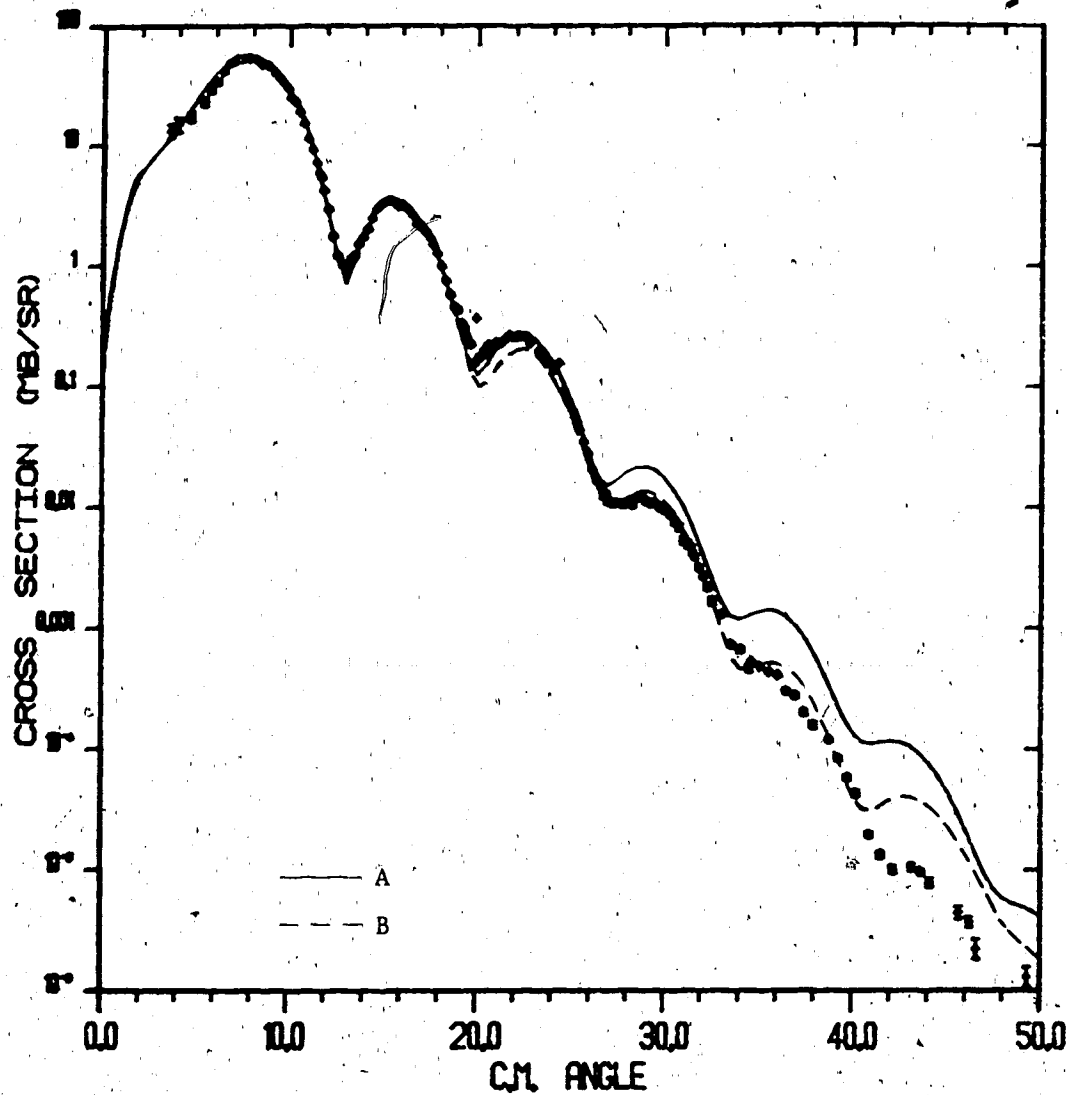The curves are RDWBA calculations using the parameters of table III-1.

Figure V-21. Analyzing power for p + ^{40}Ca inelastic scattering to the 3$^-$ state with E_x = 3.7364 Mev. and E_p = 800 Mev.

The curves are RDWBA calculations using parameter sets of table III-1.
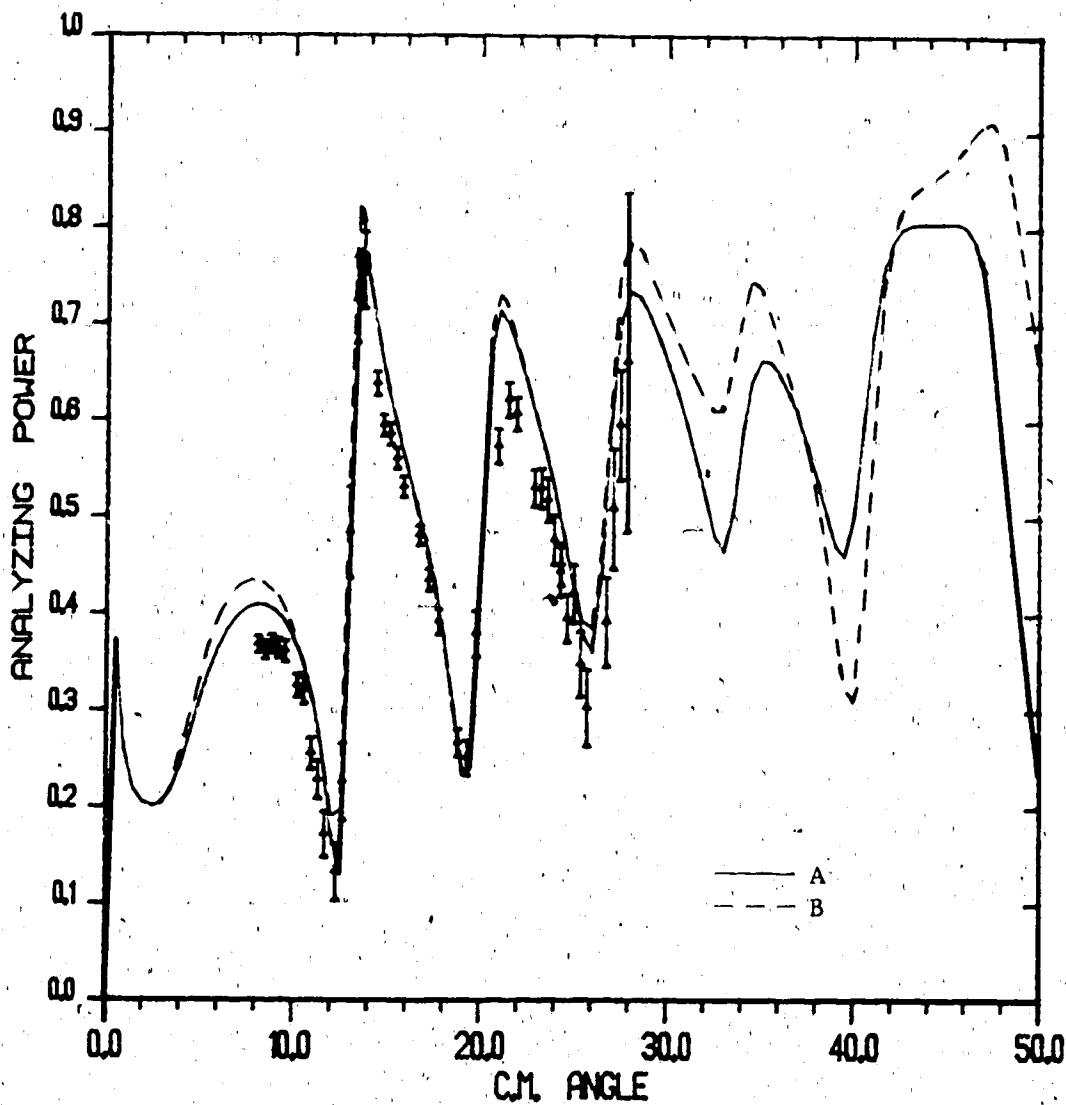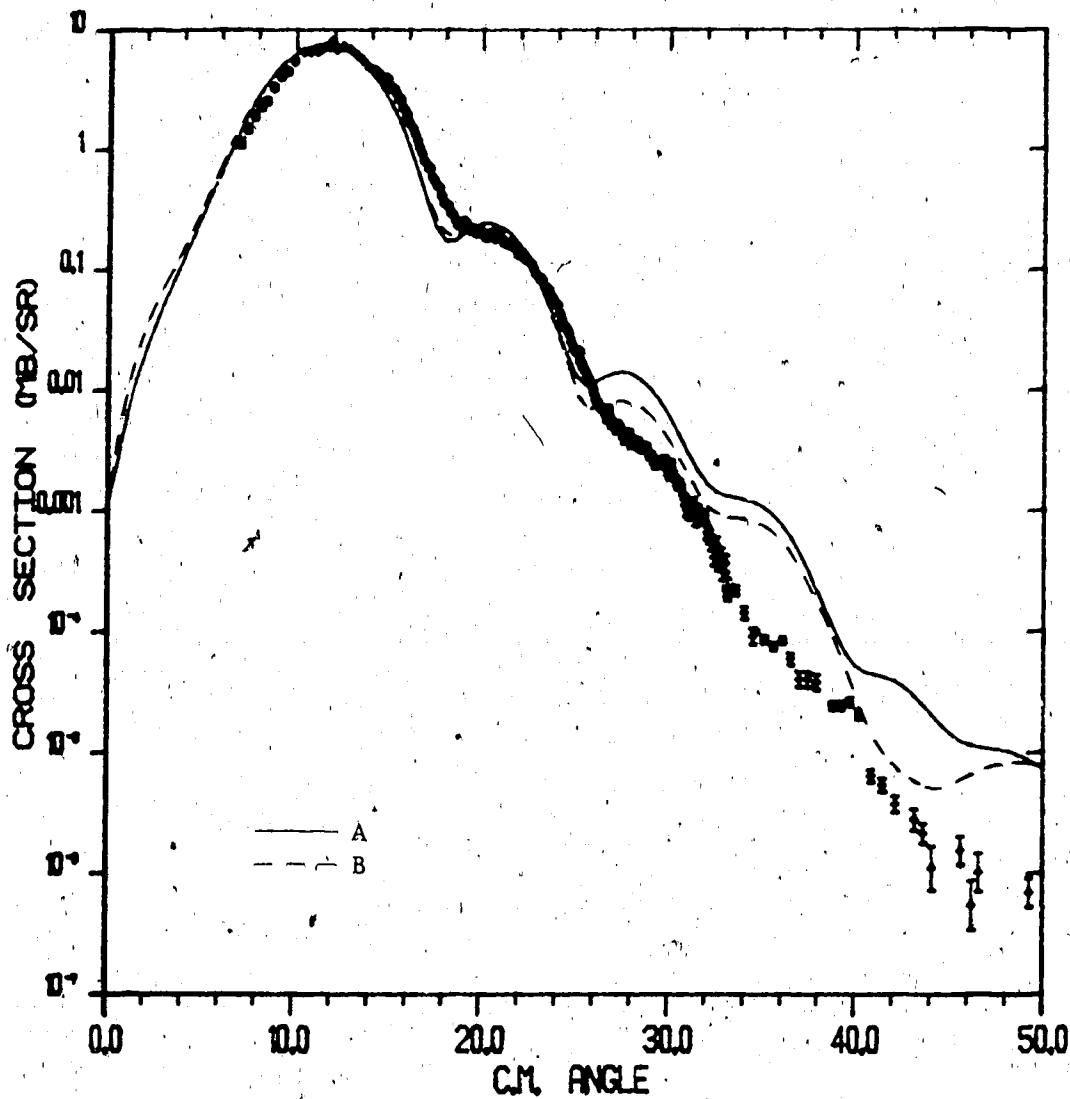
Figure V-22. Differential cross section for p + ^{40}Ca inelastic scattering to the 5^- state with E_x = 4.4915 Mev. and E_p = 800 Mev.

The curves are RDWBA calculations using the parameter sets of table III-1.

Figure V-23.   Analyzing power for p + ^{40}Ca inelastic
scattering to the 5$^-$ state with E_x = 4.4915 Mev.
and E_p = 800 Mev.

The curves are RDWBA calculations using
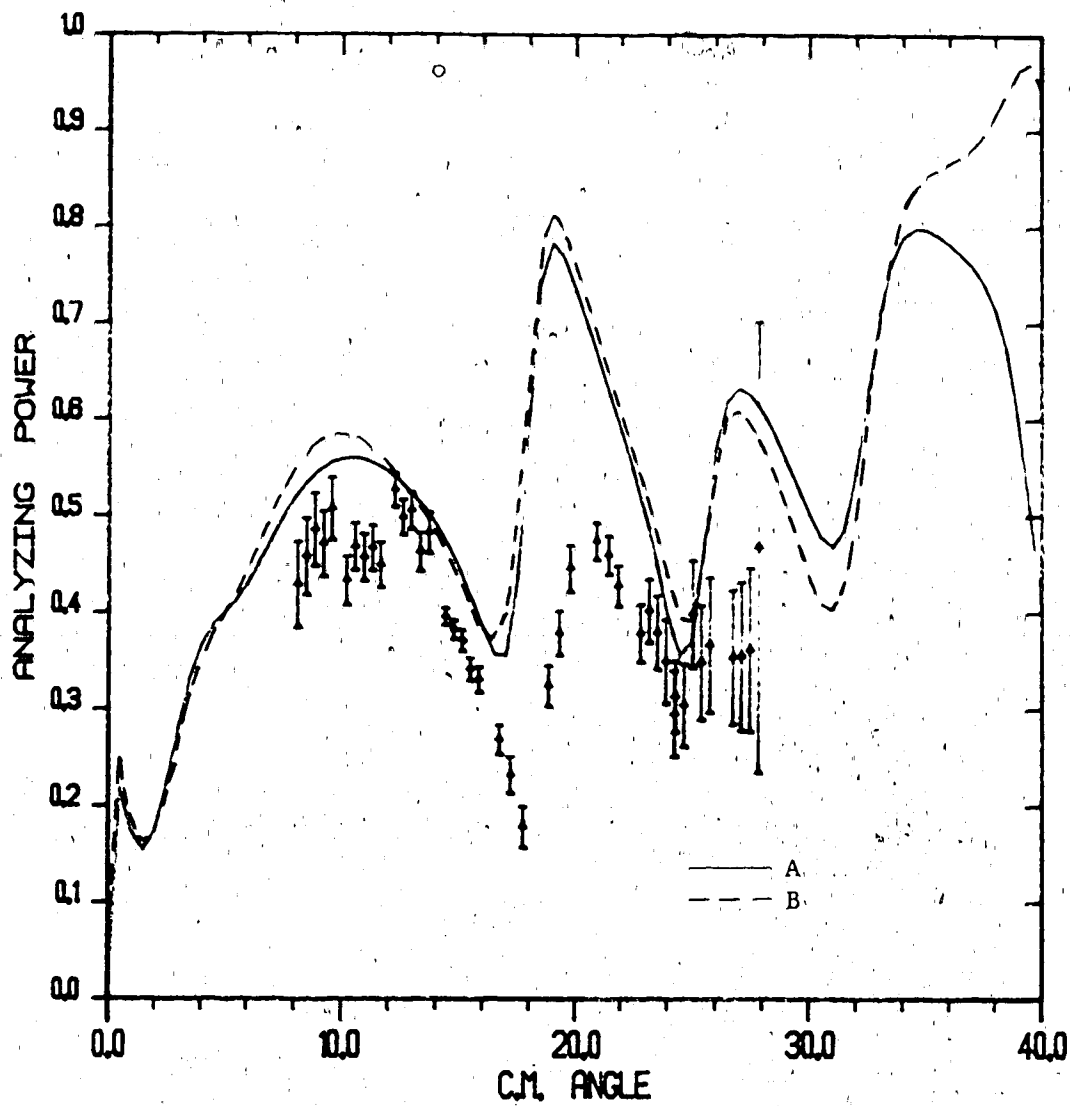the parameter sets of table III-1.

Figure V-24.   Differential cross section for $p + {}^{20}Ne$
inelastic scattering to the 2^+ state with
$E_x = 1.6338$ Mev. and $E_p = 800$ Mev.

The curve is an RDWBA calculation using
the parameter set of table III-2.

Figure V-25.   Analyzing power for p + ^{20}Ne inelastic scattering to the 2$^+$ state with E_x = 1.6338 Mev. and E_p = 800 Mev.

The curve is an RDWBA calculation using the parameter set of table III-2.

Figure V-26.   Differential cross section for p + ^{20}Ne
inelastic scattering to the 3⁻ state with
E_x = 5.622 Mev. and E_p = 800 Mev.

The curves are calculated using the parameter
set of table III-2. The solid curve is the
RDWBA calculation and the dashed curve is
the DEB calculation.

Figure V-27. Analyzing power for p + ^{20}Ne inelastic
scattering to the 3^- state with E_x = 5.622 Mev.
and E_p = 800 Mev.
The curves are calculated using the parameter
set of table III-2. The solid curve is the
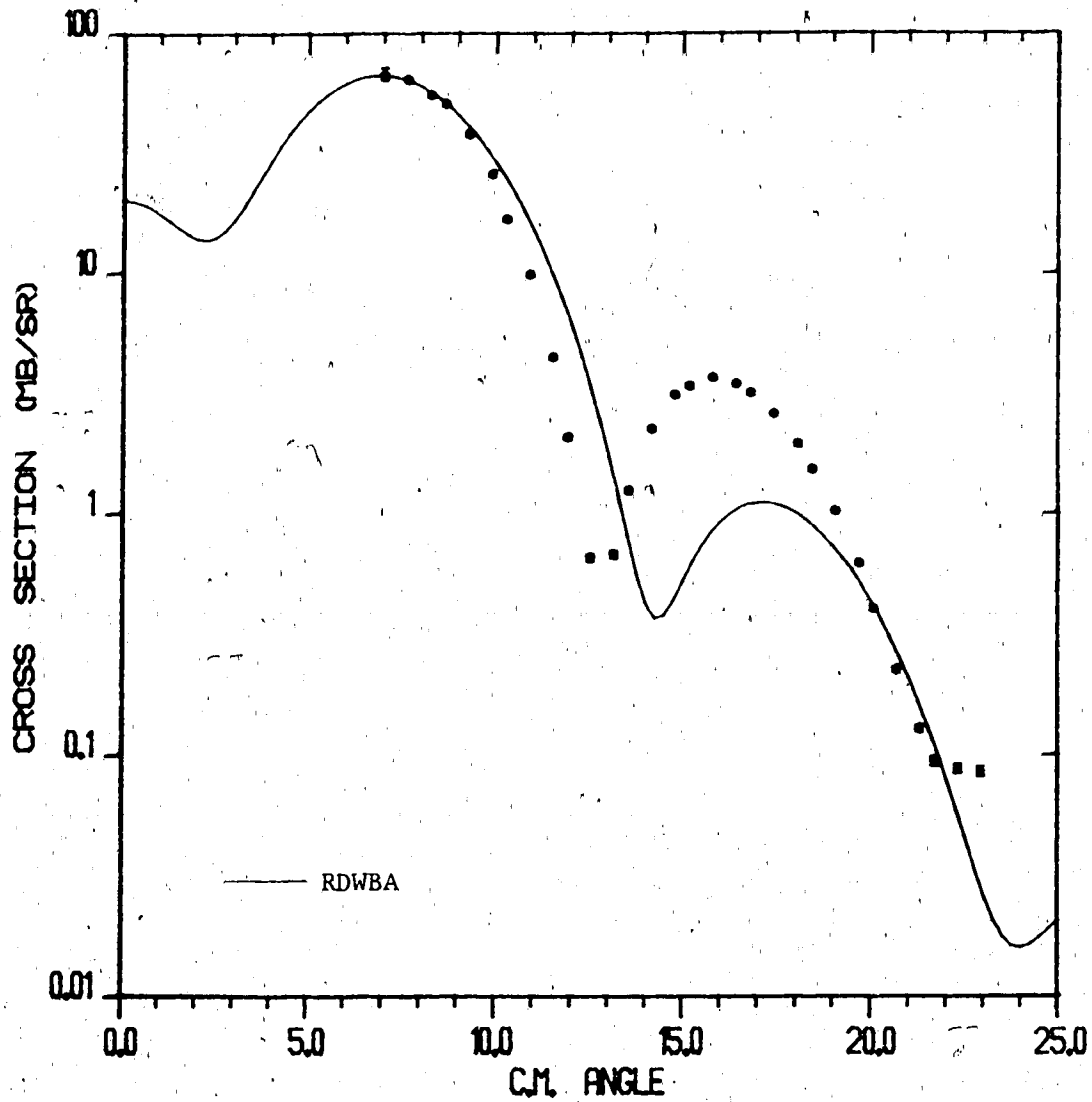RDWBA calculation and the dashed curve is
the DEB calculation.
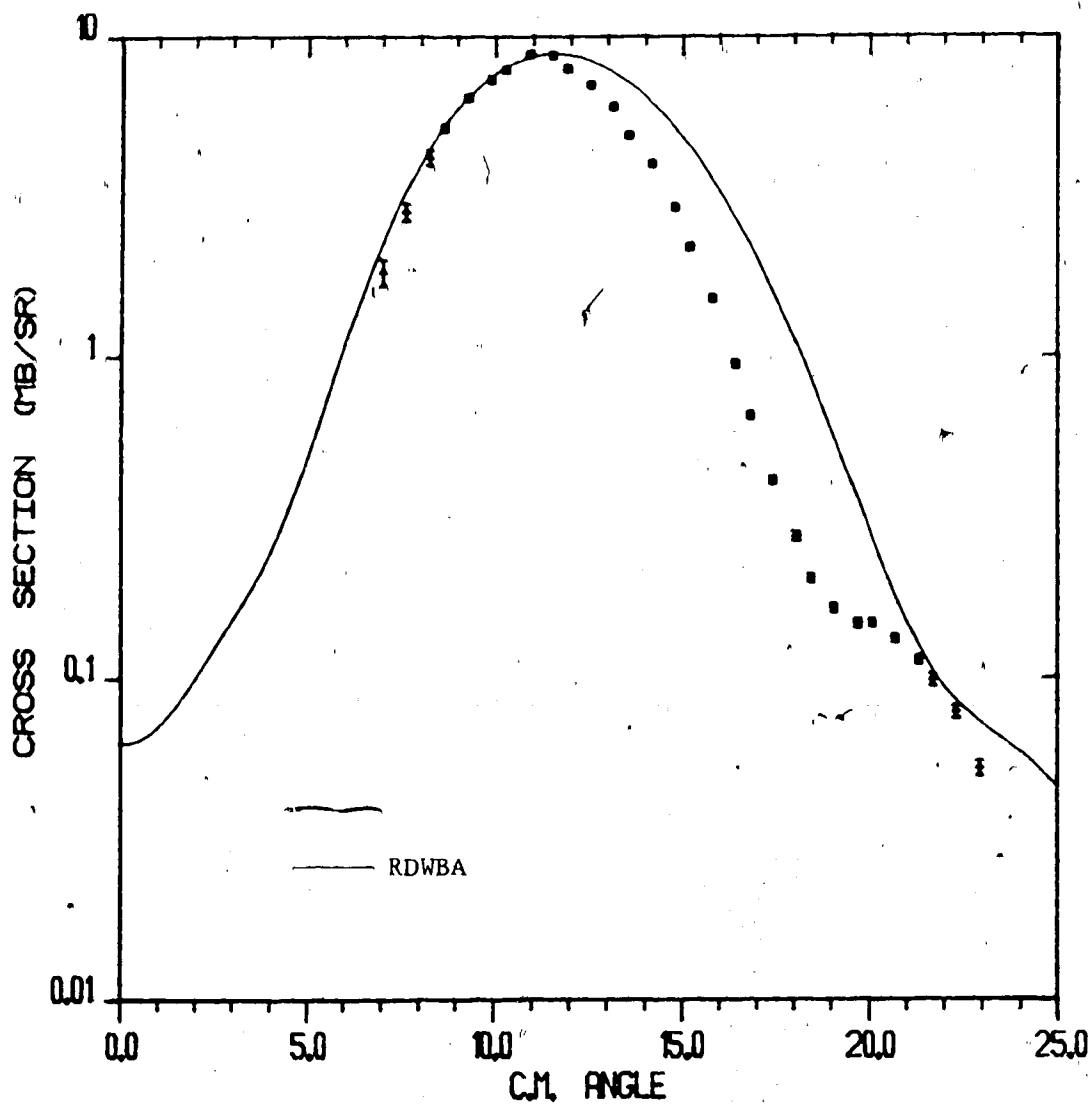
Figure V-28.   Differential cross section for $p + {}^{20}Ne$
inelastic scattering to the 4^+ state with
$E_x = 4.247$ Mev. and $E_p = 800$ Mev.

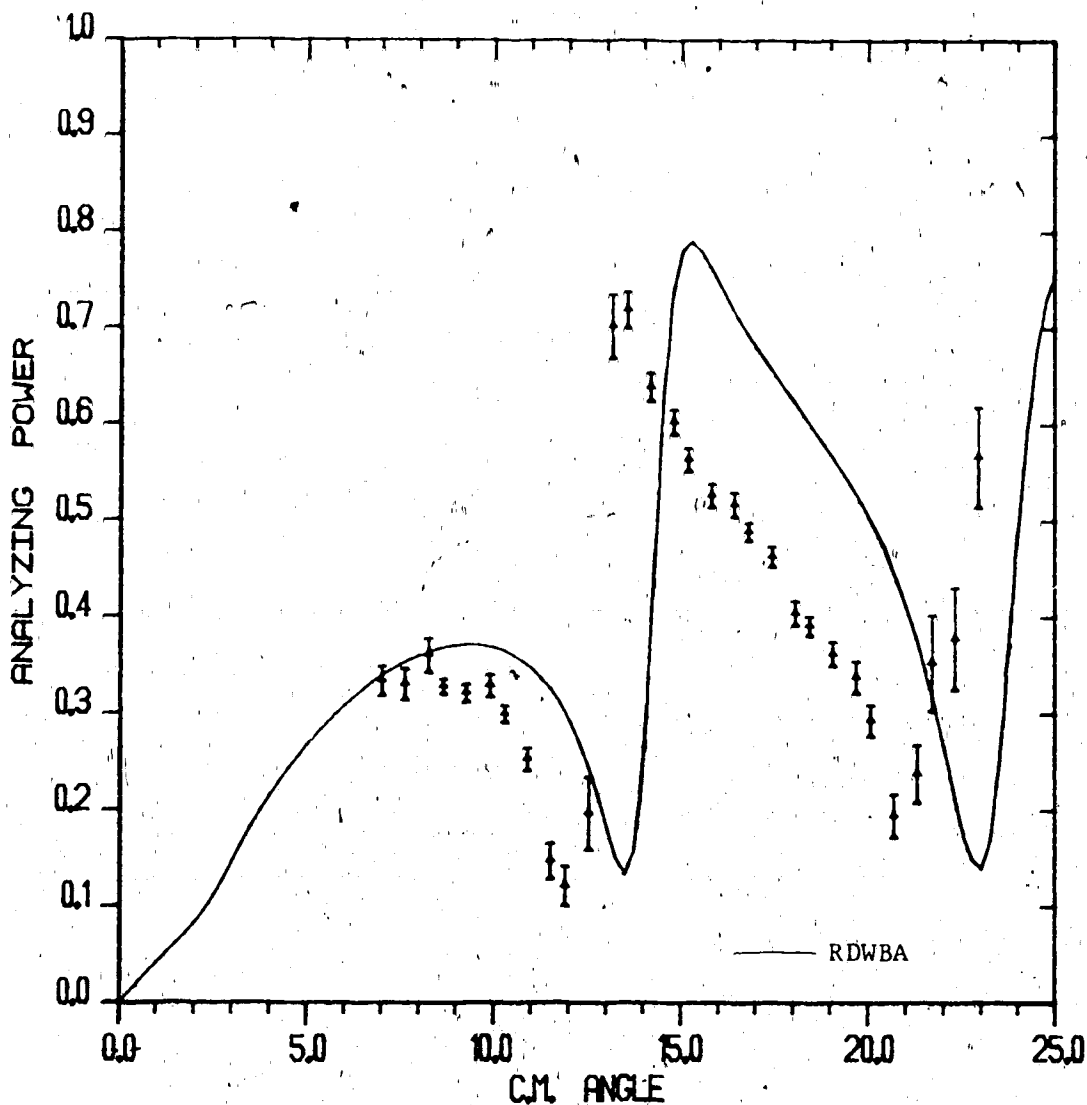The curve is an RDWBA calculation using
the parameter set of table III-2.

Figure V-29.   Analyzing power for p + ^{20}Ne inelastic
scattering to the 4$^+$ state with E_x = 4.247 Mev.
and E_p = 800 Mev.

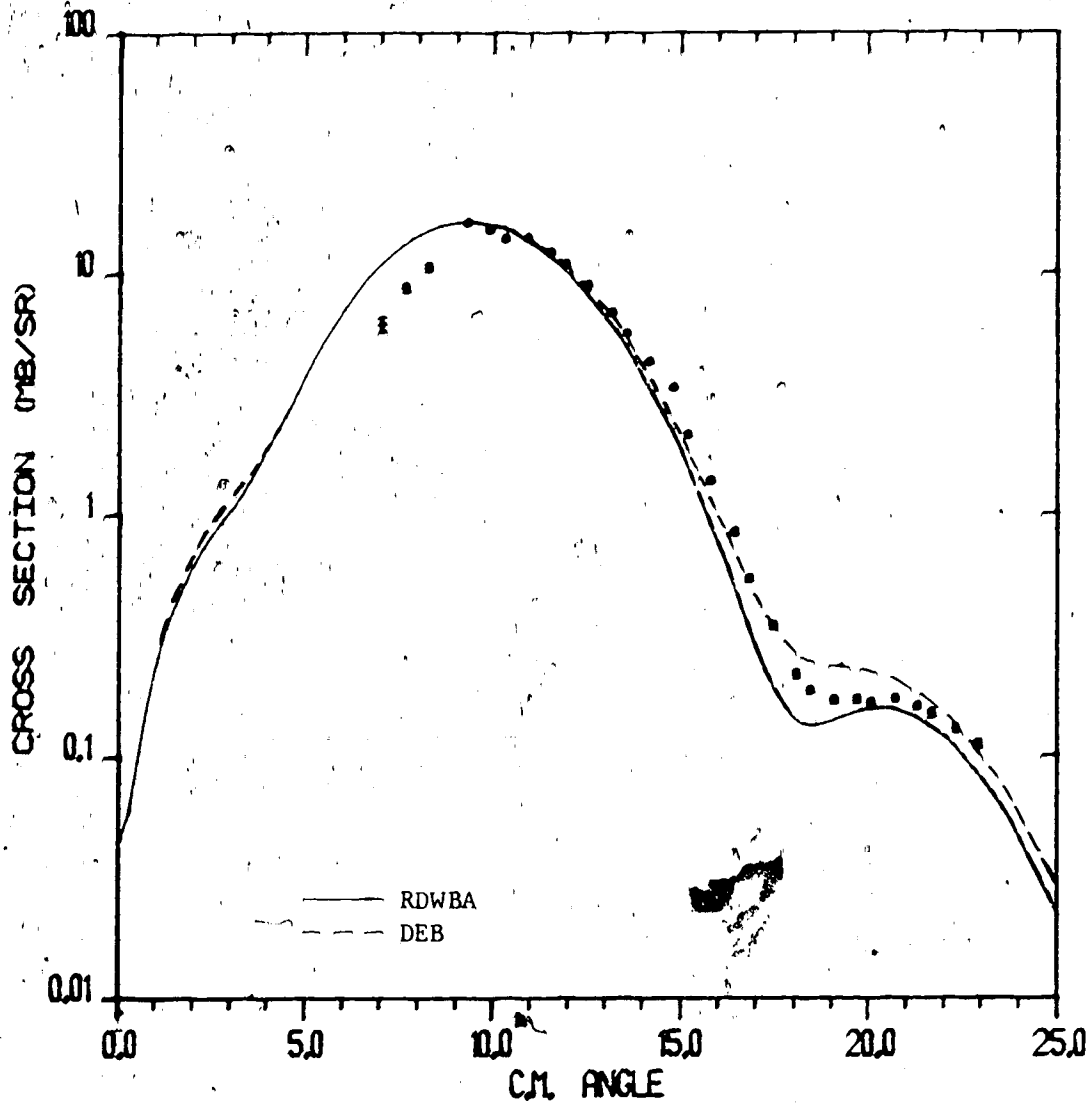The curve is an RDWBA calculation using
the parameter set of table III-2.

Figure V-30.   Differential cross section for p + ^{48}Ca
inelastic scattering to the 2^+ state with
E_x = 3.8323 Mev. and E_p = 500 Mev.

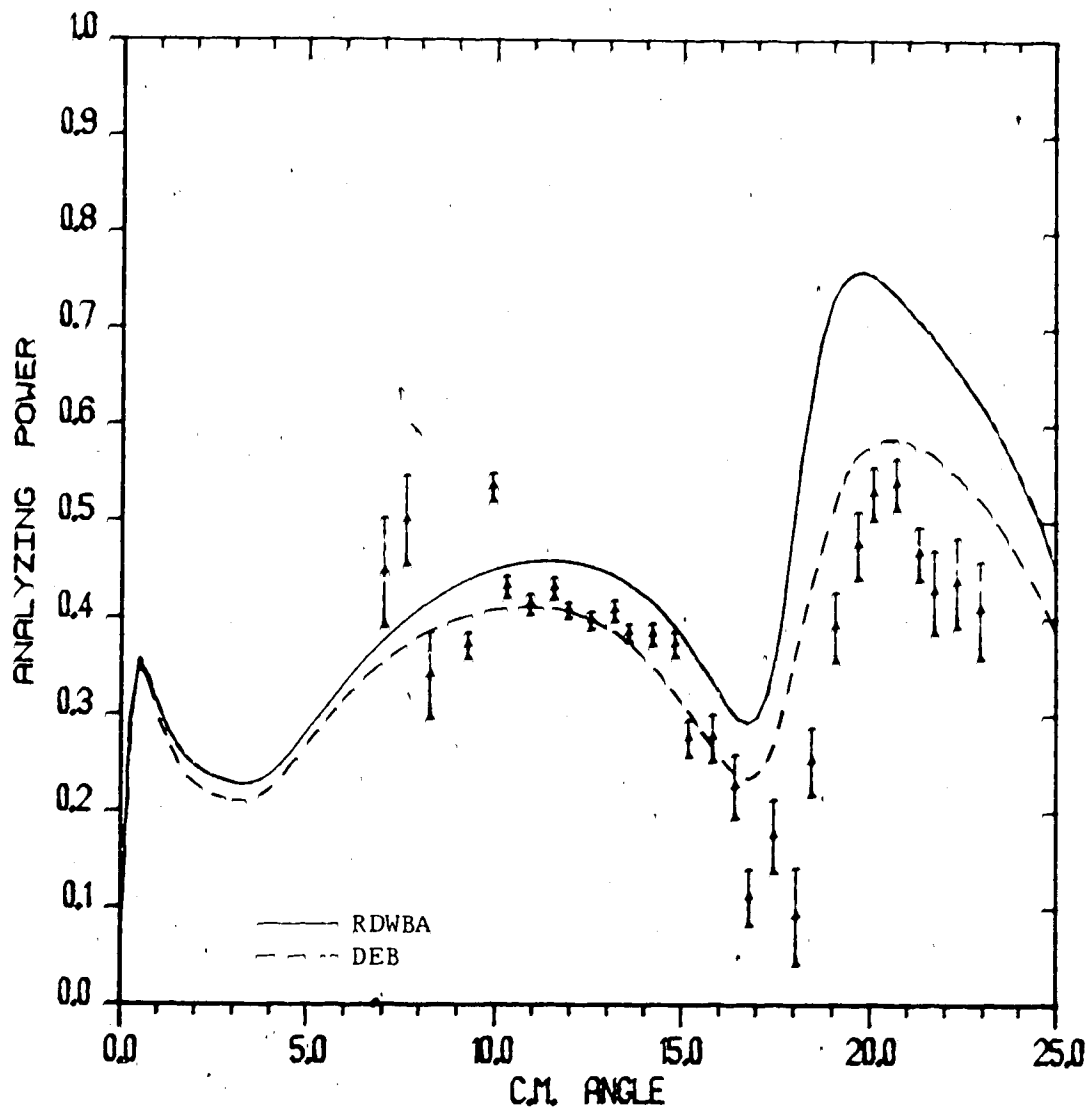The curves are RDWBA calculations using
the parameter sets of table III-2.

Figure V-31.   Analyzing power for p + ^{48}Ca inelastic
scattering to the 2^+ state with E_x = 3.8323 Mev.
and E_p = 500 Mev.

The curves are RDWBA calculations using
the parameter sets of table III-2.

Figure V-32.   Differential cross section for p + ^{48}Ca inelastic scattering to the 3$^-$ state with E_x = 4.5073 Mev. and E_p = 500 Mev.

The curves are RDWBA calculations using the parameter sets of table III-2.

Figure V-33.   Analyzing power for p + ^{48}Ca inelastic
scattering to the 3$^-$ state with E_x = 4.5073 Mev.
and E_p = 500 Mev.

The solid and short-dashed curves are
RDWBA calculations using the parameter sets
of table III-2. The long-dashed curve is
the DWBA calculation of Seth et al.
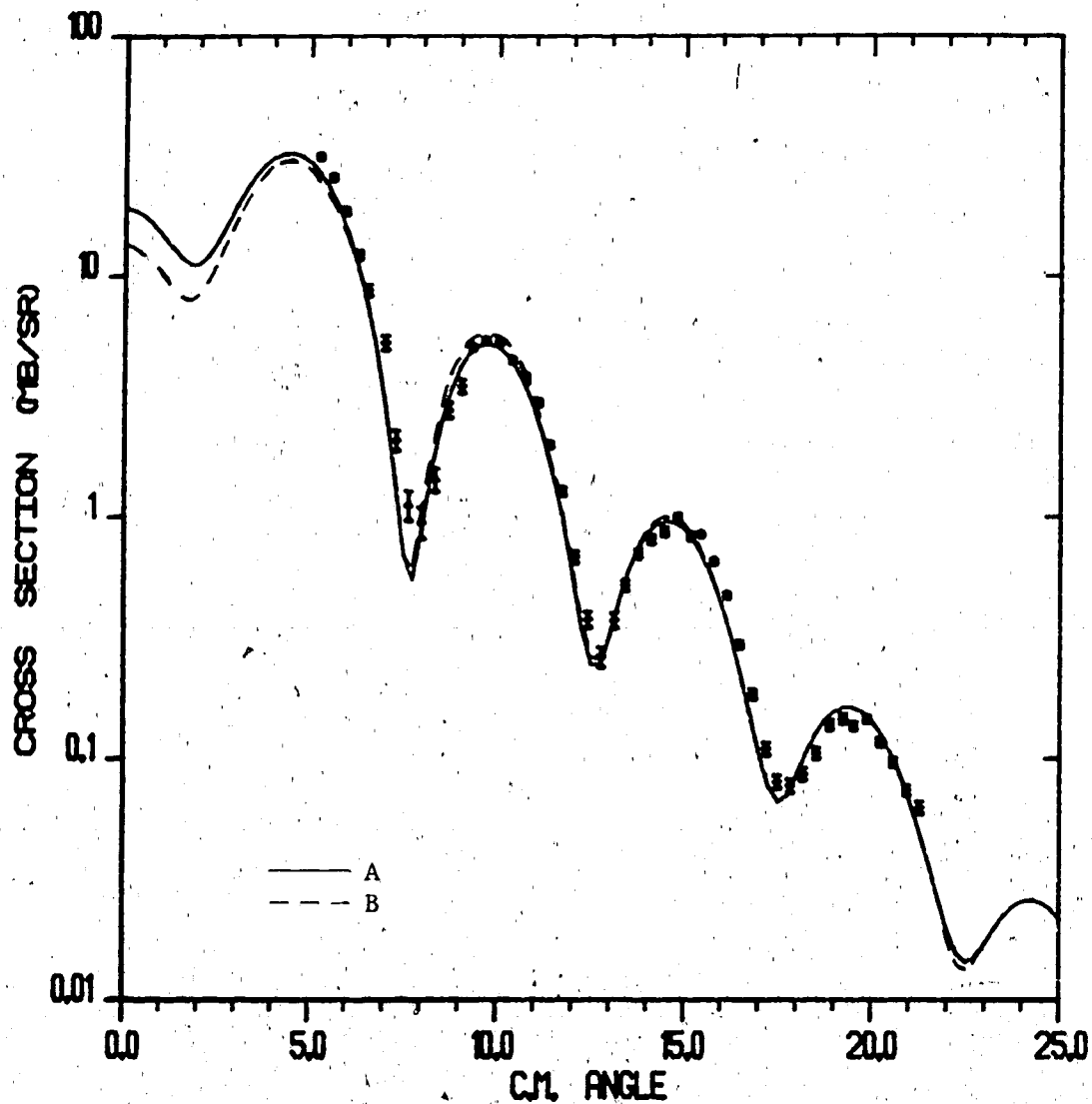
Figure V-34. Differential cross section for p + ^{90}Zr
inelastic scattering to the 2$^+$ state with
E_x = 2.1863 Mev. and E_p = 800 Mev.

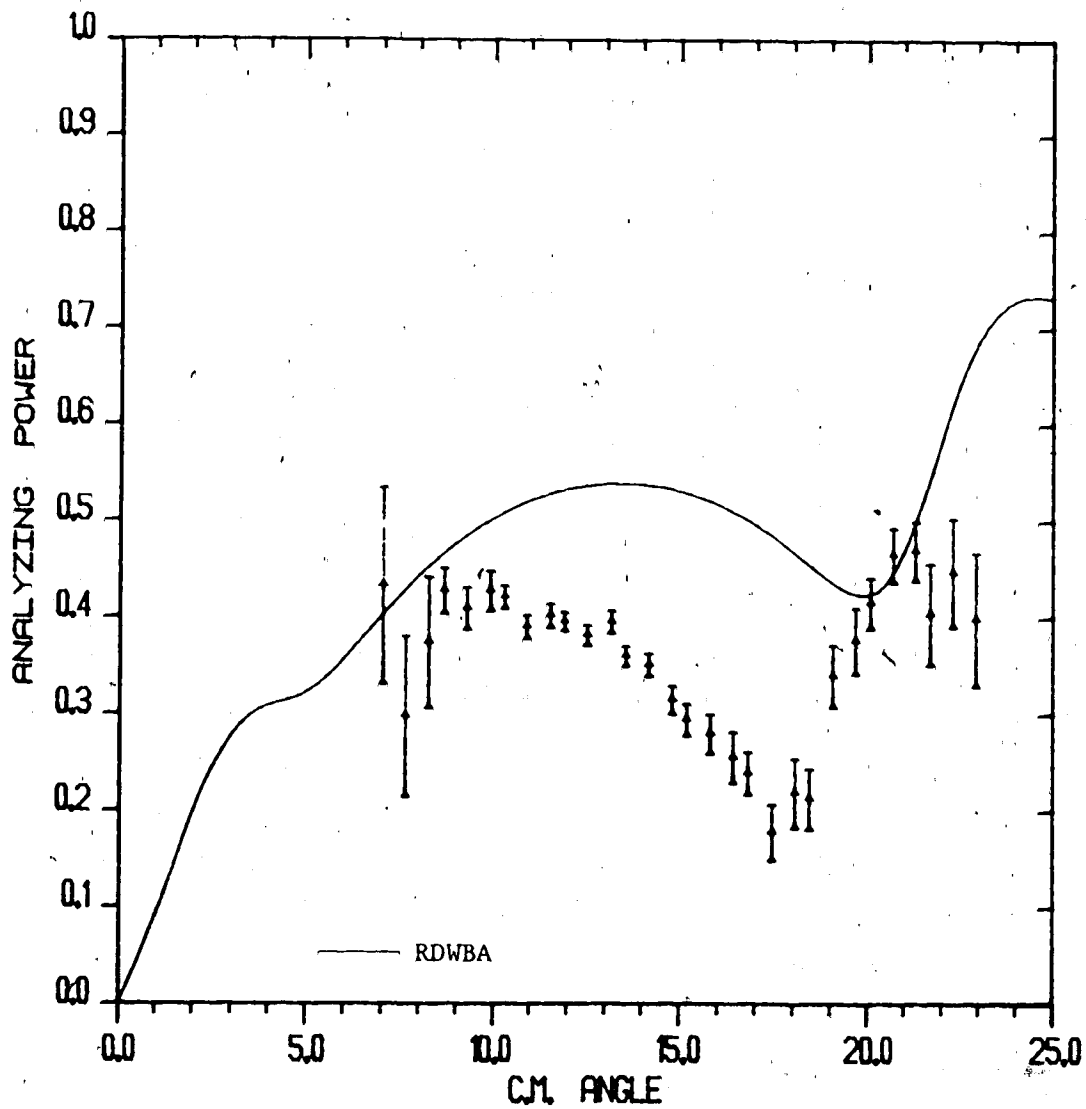The curves are RDWBA calculations using the
parameters of table III-2.
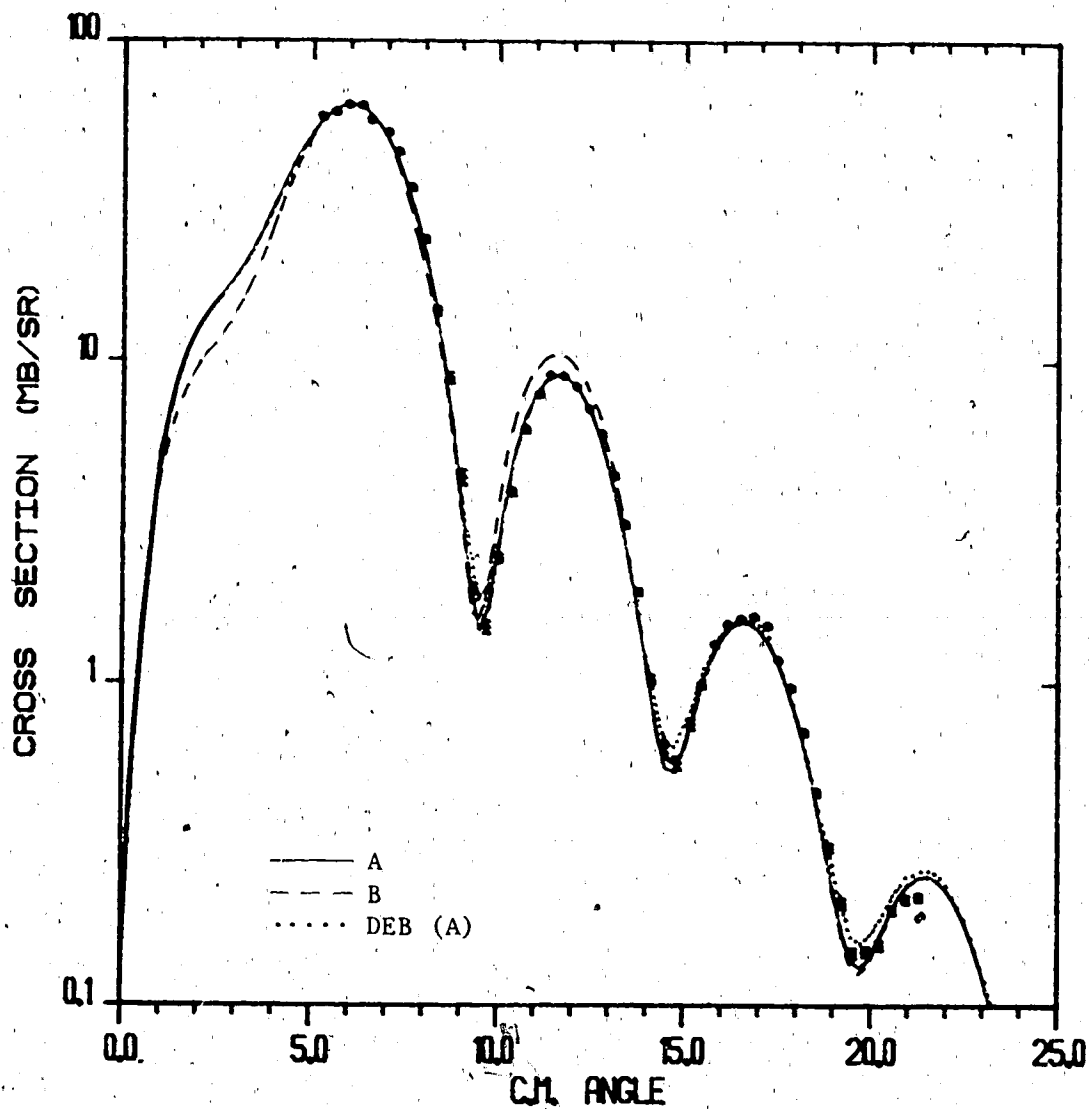
Figure V-35.   Differential cross section for p + ^{90}Zr
inelastic scattering to the 3$^-$ state with
E_x = 2.7479 Mev. and E_p = 800 Mev.

The curves are calculated using the parameter
sets of table III-2. The solid and dashed
curves are RDWBA calculations and the dotted
curve is a DEB calculation.
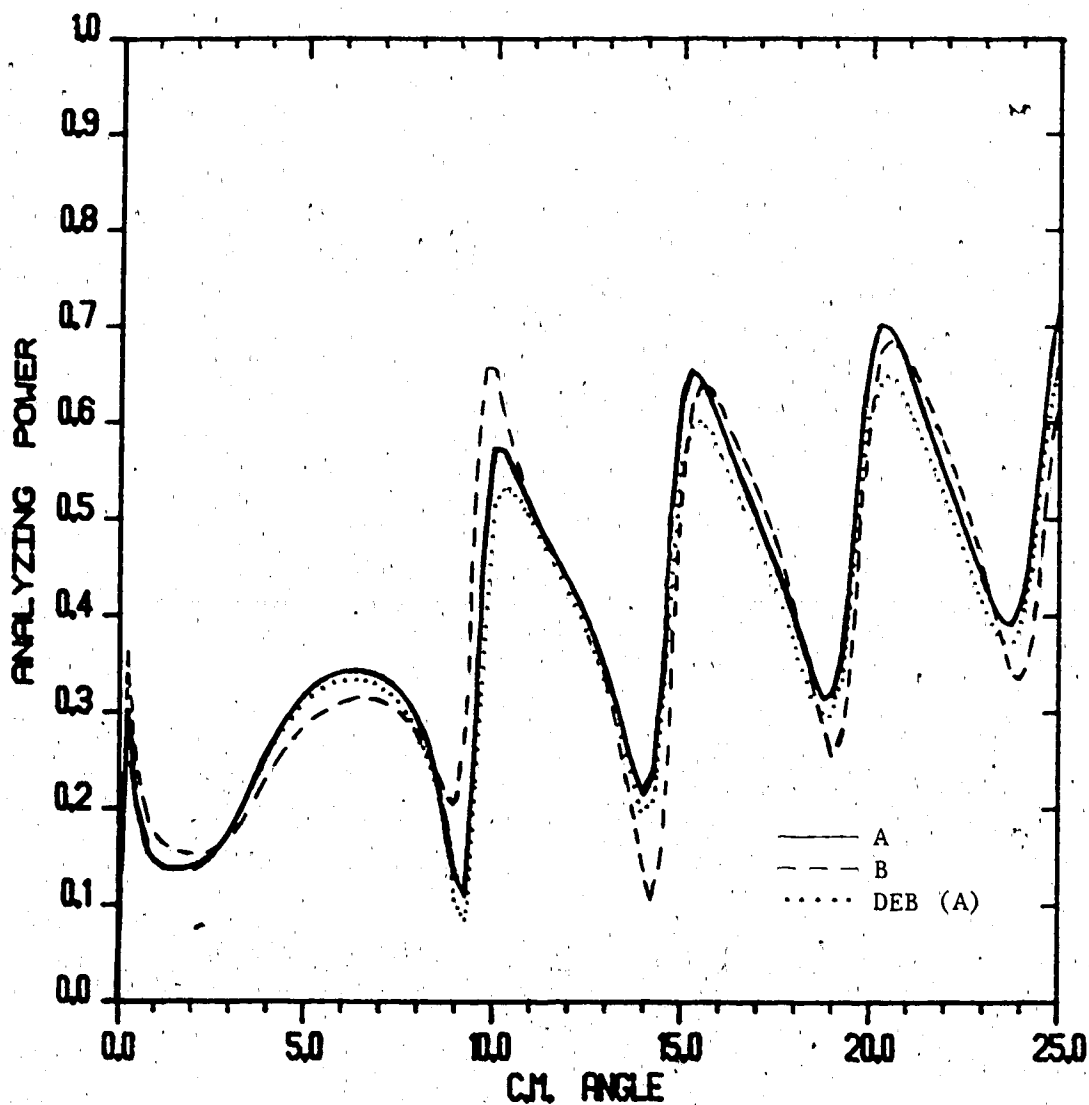
Figure V-36. Analyzing power for p + ^{90}Zr inelastic
scattering to the 3^- state with E_x = 2.7479 Mev.
and E_p = 800 Mev.

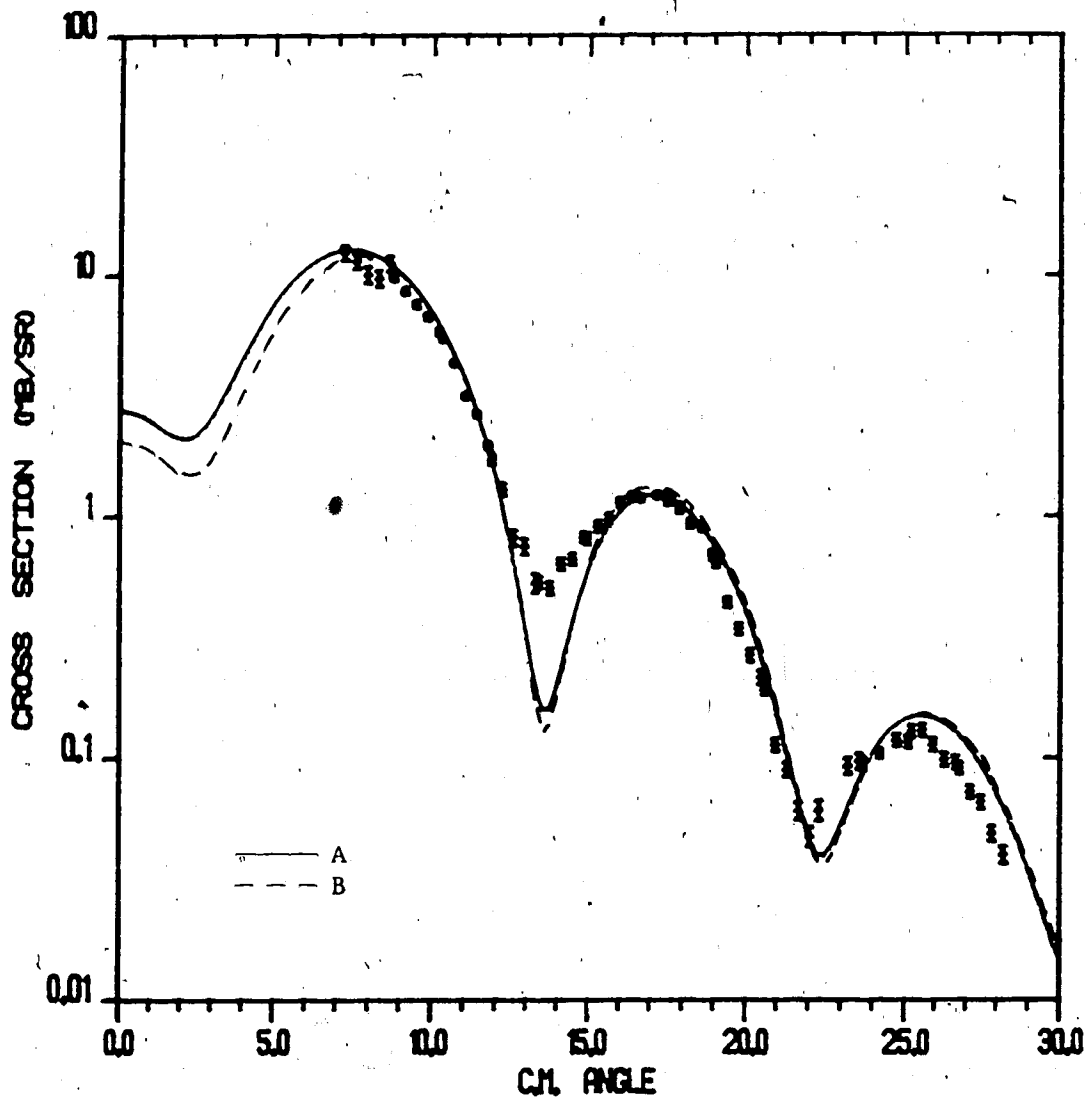The curves are calculated using the parameter
sets of table III-2. The solid and dashed
curves are RDWBA calculations and the dotted
curve is a DEB calculation using parameter set A.
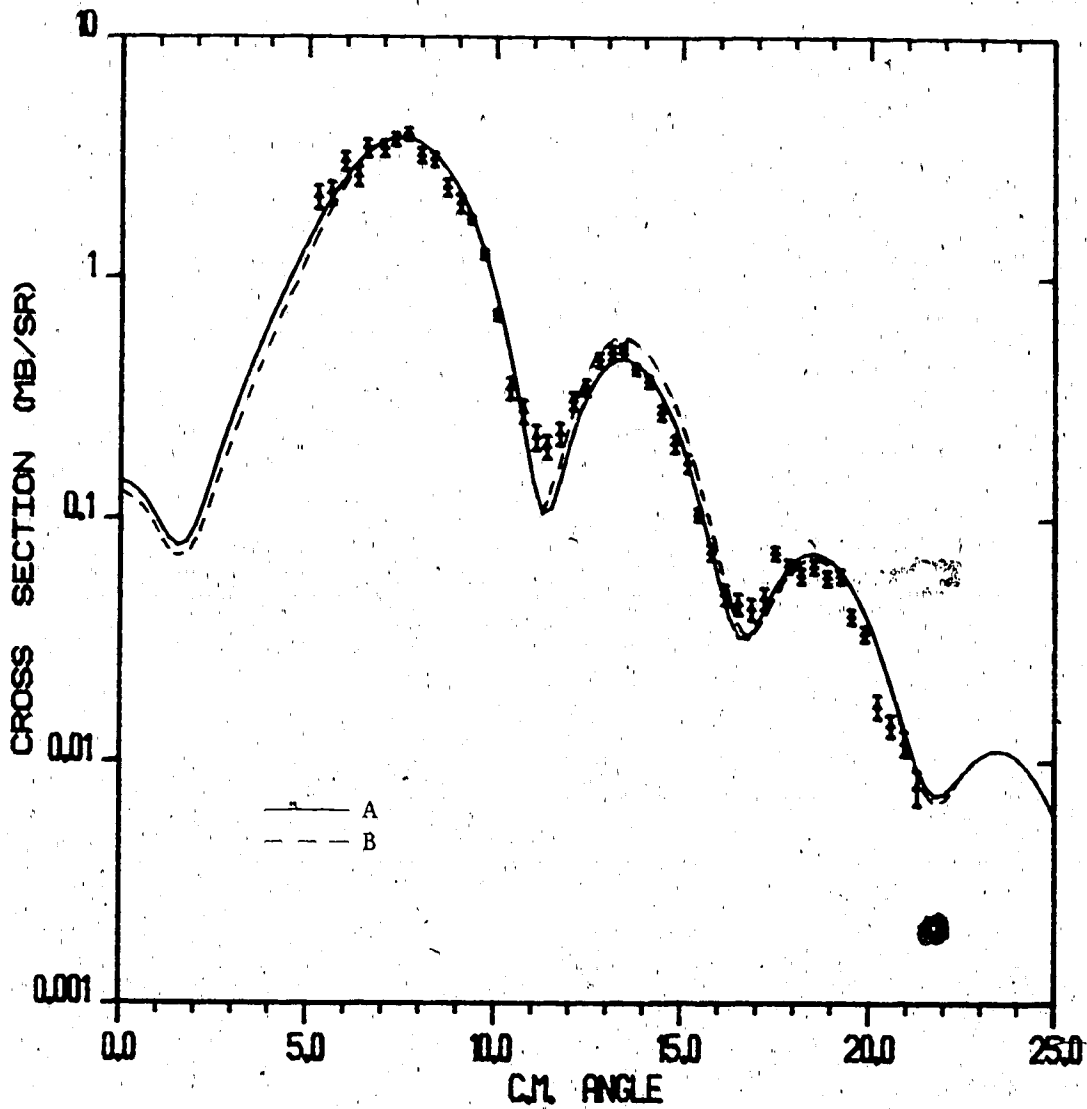
Figure V-37.   Differential cross section for p + ^{90}Zr inelastic scattering to the 4^+ state with E_x = 3.0773 Mev. and E_p = 800 Mev.

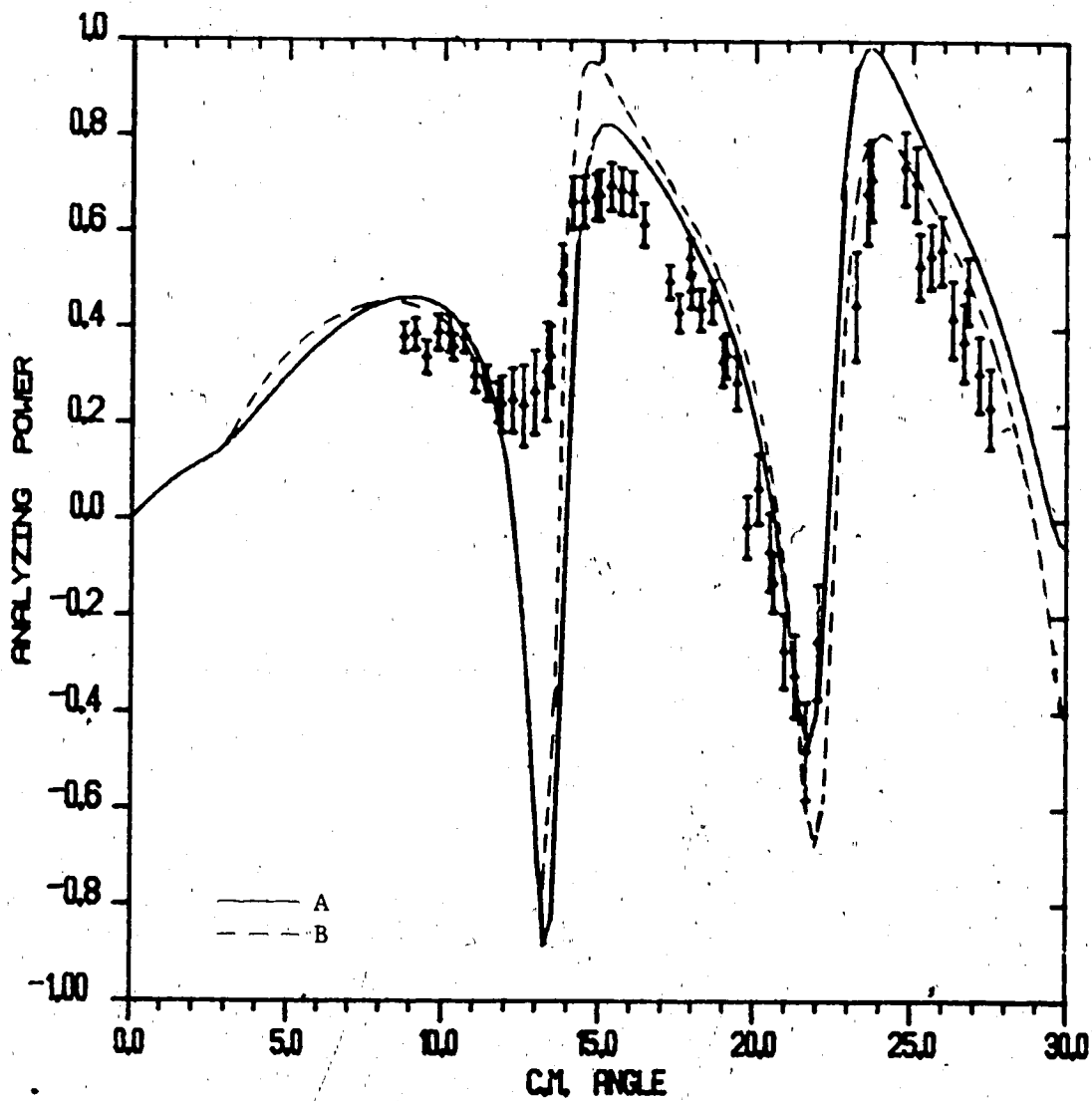The curves are RDWBA calculations using the parameter sets of table III-2.
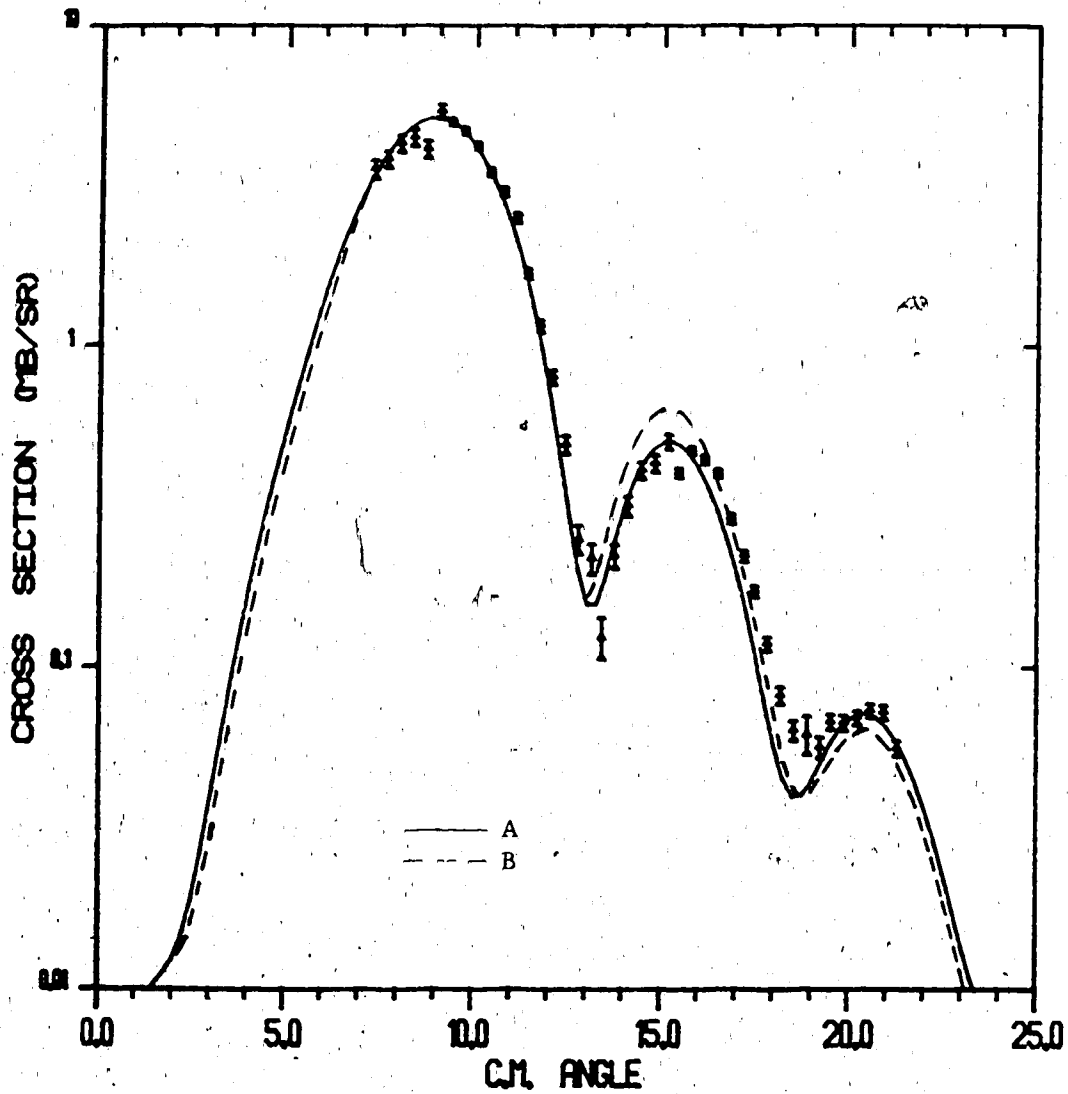
Figure V-38.   Differential cross section for p + ^{90}Zr
inelastic scattering to the 5⁻ state with
E_x = 2.3187 Mev. and E_p = 800 Mev.

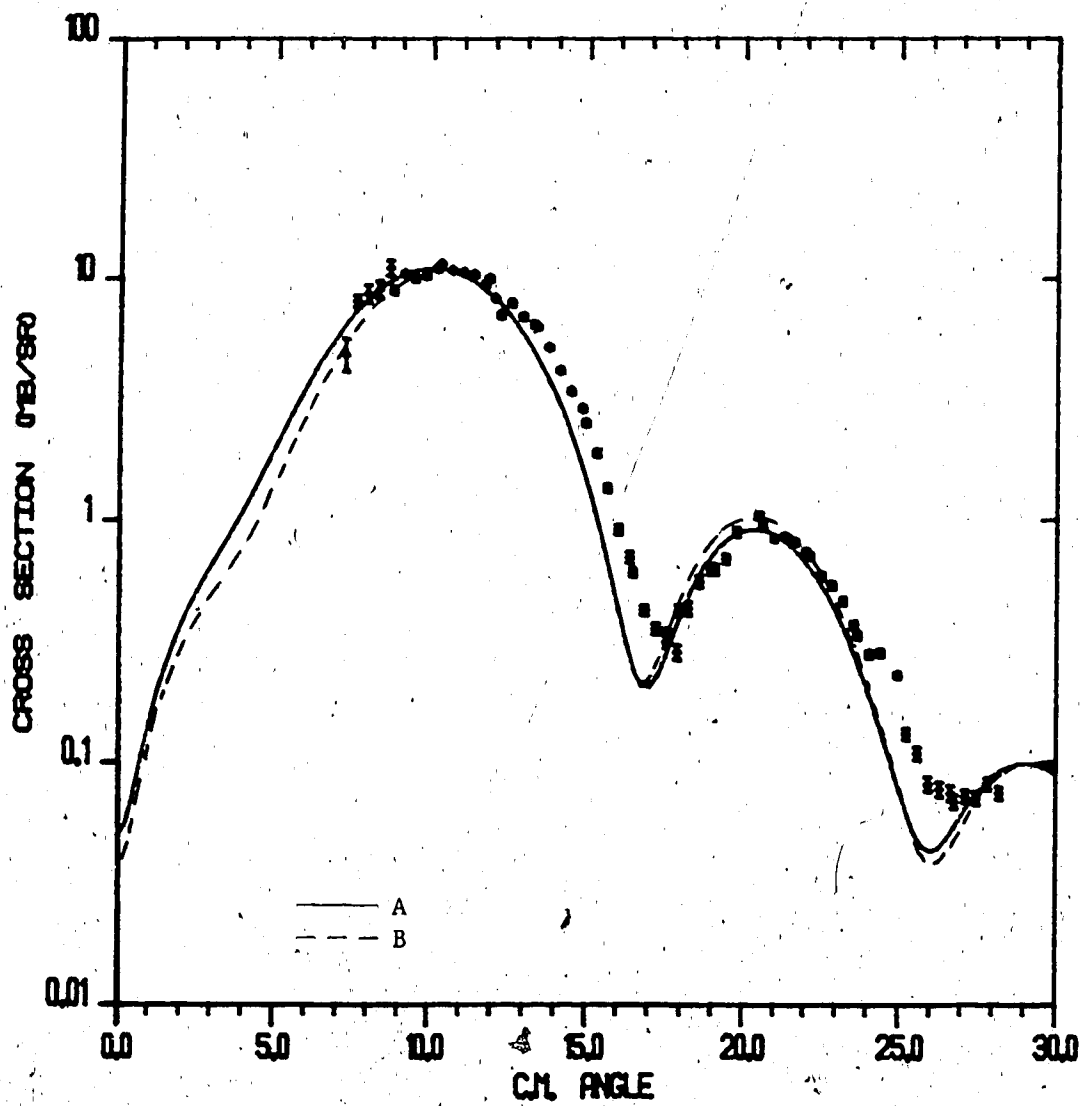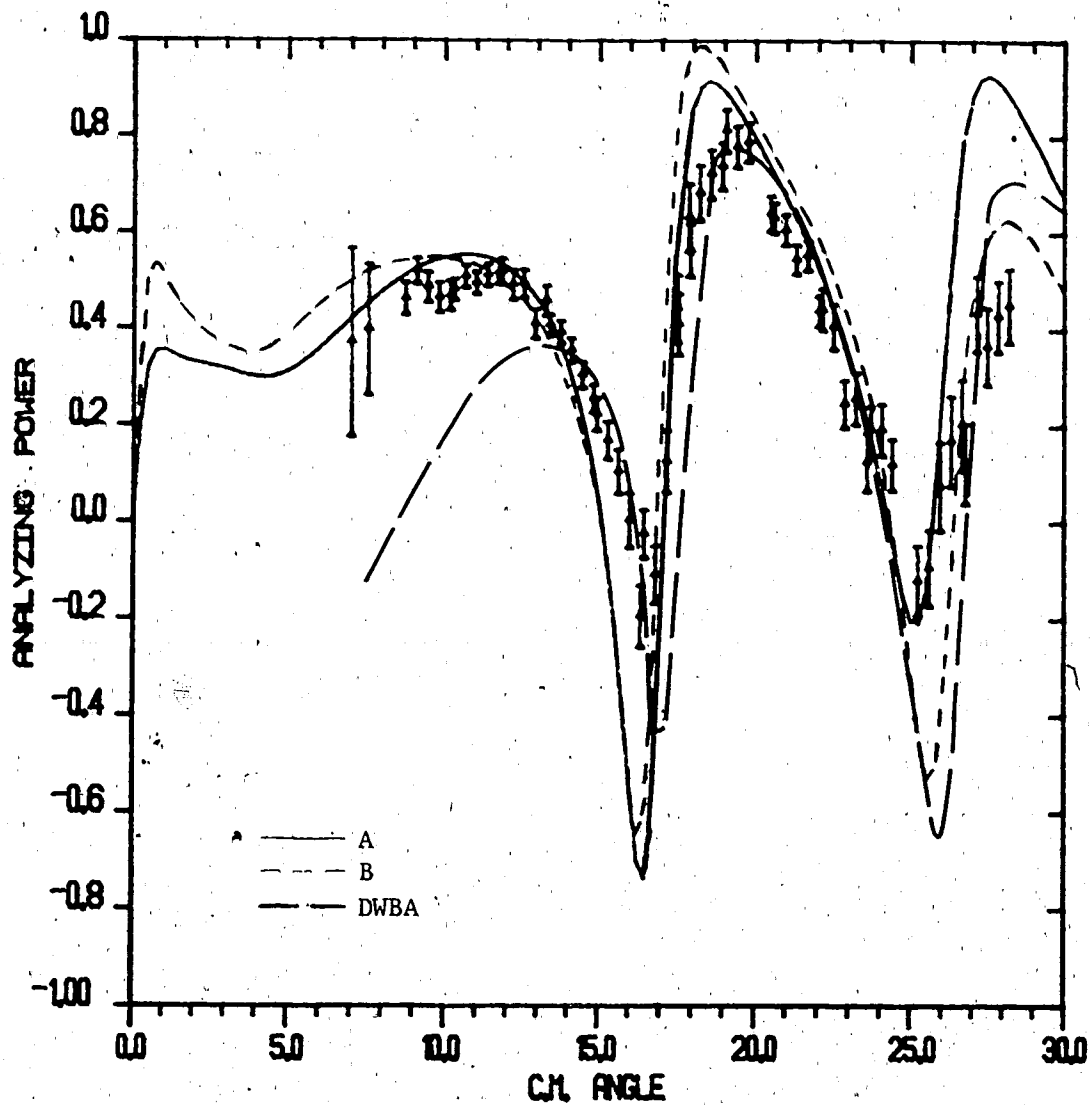The curves are RDWBA calculations using
the parameter sets of table III-2.
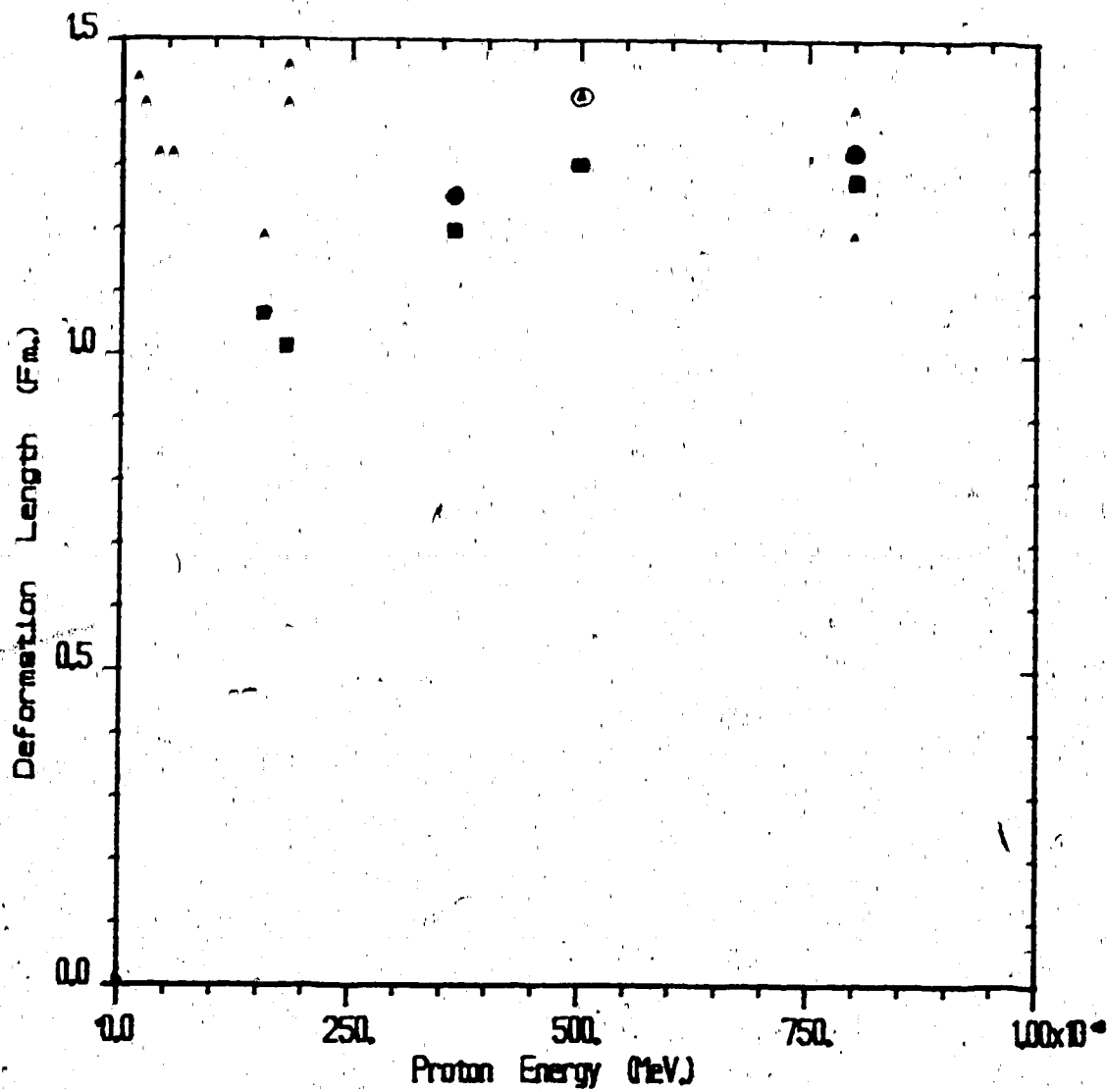
Figure V-39.   Deformation length as a function of proton
energy for the 3⁻ state of ^{40}Ca. The
triangles are from various nonrelativistic
analyses, the squares are DEB and the
circles are from this work.
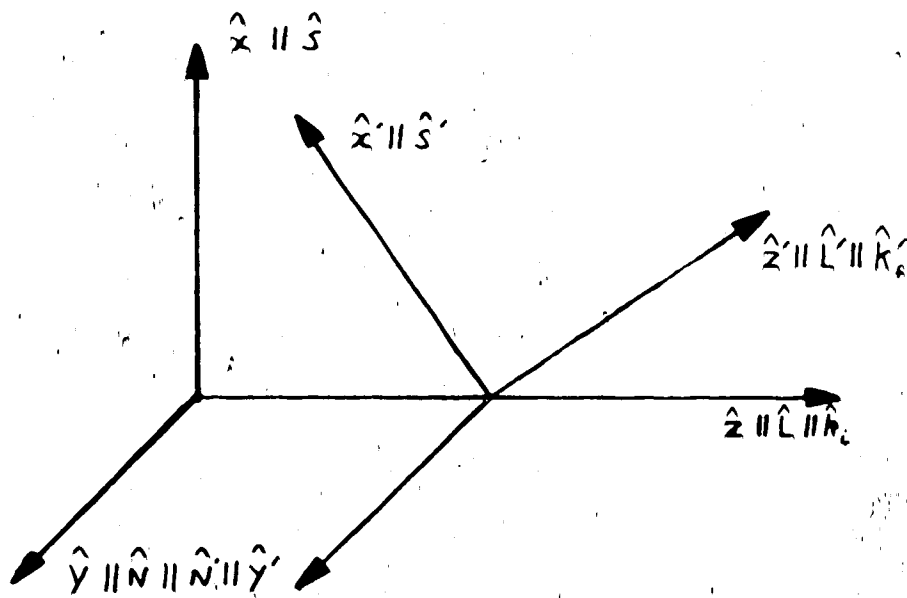
Figure B-1.   Coordinate system for the incoming
               (unprimed) and outgoing (primed) proton.

BIBLIOGRAPHY

Ca85   Anton Z. Capri, <u>Nonrelativistic Quantum Mechanics</u>,
Benjamin/Cummings Publishing Company Ltd. (1985)

Ja70·   Daphne F. Jackson, <u>Nuclear Reactions</u>,
Methuen & Company Ltd. (1970)

Ta72   John R. Taylor, <u>Scattering Theory</u>,
John Wiley & Sons, Inc. (1972)

REFERENCES

Aa82   B. Aas, E. Bleszynski, M. Bleszynski, M. Haji-Saeid, G. Igo, F. Irom,
G. Pauletta, A. Rahbar, A. T. M. Wang, J. F. Amann, T. A. Carey,
W. D. Cornelius, J. B. McClelland, C. Glashausser, S. Nanda, M. Barlett,
G. W. Hoffmann and M. Gazzaly, Phys. Rev. C26, 1770 (1982).

Am80   R. D. Amado, F. Lenz, J. A. McNeil and D. A. Sparrow, Phys. Rev. C22,
2094 (1980).

Ar83   R. A. Arndt, L. P. Roper, R. A. Bryan, R. B. Clark, B. J. Verwest and
Peter Signell, Phys. Rev. D28, 97 (1983).

Au65   N. Austern and J. S. Blair, Ann. Phys. (N. Y.) 33, 15 (1965).

Ba85   M. L. Barlett, G. W. Hoffmann and L. Ray, Phys. Lett. 158B, 289 (1985).

Bl64   J. S. Blair, in " Nuclear Spectroscopy with Direct Reactions ", ANL-6878,
143 (1964).

Bl82   E. Bleszynski, M. Bleszynski, S. Hajisaeid, G. J. Igo, F. Irom,
J. B. McClelland, G. Pauletta, A. Rahbar, A. T. M. Wang, C. A. Whitten Jr.,
G. Adams, M. Barlett, G. W. Hoffmann, J. A. Mcgill, R. Boudrie and
G. Kyle, Phys. Rev. C25, 2563 (1982).

Bl84   G. S. Blanpied, G. A. Balchin, G. E. Langston, B. G. Ritchie, M. L. Barlett,
G. W. Hoffmann, J. A. McGill, M. A. Franey, M. Gazzaly and
B. H. Wildenthal, Phys. Rev. C30, 1233 (1984).

Cl82   B. C. Clark, S. Hama and R. L. Mercer, in " The Interaction Between Medium
Energy Nucleons in Nuclei ", AIP Conference Proceedings 97, Edited by
H. Meyer, AIP New York, 260 (1982).

127

Cl83   B. C. Clark, R. L. Mercer and P. S. Schwandt, Phys. Lett. 122B, 211 (1983).

Co81   E. D. Cooper, Ph.D. Thesis, University of Alberta (1981) unpublished.

Co85a   Tim Cooper, Private communication.

Co85b   Tim Cooper, H. S. Sherif, J. Johansson and R. I. Sawafta, in the
        " Proceedings of the LAMPF Workshop on Dirac Approaches to Nuclear
        Physics ", Proceedings No. LA-10438-C, 321, (1985).

Fe58   H. Feshbach, Ann. of Phys. 5, 357 (1958).

Fe86   R. W. Fergerson, M. L. Barlett, G. W. Hoffmann; J. A. Marshall,
        E. C. Milner, G. Pauletta, L. Ray, J. F. Amann, K. W. Jones,
        J. B. McClelland, M. Gazzaly and G. J. Igo, Phys. Rev. C33, 239 (1986).

Fr86   Deiter Frekers, University of Toronto, private communication.

Ga82   M. M. Gazzaly, N. M. Hintz, G. S. Kyle, R. K. Owen, G. W. Hoffmann,
        M. Barlett and G. Blanpied, Phys. Rev. C25, 408 (1982).

Gr72   G. R. Gruhn, T. Y. T. Kno, G. J. Maggiore, H. McManus, F. Petrovich
        and B. M. Preedom, Phys. Rev. C6, 915 (1972).

Gr83   J. M. Greben and R. Gourishankar, Nucl. Phys. A405, 445 (1983).

Ho68   N. Hoshizaki, Supp. Prog. Theor. Phys. (Japan) 42, 107 (1968).

Ho81a   G. W. Hoffmann, L. Ray, M. L. Barlett, R.Fergerson, J. McGill,
        E. C. Milner, K. K. Seth, D. Barlow, M. Bosko, S. Iverson, M. Kaletka,
        A. Saha and D. Smith, Phys. Rev. Lett. 47, 1436 (1981).

Ho81b   C. J. Horowitz and B. P. Serot, Nucl. Phys. 368A, 503 (1981).

Ho85   G. W. Hoffmann, Private Communication.

In73   A. Ingemarsson, E. Hagberg and H. Sherif, Nucl. Phys. A216, 271 (1973).

Ja70   Daphne F. Jackson, Nuclear Reactions, Methuen & Company Ltd. (1970).

Jo86   K. W. Jones, C. Glashausser, R. de Swiniarski, S. Nanda, T. A. Carey,
        W. Cornelius, J. M. Moss, J. B. McClelland, J. R. Comfort, J. L. Escudie,
        M. Gazzaly, N. Hintz, G. Igo, M. Haji-Saeid and C. A. Whitten, Jr.,
        Phys. Rev. C33, 17 (1986).

Kä84   B. Kämpfer and R. Wünsch, Nucl. Phys. A426, 301 (1984).

Ko85   A. M. Kobos, E. D. Cooper, J. I. Johansson and H. S. Sherif, Nucl. Phys.
        A445, 605 (1985).

Ko86   A. M. Kobos, Private Communication.

Ma58   F. Mandl, Proc. Phys. Soc. (London) 71, 177 (1958).

Mc83   J. A. McNeil, L. Ray and S. J. Wallace, Phys. Rev. C27, 2123 (1983).
        J. A. McNeil, J. R. Shepard and S. J. Wallace, Phys. Rev. Lett. 50,
        1439 (1983).

Me81   H. O. Meyer, P. Schwandt, G. L. Moake and P. P. Singh,
        Phys. Rev. C23, 616 (1981).

Pi83   J. Piekarewicz, R. D. Amado, D. A. Sparrow and J. A. McNeil,
        Phys. Rev. C28, 2392 (1983).

Ra81   A. Rahbar, B. Aas, E. Bleszynski, M. Bleszynski, M. Haji-Saeid, J. Igo,
        F. Irom, G. Pauletta, A. T. M. Wang, J. B. McClelland, J. F. Amann,
        T. A. Carey, W. D. Cornelius, M. Barlett, G. W. Hoffmann, C. Glashausser,
        S. Nanda and M. M. Gazzaly, Phys. Rev. Lett. 47, 1811 (1981).

Ra86   J. Raynal, private communication.

Ro57   M. E. Rose, Elementary Theory of Angular Momentum, John Wiley & Sons
        Inc. (1957).

Ro84   E. Rost, J. R. Shepard, E. R. Siciliano and J. A. McNeil, Phys. Rev. C29,
        209 (1984).

Ro85   E. Rost, in the " Proceedings of the LAMPF Workshop on Dirac
        Approaches to Nuclear Physics ", Proceedings No. LA-10438-C, 182, (1985).

Sa65   G. R. Satchler, in " Lectures In Theoretical Physics", University of Colorado
        Press (1965).

Sa84   R. I. Sawafta, M.Sc. Thesis, University of Alberta (1984) unpublished.

Sa83   G. R. Satchler, Nucl. Phys. A394, 349 (1983).

Se85   K. K. Seth, D. Barlow, A. Saha, R. Soundranayagam, S. Iversen, M. Kaletka,
        M. Basko, D. Smith, G. W. Hoffmann, M. L. Barlett, R. Fergerson,
        J. McGill and E. C. Milner, Phys. Lett. 158B, 23 (1985).

Sh68   H. S. Sherif, Ph.D. Thesis, University of Washington (1968) unpublished.

Sh83   J. R. Shepard, J. A. McNeil and S. J. Wallace, Phys. Rev. Lett. 50,
        1443 (1983).

Sh85   H. S. Sherif, E. D. Cooper and R. I. Sawafta, Phys. Lett. 158B, 193 (1985).

Sh86   H. S. Sherif, R. I. Sawafta and E. D. Cooper, Nucl. Phys. A449, 709 (1986).

Wa85   S. J. Wallace, in the " Proceedings of the LAMPF Workshop on Dirac
        Approaches to Nuclear Physics ", Proceedings No. LA-10438-C, 87, (1985).

APPENDIX A - DIRAC DWBA

We consider here the excitation of a nucleus to a collective excited state during an inelastic collision with a proton. We assume that the vector and scalar fields follow the nuclear matter distribution and that the total Hamiltonian for the system can be written as the sum of three parts [Co85b]

$$H_1 = \alpha \cdot p + \beta m + U_{Opt}(r) \qquad\qquad \text{A-1a}$$

$$H_2 = \sum_{\ell m} \hbar\omega_{\ell m} a^\dagger_{\ell m} a_{\ell m} \qquad\qquad \text{A-1b}$$

$$H_3 = \sum_{\ell m} \Delta V_{\ell m}(r) \, (a^\dagger_{\ell m} + a_{\ell m}) \qquad\qquad \text{A-1c}$$

where $a^\dagger_{\ell m}$ creates a phonon with energy $\hbar\omega_{\ell m}$, spin ℓ and projection m, and $\Delta V_{\ell m}(r)$ is the transition density IV-14 which is proportional to the derivative of the optical potential. The collective motion is described by H_2 and the transition is described by H_3. The transition we are interested in has a definite spin I and projection M so the sums in equations A-1b and A-1c are removed and we set ℓ=I and m=M. The equation that describes the process is

$$H \Psi = E \Psi \qquad\qquad \text{A-2}$$

where the total Hamiltonian is

$$H = H_1 + H_2 + H_3 \qquad\qquad \text{A-3}$$

H_2 is assumed to have a complete set of eigenfunctions $|n>$ which therefore obey

$$H_2 |n> = \varepsilon_n |n> \qquad\qquad \text{A-4}$$

where n is the set of all quantum numbers necessary to describe the state and ε_n is the excitation energy of that state. We follow the usual procedure of expanding the total wave function in terms of the eigenfunctions of the intrinsic Hamiltonian as

$$\Psi(r,\xi) = \sum_n \phi_n(r) \mid n > \qquad\qquad \text{A-5}$$

Now substitute A-5 into A-2 and with A-4 we can write

$$\sum_n (H_1 + \varepsilon_n + H_3 - E) \phi_n(r) \mid n > = 0 \qquad\qquad \text{A-6}$$

Multipying on the left by $< m \mid$ gives a set of coupled equations for the $\phi_m(r)$'s

$$(H_1 + \varepsilon_m - E) \phi_m(r) = \sum_n < m \mid H_3 \mid n > \phi_n(r) \qquad\qquad \text{A-7}$$

where H_3 either annihilates or creates a phonon. The problem can be simplified a great deal if we recall that we are trying to describe just two channels, the ground state with no phonons and an excited state with one phonon which has spin I and projection M. We write these states as $\mid 0 >$ and $\mid IM >$ respectively. Then we have that

$$a_{IM} \mid 0 > = a^\dagger_{IM} \mid IM > = 0 \qquad\qquad \text{A-8a}$$

$$a_{IM} \mid IM > = \mid 0 > \qquad\qquad \text{A-8b}$$

$$a^\dagger_{IM} \mid 0 > = \mid IM > \qquad\qquad \text{A-8c}$$

With just these two states it is necessary to evaluate only four matrix elements of H_3 in equation A-7. The results are:

$$< 0 \mid H_3 \mid 0 > = < IM \mid H_3 \mid IM > = 0 \qquad\qquad \text{A-9a}$$

$$< 0 \mid H_3 \mid IM > = < IM \mid H_3 \mid 0 > = \Delta V_{IM}(r) \qquad\qquad \text{A-9a}$$

We now have two coupled equations describing the excitation of the nucleus by the

133.

passing proton. These are written explicitly as

$$(H_1 + \varepsilon_0 - E) \phi_0(r) = - \Delta V_{IM}(r) \phi_{IM}(r) \qquad\qquad \text{A-10a}$$

$$(H_1 + \varepsilon_1 - E) \phi_{IM}(r) = - \Delta V_{IM}(r) \phi_0(r) \qquad\qquad \text{A-10b}$$

where the excitation energy of the state $| \, IM >$ is ε_1. Now we define Green functions

$G_0(r,r')$ and $G_1(r,r')$ by

$$(H_1 + \varepsilon_0 - E) G_0(r,r') = \delta(r - r') \qquad\qquad \text{A-11a}$$

$$(H_1 + \varepsilon_1 - E) G_1(r,r') = \delta(r - r') \qquad\qquad \text{A-11b}$$

Equations A-10 can then be written as integral equations

$$\phi_0(r) = \chi_\mu^{(+)}(r) - \int G_0(r,r') \Delta V_{IM}(r') \phi_{IM}(r') \, d^3r' \qquad\qquad \text{A-12a}$$

$$\phi_{IM}(r) = - \int G_1(r,r') \Delta V_{IM}(r') \phi_0(r') \, d^3r' \qquad\qquad \text{A-12b}$$

We iterate these equations once, i.e. we substitute the solution of A-10a (or A-12a)

which solves

$$(H_1 + \varepsilon_0 - E) \chi_\mu^{(+)}(r) = 0 \qquad\qquad \text{A-13}$$

into A-12b to get

$$\phi_{IM}(r) = - \int G_1(r,r') \Delta V_{IM}(r') \chi_\mu^{(+)}(r') \, d^3r' \qquad\qquad \text{A-14}$$

where $\chi_\mu^{(+)}(r')$ is the distorted wave for the incoming channel and we have explicitly

included the dependence of the spin projection of the incoming particle. All we need now

is the Green function which satisfies A-12b and the following boundary conditions:

i) $\phi_{IM}(r)$ is finite everywhere so $LIM_{r\to 0} G_1(r,r') = $ const.

ii) $LIM_{r\to\infty} G_1(r,r')$ gives an outgoing spherical wave in channel $| \, IM >$ i.e.

$$LIM_{r\to\infty} G_1(r,r') = LIM_{r\to\infty} \{ \exp(ikr) / r \, [\, 1 \, , k_1 \sigma \cdot \hat{r}/(E_1+m) \,]^\dagger \, G^\mu(r') \, | \, \mu > \}$$

where $G^{\mu}(r')$ is some function to be determined i.e. we have only outgoing

spherical waves.

The solution to the problem is

$$G_1(r,r') = k_1 \, (4\pi)^2 \, (E_1 + m) / (2m)$$

$$\sum_{j\ell m} [\, f_{\ell j}^{*}(r) \,, \, i \, \sigma \cdot \hat{r} \, g_{\ell j}^{*}(r) \,]^{\dagger} \, \mathcal{Y}^{m}_{\ell\,1/2\,j}(\hat{r}) \, \exp(-i\delta_{\ell j})$$

$$\mathcal{Y}^{m}_{\ell\,1/2\,j}{}^{\dagger}(\hat{r}') \, [\, f_{\ell j}^{(+)}(r') \,, \, i \, \sigma \cdot \hat{r} \, g_{\ell j}^{(+)}(r') \,] \qquad r < r' \qquad \text{A-15a}$$

$$\sum_{j\ell m} [\, f_{\ell j}^{(+)*}(r) \,, \, i \, \sigma \cdot \hat{r} \, g_{\ell j}^{(+)*}(r) \,]^{\dagger} \, \mathcal{Y}^{m}_{\ell\,1/2\,j}(\hat{r}) \, \exp(-i\delta_{\ell j})$$

$$\mathcal{Y}^{m}_{\ell\,1/2\,j}{}^{\dagger}(\hat{r}') \, [\, f_{\ell j}(r') \,, \, i \, \sigma \cdot \hat{r} \, g_{\ell j}(r') \,] \qquad r > r' \qquad \text{A-15b}$$

where k_1 and E_1 are the momentum and energy of the outgoing proton. Assymptotically

the incoming radial waves are Bessel functions and the outgoing waves are Hankel

functions of the first kind, so we can write

$$f_{\ell j}(r) \to_{r\to\infty} \sin(\, k_1 r - \ell\pi/2 + \delta_{\ell j}\,) / (k_1 r) \qquad \text{A-16a}$$

$$g_{\ell j}(r) \to_{r\to\infty} [\, k_1 / (E_1 + m)\,] \cos(\, k_1 r - \ell\pi/2 + \delta_{\ell j}\,) / (k_1 r) \qquad \text{A-16b}$$

$$f_{\ell j}^{(+)}(r) \to_{r\to\infty} \exp i(\, k_1 r - \ell\pi/2 + \delta_{\ell j}\,) / (k_1 r) \qquad \text{A-16c}$$

$$g_{\ell j}^{(+)}(r) \to_{r\to\infty} [\, i k_1 / (E_1 + m)\,] \exp i(\, k_1 r - \ell\pi/2 + \delta_{\ell j}\,) / (k_1 r) \qquad \text{A-16d}$$

The calculation of the probability of observing a proton in channel $| \, IM >$ given a proton

incident in channel $| \, 0 >$ requires that we examine the flux at a large distance from the

scatterer so we must examine

$$\text{LIM}_{r\to\infty} \, \phi_{IM}(r) = - \text{LIM}_{r\to\infty} \int G_1(r,r') \, \Delta V_{IM}(r') \, \chi_{\mu}^{(+)}(r') \, d^3 r' \qquad \text{A-17}$$

Note that there are no contributions to this integral for r' outside the range of $\Delta V_{IM}(r')$

so we are only interested in the form of the Green function for $r > r'$. Using A-15b, A-16c and A-16d in A-17 leads to

$$\text{LIM}_{r \to \infty} \phi_{IM}(r) = -4\pi (E_1 + m)/(2m) \exp(ik_1 r)/r \ [\ 1, k_1 \sigma \cdot \hat{r}/(E_1 + m)\ ]^\dagger$$

$$\sum_{j \ell m} i^\ell \ \mathcal{Y}^m_{\ell 1/2 j}(\hat{r}) \int \mathcal{Y}^m_{\ell 1/2 j}{}^\dagger(\hat{r}') \ [\ f_{\ell j}(r'), i \ \sigma \cdot \hat{r}' g_{\ell j}(r')\ ]$$

$$\Delta V_{IM}(r') \chi_\mu^{(+)}(r') \ d^3 r' \qquad\qquad \text{A-18}$$

Now expand the generalized spherical harmonic as in IV-20. Then we can write A-18 as

$$\text{LIM}_{r \to \infty} \phi_{IM}^{\mu'}(r) = [(E_1 + m)/(2m)]^{1/2} \exp(ik_1 r)/r \ [1, k_1 \sigma \cdot \hat{r}/(E_1 + m)\ ]^\dagger \ m/2\pi$$

$$\sum_\mu T^M_{\mu\mu'} \ |\mu\rangle \qquad\qquad \text{A-19}$$

where a factor of $-m/2\pi$ enters because we are looking at the T-matrix and not the scattering amplitude of the scattered wave. Notice also that we have labelled $\phi_{IM}(r)$ with the spin projection of the outgoing proton in A-19. The scattered particles are moving radially outward in the direction of $\hat{r}$ so we set

$$Y_\ell^{m-\mu}(\hat{r}) = Y_\ell^{m-\mu}(\hat{k}_f) \qquad\qquad \text{A-20}$$

and define the final state distorted wave by

$$\chi_\mu^{(-)}(r') = 4\pi \ [(E_1 + m)/(2m)]^{1/2} \sum_{j \ell m} i^\ell \ Y_\ell^{m-\mu'}(\hat{k}_f) \ (\ell, 1/2\ ; m-\mu', \mu' \ | \ j, m)$$

$$\mathcal{Y}^m_{\ell 1/2 j}{}^\dagger(\hat{r}') \ [\ f_{\ell j}(r'), i \ \sigma \cdot \hat{r}' g_{\ell j}(r')\ ] \qquad\qquad \text{A-21}$$

then we can write the T-matrix in the conventional looking form

$$T^M_{\mu\mu'} = \int \chi_\mu^{(-)}(r') \ \Delta V_{IM}(r') \ \chi_\mu^{(+)}(r') \ d^3 r' \qquad : \qquad \text{A-22}$$

APPENDIX B - OBSERVABLES

B-1 Elastic Observables

The scattering amplitude for elastic scattering can be expressed in terms of two amplitudes [Co81] which in turn can be written as functions of the phase shifts extracted when the radial wave functions are normalized to the Coulomb wave functions. These two amplitudes are

$$A = (2ik)^{-1} \sum_{\ell=1,\infty} [((\ell+1) (s_\ell^{(+)} - 1) + \ell (s_\ell^{(-)} - 1)] P_\ell(\cos\theta)] \qquad \text{B-1}$$

$$B = (2ik)^{-1} \sum_{\ell=1,\infty} [s_\ell^{(-)} - s_\ell^{(+)}] P_\ell^1 (\cos\theta)] \qquad \text{B-2}$$

where the S-matrix elements are similar to II-62 but depend on the total spin j, as well as ℓ

$$s_\ell^{(\pm)} = s_{\ell, j=\ell\pm1/2}$$

$$= \exp(2i\delta_{\ell j}) \qquad \text{B-3}$$

The differential cross section can then be written in terms of these amplitudes as

$$d\sigma/d\Omega = | A |^2 + | B |^2 \qquad \text{B-4}$$

This looks just the same as the nonrelativistic case outlined by Jackson [Ja70], the only difference is that we calculate the phase shifts using the Dirac wave functions instead of Schrödinger wave functions.

The analyzing power is defined as

$$A = \text{Tr } T\sigma T^\dagger / \text{Tr } TT^\dagger$$

and interms of the amplitudes this is

$$A = 2 \text{ Im}(A^*B) / (|A|^2 + |B|^2) \qquad\qquad \text{B-5}$$

The spin rotation parameter, Q, is

$$Q = \text{Tr } T\sigma_z T^\dagger \sigma_x / \text{Tr } TT^\dagger$$

which in terms of the amplitudes is

$$Q = 2 \text{ Re}(A^*B) / (|A|^2 + |B|^2) \qquad . \qquad\qquad \text{B-6}$$

This is how the optical model program RUNT, which we have used for the fitting,

calculates the observables.

B-2 Inelastic Cross Section

Recall equation A-19 for the final state wave function

$$\text{LIM}_{r\to\infty} \phi^M_\mu(r) = [(E_f+m)/(2m)]^{1/2} \exp(ik_f r)/r$$

$$[1, k_f\sigma\cdot\hat{r}/(E_f+m)]^\dagger m/2\pi \sum_\mu T^M_{\mu\mu'} |\mu> \qquad\qquad \text{B-7}$$

We define a wave function with all the spin indices by removing the sum over the

initial projection

$$\phi^M_{\mu\mu'}(r) = [(E_f+m)/(2m)]^{1/2} \exp(ik_f r)/r [1, k_f\sigma\cdot\hat{r}/(E_f+m)]^\dagger$$

$$m/2\pi T^M_{\mu\mu'} |\mu> \qquad\qquad \text{B-8}$$

The outgoing flux associated with $\phi^M_{\mu\mu'}(r)$ is

$$J^M_{\mu\mu'} = [\, \phi^M_{\mu\mu'}(r)\,]^\dagger \, \alpha \, \phi^M_{\mu\mu'}(r)$$

$$= \hat{r}/r^2 \; k_f/m \, (m/2\pi)^2 \,|\, T^M_{\mu\mu'}\,|^2 \qquad\qquad \text{B-9}$$

where we have used $[\,\sigma\,,\,\sigma\cdot\hat{r}\,]_+ = 2\hat{r}$. The total outgoing current is obtained by summing over all the final spin projections and averaging over the initial spin so

$$J_{Fin} = (\,2S_i + 1\,)^{-1} \sum_{M\mu\mu'} J^M_{\mu\mu'} \qquad\qquad \text{B-10}$$

where S_i is the spin of the incoming particle (1/2 for protons).

.The incident wave function is a plane wave at large r

$$\phi_\mu(r) \to_{r\to\infty} [\, (E_i+m)/(2m)\,]^{1/2} \exp(ik_i r) \, [1,\, k_i \sigma\cdot\hat{r}/(E_i+m)\,]^\dagger \,|\mu\rangle \qquad \text{B-11}$$

and the incoming flux is (choosing the beam in the z direction)

$$J_{Inc} = (\,2S_i + 1\,)^{-1} \sum_\mu \phi_\mu^\dagger(r)\, \alpha\, \phi_\mu(r)$$

$$= \hat{z}\, 2\,(\,2S_i + 1\,)^{-1} k_i/m \qquad\qquad \text{B-12}$$

The differential cross section is the outgoing flux per unit solid angle divided by the incoming flux so

$$d\sigma/d\Omega = 1/2\, k_f/k_i \,(m/2\pi)^2 \sum_{m\mu\mu'} |\, T^M_{\mu\mu'}\,|^2 \qquad\qquad \text{B-13}$$

B-3   Inelastic Spin Observables

The sum over the spin indices in B-7 can be written as the trace of $TT^\dagger$

$$Tr\, TT^\dagger = \sum_{\mu\lambda M} T^M_{\mu\lambda}\, T^{*M}_{\mu\lambda} \qquad\qquad \text{B-14}$$

then the analyzing power is given by

$$A = \text{Tr } T\sigma T^\dagger / \text{Tr } TT^\dagger$$

B-15

and the polarization transfer coefficients are defined as

$$D_{jk'} = \text{Tr } T\sigma_j T^\dagger \sigma_{k'} / \text{Tr } TT^\dagger$$

B-16

where j refers to the incident projectile frame and k' refers to the outgoing projectile frame. The coordinate system for the scattering is shown in Figure B-1. For the incident projectile the frame we choose has the z-axis parallel to k_i, the y-axis normal to the scattering plane and the x-axis placed to form a right-handed system. The coordinate system for the outgoing particle is defined similarly, with the z'-axis parallel to k_f, the y'-axis parallel to the y-axis and the x'-axis placed to form a right-handed coordinate system. We also use another notation for the coordinate system in this work, and that is the right handed system formed by the unit vectors s, n and l (sideways, normal and longitudinal) as shown in figure B-1.

Note that a relativistic correction must be applied to the expression for $D_{jk'}$ since the use of the σ operator implies a particle rest frame [Ho68, Gr83]. This correction is not shown in B-16 but is included in our calculations.

Aas et al. [Aa82] have found that in the adiabatic limit $D_{LS'} = D_{SL'}$. They also find that for collective, natural parity transitions, as we discuss in this work, $D_{LL'}$ is approximately the same as $D_{SS'}$.